UNIVERSITAT POLITÈCNICA
DE CATALUNYA
BARCELONATECH

ELECTRICAL AND MAGNETIC FAULTS DIAGNOSIS IN PERMANENT MAGNET SYNCHRONOUS MOTORS

By

Julio César Urresty Betancourt

Thesis submitted in partial fulfillment of the requirements of the degree of Doctor in Electronic Engineering

Advisers:

José Luis Romeral Martínez

Jordi-Roger Riba Ruiz

Department of Electronic Engineering

Terrassa Barcelona, Spain

June, 2012

ABSTRACT

Permanent magnet synchronous motors (PMSMs) are an alternative in critical applications where high-speed operation, compactness and high efficiency are required. In these applications it is highly desired to dispose of an on-line, reliable and cost-effective fault diagnosis method. Fault prediction and diagnosis allows increasing electric machines performance and raising their lifespan, thus reducing maintenance costs, while ensuring optimum reliability, safe operation and timely maintenance. Consequently this thesis is dedicated to the diagnosis of magnetic and electrical faults in PMSMs.

As a first step, the behavior of a healthy machine is studied, and with this aim a new 2D finite element method (FEM) model-based system for analyzing surface-mounted PSMSs with skewed rotor magnets is proposed. It is based on generating a geometric equivalent non-skewed permanent magnet distribution which accounts for the skewed distribution of the practical rotor, thus avoiding 3D geometries and greatly reducing the computational burden of the problem.

To diagnose demagnetization faults, this thesis proposes an on-line methodology based on monitoring the zero-sequence voltage component (ZSVC). Attributes of the proposed method include simplicity, very low computational burden and high sensibility when compared with the well known stator currents analysis method. A simple expression of the ZSVC is deduced, which can be used as a fault indicator parameter. Furthermore, mechanical effects arising from demagnetization faults are studied. These effects are analyzed by means of FEM simulations and experimental tests based on direct measurements of the shaft trajectory through self-mixing interferometry. For that purpose two perpendicular laser diodes are used to measure displacements in both X and Y axes. Laser measurements proved that demagnetization faults may induce a quantifiable deviation of the rotor trajectory.

In the case of electrical faults, this thesis studies the effects of resistive unbalance and stator winding inter-turn short-circuits in PMSMs and compares two methods for detecting and discriminating both faults. These methods are based on monitoring and analyzing the third harmonic component of the stator currents and the first harmonic of the ZSVC.

Finally, the Vold-Kalman filtering order tracking algorithm is introduced and applied to extract selected harmonics related to magnetic and electrical faults when the machine operates under variable speed and different load levels. Furthermore, different fault indicators are proposed and their behavior is validated by means of experimental data. Both simulation and experimental results show the potential of the proposed methods to provide helpful and reliable data to carry out a simultaneous diagnosis of resistive unbalance and stator winding inter-turn faults.

ACKNOWLEDGMENTS

First of all I thank my supervisors, Prof. José Luis Romeral and Jordi Roger Riba, for their guidance, support, patience and trust during my studies in the Universitat Politècnica de Catalunya. I am forever grateful as this work has not been possible without their knowledge and experience.

To the members of MCIA research group, to all of them many thanks for their friendship and support during this time.

To Reza Atashkhooei from CD6 research center, thanks for his support with his laser system for the shaft trajectory measurements.

To my parents Rafael and Bertha who with their example, efforts and love make the dreams of their children into reality. I would like to express my gratitude to my siblings Rafael and Bertha and my girlfriend Beatriz, they all in a distance place, but with the same unconditionally and support, were inspiring me during this period.

To my friends in Spain, who have given me great moments and make me feel at home.

CONTENTS

LIST OF FIGURES

LIST OF TABLES

ACRONYMS

HCF: Highest common factor

MMF: Magnetomotive force

Back-emf: Back electromotive force

PMSM: Permanent magnet synchronous motor

SPMSM: Surface permanent magnet synchronous motor

ZSVC: Zero sequence voltage component

CBM: Condition-based maintenance

FFT: Fast Fourier transform

OT: Order tracking

VKF-OT: Vold-Kalman Filtering Order Tracking

SMI: Self-mixing interferometry

SMLDs: Self-mixing laser diodes

SYMBOLS

f_{dmg}: Demagnetization frequency

f_s: Supply frequency

k: Integer number

p: Pole pairs

q: Number of slots/pole/phase

f_{slot}: Slot frequency

ν: Harmonic order

Z_1: Number of stator slots

f_e: Eccentricity fault frequency

f_{bng}: Bearings fault frequency

$f_{i,o}$: Characteristic vibration frequency

n_b: Number of bearing balls

f_r: Mechanical frequency of the rotor

bd: Ball diameter

pd: Bearing pitch diameter

β: Contact angle of the balls

k_M: MMF reduction factor

k_d: Winding distribution factor

k_p: Short pitching factor

k_s: Skewed factor

θ_{skew}: Skew angle of the rotor magnets

ϕ_τ: Net magnetic flux per pole

n_s: Number of magnet segments

B_r: Magnet Remanent flux density

τ': Magnetic arc

r: Magnet radius

l: Axial length of the rotor

k_s: Skewed reduction factor

B_k: Remanent flux density of a magnet segment

θ: Mechanical angle of the rotor

φ: Angle between magnet segments

i_d: Direct axis current

$y(t)$: Pulsating waveform

$x(t)$: Square waveform

d: Duty cycle of Square waveform

N: Number of turns in a slot

k_{dem}: Demagnetization factor in p.u

V_{slot}: Voltage in a slot of a healthy machine

e_{slot}: Back-emf voltage in a single slot

e_{phase}: Back-emf voltage in phase of the machine

λ_{phase}: Magnetic flux in phase of the machine

λ_{slot}: Magnetic flux in a slot of a healthy machine

λ_1: Fundamental Magnetic flux in a slot

λ_{PM1}: Fundamental Magnet flux

$\lambda_{PM\nu}$: ν-th harmonic of magnet flux

$[\lambda_{s,abc}]$: Stator three-phase magnetic flux matrix

λ_{PM0}: Magnets zero-sequence flux component

$[V_{s,abc}]$: Stator three-phase voltage matrix

$[i_{s,abc}]$: Stator three-phase current matrix

$[R_{sh}]$: Stator resistance matrix

$[L_{sh}]$: Stator inductances matrix

n: Number of shorted turns

υ: Ratio between faulty and healthy turns

i_f: Current through the short-circuited turns

R_f: Resistance which models the insulation failure

1. INTRODUCTION

Electric motors are one of the most important components of industrial machinery, playing a decisive role in applications such as robotics and motion control. It is well known that industry continuously demands faster and more reliable manufacturing machinery. In the last decade, different electric motor technologies have become popular because high power density, accurate dynamic performance and high efficiency are being demanded in industrial applications. Additionally, a number of different control methods have been widespread, such as adaptive motor control [1-3].

PMSMs are currently being widely applied and are being object of an intense research [4] because they accomplish with the abovementioned features and are well suited for new adjustable speed ac inverter drives. Appealing features of PMSMs include high-speed operation, precise torque control even at low speed, high power to weight ratio, compactness, and high efficiency [5]. The development of rare earth magnets such as Sm-Co and Nd-Fe-B has made possible the development of efficient and compact PMSMs. Furthermore, PMSMs efficiency and power factor do not depend on the pole number and speed to the same extent as it is the case of induction motors. All of these reasons lead to PMSMs to gain ground in automotive, robotics and aeronautical industry [6].

On the other hand, for safety-critical systems, the consequences of a minor fault in a component can be catastrophic [7]. Therefore, demand on reliability, safety and fault tolerance is generally high. It is necessary to design control systems which are capable of diagnose and tolerate potential faults in order to improve the reliability and availability while providing a desirable performance[8]. There are different fault detection techniques for electric motors such as temperature measurement, radio frequency emission monitoring, noise and vibration monitoring, acoustic noise measurements, motor torque and speed harmonic analysis and stator currents monitoring among others [9]. Stator currents monitoring [10] is the most widely employed method since can provide unique fault patterns [10], it is non-intrusive and does not require extra equipment because it uses the stator winding as search coil and performs a numerical processing of the acquired stator currents. Stator currents monitoring relies on several mathematical processing techniques. Among them, Fourier transform based methods have been widely applied when the motor operates under stationary conditions [11]. However, when operating under non-stationary conditions, time-frequency based methods still remain preferred [5].

PMSMs faults can be classified in magnetic, electrical and mechanical faults. Magnetic faults include damaged or demagnetized magnets, whereas electrical faults include abnormal connection, stator open turns, stator short circuited turns, phase-to-phase and phase-to-ground short-circuits. Mechanical faults include static and dynamic air-gap irregularities, bent shaft or dynamic eccentricity, and damaged

bearings [12]. In this work magnetic and electrical faults (unbalance connections and inter-turns short-circuits) are analyzed in surface-mounted permanent magnet synchronous motors (SPMSMs).

Partial demagnetization has adverse mechanical effects because it causes unbalanced magnetic pull, magnetic force harmonics, acoustic noise and vibrations [13], thus reducing mechanical torque of the SPMSM and affecting motor performance [14]. Due to partial demagnetization, the SPMSM requires a stator current higher than the rated one to generate the same output torque. This in turn increases the temperature of the PMSM and may cause a higher demagnetization, which again increases the stator current [15]. Additionally, over-currents due to inter-turn short-circuits may produce partial demagnetization [14]. The worst-case condition happens when a whole stator coil is in short circuit when the armature reaction is at its highest, during transients or when the motor drives high loads [13]. Stator short-circuits increase fault effects and may shift the permanent magnet operation point below the irreversible demagnetization region [16].

In this work it is proved that partial demagnetization faults generate harmonics in the back-emf spectrum of a single slot because the flux is not symmetrical. However, depending on windings configuration, when analyzing the global back-emf induced in all the slots of a phase, in some cases it is not possible to detect such harmonics because they cancel each other. Hence, when diagnosing this specific type of fault, in some motors it is not feasible to detect fault harmonics in the current spectrum due to demagnetization. In this work it is proposed to diagnose incipient demagnetization faults by applying an on-line monitoring of the zero-sequence voltage component (ZSVC) [17]. This method is also appropriate for inverter-fed machines. An accessible neutral point of the stator windings is needed to measure the ZSVC, just as required by the fault tolerant schemes that add an extra inverter branch which, under a fault condition, is connected to the neutral point of the SPMSM by replacing the faulty phase [15]. Additionally, a simple-to-extract fault severity factor is presented and its behavior is evaluated and validated by means of experiments when the SPMSM operates under different speed and load conditions.

In the case of electrical faults, most problems are caused by deterioration and failure of the turn-to-turn insulation and subsequently they develop into more severe insulation faults [18]. Such faults generate large circulating currents in the shorted turns of the order of twice the blocked rotor current [19] which in turn produce winding overheating. It results in severe coil-to-coil short-circuits in which coils from the same phase get shorted and also can result in phase-to-phase short-circuits, where the fault occurs between two or more different phases. These faults can again develop into phase-to-ground faults, which can cause substantial damage to the motor [18]. According to [19], ground current may lead to irreversible damage to the core and the machine might have to be pulled out of service. In the case of PMSMs, stator over-currents due to inter-turn short-circuits may create a magnetic flux opposed to the natural flux of the permanent magnets, which may lead to a demagnetization of the rotor magnets [14]. On the other hand in a three-phase motor, phase resistances should be as balanced as possible. Unbalanced connections occur frequently in industrial applications. Usually they are due to corrosion or

contamination problems. Moreover, vibrations and thermal cycling process may deteriorate connections [20]. Poor contacts may generate local overheating, unbalanced voltages and currents as well as electrical failures such as short-circuits or open-circuits [21]. Unbalanced conditions generate negative-sequence voltages and currents that have a negative impact on the motor efficiency and performance and may lead to excessive thermal stress. Furthermore, voltage unbalance may generate a current unbalance several times larger than the magnitude of voltage unbalance. The impedance unbalance may increase with time because of the heating of the stator windings [22].The objective of this thesis is to study both resistive unbalance and inter-turn faults in SPMSMs while providing a fault detection method for distinguishing them, even when fed by a voltage-source inverter. For this purpose, two methods are proposed. The first one is based on the analysis of the amplitude of the third harmonic of the stator currents for different operating points of the SPMSM, whereas the second one is based on the analysis of the first harmonic of the ZSVC [23].

1.1 Objectives

This works aims to contribute to the detection and diagnosis of magnetic and electrical faults in permanent magnet synchronous motors. The main objectives of this work are as follows:

- Carry out an exhaustive theoretical and experimental analysis of demagnetization and electrical faults, including winding configuration effects.
- Identify relevant fault harmonics in stator currents and voltage signals caused by each fault type.
- Determine fault harmonics behavior under stationary and variable load and speed conditions.
- Select and implement and appropriate signal processing technique for tracking relevant harmonics from variable frequency signals.
- Propose fault indicators to diagnose electric and magnetic faults.

1.2 Main contributions of the thesis

The most important scientific contributions of this work are as follows:

- A new 2D finite element method (FEM) based system for analyzing SPMSMs with skewed rotor magnets is presented. It is based on generating a geometric equivalent non-skewed permanent magnet distribution which accounts for a skewed distribution of a practical rotor. An appealing feature of the proposed system is that it can be easily performed in any 2D electromagnetic FEM package by performing a simple change in the magnets geometry instead of using 3D models which require a large computational burden.

- It is presented a novel mathematical model to study partial demagnetization effects in the back-emf on both a single slot and the resultant effect on all slots in an integral (q = 1) concentrated winding.
- It is proposed and studied the diagnosis of demagnetization faults in SPMSMs by means of an on-line monitoring of the ZSVC instead of applying the classical stator currents method. Furthermore, a simple expression of the ZSVC is deduced, which is proposed as a new fault indicator parameter in SPMSMs with integral slot windings.
- Based on FEM simulations, it is investigated the winding configuration influence on the currents and ZSVC spectra in a demagnetized motor. New motor models are studied that include fractional and integral stator slot windings, single- and double-layer, full-, short-, and variable-pitch, and series- and parallel-connected windings.
- Mechanical effects arising from demagnetization faults are studied. These effects are analyzed by means of FEM simulations and experimental tests based on direct measurements of the shaft trajectory by means of self-mixing interferometry, to which result on a new hybrid detection method for motor faults. Additionally, a FEM model that includes the motor shaft displacement is presented.
- It is proposed and analyzed a new parametric model which allows studying windings inter-turn short-circuit faults effects. From this model a new methodology based on the analysis of the first ZSVC harmonic is proposed for detecting such a fault.
- A new mathematical model of the SPMSM including saturation effects which accounts for inter-turns short-circuits and unbalance stator resistance faults is developed.
- The Vold-Kalman filtering order tracking algorithm is introduced and applied to track relevant harmonics when the machine running under variable speed and different load levels.
- Two reliable new fault indicators especially focused on stator windings inter-turn faults diagnosis under non-stationary speed conditions are proposed.

1.3 Thesis outline

The contents of the thesis are:

- Chapter 2. Condition monitoring of electrical machines: this chapter presents the main definitions related to condition monitoring with the aim of highlight the importance of studying faults in SPMSMs. Additionally in this chapter some general aspects about SPMSMs faults are described.
- Chapter 3. Healthy SPMSM: In this chapter it is studied the healthy machine state in order to examine the main constructive harmonics in the back-emf and stator currents. Furthermore it is proposed a new method to study SPMSMs with skewed magnets with a 2D FEM model.

- Chapter 4. Demagnetization faults in SPMSM: In this chapter it is presented a theoretical and experimental analysis of demagnetization faults, including winding configuration influence and mechanical effects.
- Chapter 5. Electrical faults in SPMSM: In this chapter it is analyzed stator unbalance resistance and winding inter-turns short-circuits, a model for both faults is developed and a diagnosis method from proposed models is derived. Moreover, SPMSM with shorted turns and different winding configurations are studied.
- Chapter 6. Diagnosis of SPMSMs operating under non-stationary conditions by means of order tracking filtering: In this chapter, the Vold-Kalman filtering order tracking is introduced and applied for tracking demagnetization and inter-turns short-circuits harmonics from non-stationary signals.
- Chapter 7. Conclusions and future work.

1.4 Thesis publications

The publications related to the thesis are as follows:

1.4.1 Journals

The papers already published or submitted to international scientific journals (JCR indexed) can be divided according to each chapter of this thesis as follows:

Chapter 3. Healthy SPMSM:

1. Urresty, J.-C.; Riba, J.-R.; Romeral, L.; Garcia, A., "A Simple 2-D Finite-Element Geometry for Analyzing Surface-Mounted Synchronous Machines With Skewed Rotor Magnets," IEEE Transactions on Magnetics, vol.46, no.11, pp.3948-3954, Nov. 2010.

Chapter 4. Demagnetization faults in SPMSM:

2. Urresty, J.; Riba, J.-R.; Delgado, M.; Romeral, L., "Detection of Demagnetization Faults in Surface-Mounted Permanent Magnet Synchronous Motors by Means of the Zero-Sequence Voltage Component," IEEE Transactions on Energy Conversion, vol.27, no.1, pp.42-51, March 2012
3. Prieto, M.D.; Espinosa, A.G.; Ruiz, J.-R.R.; Urresty, J.C.; Ortega, J.A., "Feature Extraction of Demagnetization Faults in Permanent-Magnet Synchronous Motors Based on Box-Counting Fractal Dimension," IEEE Transactions on Industrial Electronics, vol.58, no.5, pp.1594-1605, May 2011

4. Urresty, J.-C.; Riba, J.-R.; Romeral, L, Saavedra, H., “A Fault Severity Index to Detect Magnet Failures in PMSMs,” Submitted to IEEE Transactions on Magnetics
5. Urresty, J.-C.; Atashkhooei, R.; Riba, J.-R.; Romeral, L, Royo, S., “Mechanical Effects of Demagnetization Faults in Permanent Magnet Synchronous Motors,” Submitted to IEEE Transactions on Industrial Electronics

Chapter 5. Electrical faults in SPMSM:

6. Urresty, J.C.; Riba Ruiz, J.-R.; Romeral, L., "Application of the zero-sequence voltage component to detect stator winding inter-turn faults in PMSMs” Electric Power Systems Research, Vol.89 pp.38-44, August 2012
7. Romeral, L.; Urresty, J.C.; Riba Ruiz, J.-R.; Garcia Espinosa, A., "Modeling of Surface-Mounted Permanent Magnet Synchronous Motors With Stator Winding Inter-turn Faults," IEEE Transactions on Industrial Electronics, vol.58, no.5, pp.1576-1585, May 2011

Chapter 6. Diagnosis of SPMSMs operating under non-stationary conditions by means of order tracking filtering:

8. Urresty, J.C.; Riba Ruiz, J.-R.; Romeral, L.; “Diagnosis of Inter-Turn Faults in PMSMs Operating Under Non-Stationary Conditions by applying Order Tracking Filtering” IEEE Transactions on Power Electronics, Accepted for future publication

1.4.2 Conferences

1. Urresty, J.-C.; Riba, J.-R.; Saavedra, H.; Romeral, L., "Detection of inter-turns short circuits in permanent magnet synchronous motors operating under transient conditions by means of the zero sequence voltage," Proceedings of the 2011-14th European Conference on Power Electronics and Applications (EPE 2011), pp.1-9, Aug. 30-Sept. 1, 2011
2. Urresty, J.; Riba, J.; Saavedra, H.; Romeral, J., "Analysis of demagnetization faults in surface-mounted permanent magnet synchronous motors with symmetric windings," IEEE International Symposium on Diagnostics for Electric Machines, Power Electronics & Drives (SDEMPED 2011), pp.240-245, 5-8 Sept. 2011
3. Delgado, M.; Urresty, J.C.; Albiol, L.; Ortega, J.A.; Garcia, A.; Romeral, L.; Vidal, E., "Motor fault classification system including a novel hybrid feature reduction methodology," IEEE Industrial Electronics Society Annual Conference (IECON 2011), pp.2388-2393, 7-10 Nov. 2011
4. Delgado, M.; Garcia, A.; Urresty, J.C.; Riba, J.-R.; Ortega, J.A., "Evaluation of machine learning techniques for electro-mechanical system diagnosis," Proceedings of the 14th European Conference on Power Electronics and Applications (EPE 2011), pp.1-10, Aug. 30-Sept. 1, 2011

5. Navarro, L.; Delgado, M.; Urresty, J.; Cusido, J.; Romeral, L., "Condition monitoring system for characterization of electric motor ball bearings with distributed fault using fuzzy inference tools," Instrumentation and Measurement Technology Conference (I2MTC), 2010 IEEE , vol., no, pp.1159-1163, 3-6 May 2010
6. Urresty, J.; Riba, J.; Romeral, L.; Rosero, J.; Serna, J, "Stator short circuits detection in PMSM by means of Hilbert-Huang transform and energy calculation," IEEE International Symposium on Diagnostics for Electric Machines, Power Electronics and Drives, SDEMPED 2009., pp.1-7, Aug. 31-Sept. 3 2009
7. Urresty, J.; Riba, J.; Ortega, J.; Cardenas, J.; , "Stator short circuits detection in PMSM by means of Zhao-Atlas-Marks distribution and energy calculation," 13th European Conference on Power Electronics and Applications, EPE '09., pp.1-9, 8-10 Sept. 2009
8. Delgado, M.; Garcia, A.; Ortega, J.A.; Urresty, J.; Riba, J.R.; , "Bearing diagnosis methodologies by means of Common Mode Current," 13th European Conference on Power Electronics and Applications, EPE '09, pp.1-10, 8-10 Sept. 2009
9. Rosero, J.; Romeral, L.; Rosero, E.; Urresty, J.; , "Fault Detection in dynamic conditions by means of Discrete Wavelet Decomposition for PMSM running under Bearing Damage," Twenty-Fourth Annual IEEE Applied Power Electronics Conference and Exposition, APEC 2009., pp.951-956, 15-19 Feb. 2009

1.5 Patents

1. Urresty, J.C.; Riba Ruiz, J.R.; Romeral, J.L, "Equipo de diagnóstico de fallos de corto circuito para motores síncronos de imanes permanentes y método de utilización de este", Spanish Patent P201130006, January 2011
2. Urresty, J.C.; Riba Ruiz, J.-R.; Romeral, J.L, "Equipo de diagnóstico de fallos de desmagnetización para motores síncronos de imanes permanentes y método de utilización de este", Spanish Patent P201130332, March 2011
3. Atashkhooei, R.; Urresty, J.-C.; Royo, S.; Riba, J.-R.; Romeral, L, “Sistema y método de medida del desplazamiento transversal de un eje físico giratorio”, Spanish Patent P201132100, December 2011

2. CONDITION MONITORING OF ELECTRICAL MACHINES

This chapter presents an overview of condition monitoring techniques and the main concepts in regard to PMSM faults.

Most of electrical machines have to operate within a close set of limits. These are selected to ensure safe operation and to guarantee that design specifications are not exceeded. In many applications such as electrical vehicles, electrical motors operate within a particular range of speeds and loads. This includes both steady-state and variable operation. Intermittently, electrical machines are required to operate outside of design constrains for short time periods (start-up, shutdown, and momentary overloads) [24].

The most important reason for using condition monitoring and fault diagnostics is to generate precise information about the actual condition of the motor. This allows more realistic expectations about machine performance. With this type of information is possible to determinate the following key aspects[25]:

- Expected time to failure
- Expected failure mode
- Required maintenance activities

Failures can be divided into incipient and catastrophic. In most type of failures there are some previous alarms to detect the failure. The aim of condition monitoring and fault diagnosis is to detect any failure in its incipient phase and its progression over the time. This will allows to design actuation plans to avoid catastrophic stages [24].

2.1 Maintenance strategies

Maintenance strategies can be classified into three types: run-to-failure, programmed and condition-based maintenance (CBM) [26].

Run-to-failure is an approach where maintenance actions or replacements are performed when machinery has failed. Run-to-failure maintenance is recommended in the following situations:

- With redundant machines
- Low costs spares or replacements are possible
- All failures modes are safe
- In the case of a low cost secondary damage

In the case of programmed or preventive maintenance, specific tasks are performed at defined time intervals in order to keep a significant period between machine capacities and actual duty. Preventive maintenance is effective under the following circumstances:

- Statistics of the failure time is known
- Maintenance actions return the reliability of the machine
- A dominant single known failure type
- A usual low cost associated with regular substitution of the equipment
- With a low cost secondary damage

An example of preventive maintenance practice can be found in a car, in which the engine oil is replaced at regular time intervals with a relative low cost.

2.2 Condition-based maintenance

In CBM, components are periodically inspected in order to determine their condition and to identify their degradation rates. A maintenance decision is based upon an examination of the monitored data and only when it is necessary. The main advantages of CBM is that actual condition and precise failure prediction permit flexibility for maintenance at a suitable time, therefore improving system availability and reducing random breakdowns.

The fundamental component in a CBM program is the failure prediction and consequently an effective method of condition monitoring. The ideal method would be one in which the state of the equipment would be identified continuously and would provide an accurate prediction of any possible failure on demand. As a result, condition monitoring is the way by which CBM can be carried out.

CBM should be used when the following circumstances apply:

- In expensive or vital machinery
- There is a long time for replacements parts
- In uninterruptible processes
- Equipment with expensive maintenance
- Acceptable cost of monitoring program
- In remote equipment
- Failures may be dangerous

2.3 Condition monitoring

Condition monitoring can be defined as a method or a practice of monitoring the working characteristics of a machine in order to use changes and trends in collected data to predict the requirements of

maintenance before severe deterioration occurs and to estimate the machine condition. Machine monitoring can be carried out periodically or continuously [24].

In periodic monitoring, machine data is only collected at specific time intervals with portable removable sensors. This type of monitoring is typically applied to equipment where failure modes are known. Trending of state and severity levels checks are the main focus. On the other hand in continuous monitoring, the data from fixed sensors in the machine is analyzed automatically. This type of monitoring is carried out on critical equipment [27].

A condition monitoring system should include the following three main steps [28]:

- Data acquisition
- Fault detection
- Fault identification and Diagnosis

2.3.1 Data acquisition

Data acquisition is an essential step in fault diagnosis. Condition monitoring data are the measurements related to the state of the system.

The source data can be vibration data, acoustic data, oil analysis data, temperature, pressure, moisture, humidity, and weather or environment data among others. Various sensors, such as micro-sensors, ultrasonic sensors, acoustic emission sensors, etc., have been designed to collect different types of data. Selection of sensors will rely on the monitoring method and are related to the knowledge on failure mechanisms of the machine [29].

In this project, the signals acquired for fault diagnosis purposes are stator currents and voltages.

2.3.2 Fault detection

The aim of fault detection schemes is to determine the possible occurrence of an incipient fault appearing in the machine and the need of further corrective actions.

Fault detection can be done by means of feature extraction methods, time domain, frequency domain or time-frequency domain signal processing technologies in order to obtain “signatures” which can represent normal and faulty states[30].

Various signal processing techniques have been developed to analyze and interpret collected data with the aim of extracting useful information for further diagnostic and prognostic purposes. The selection of appropriate signal data processing algorithm among a wide number of possibilities is an important task which depends of the selected sensors and motor application.

The most widely used conventional analysis is the spectral analysis by means of fast Fourier transform (FFT). The main idea of spectral analysis in fault diagnosis is to either analyze the whole spectrum or study closely at a certain frequency interval of interest and thus extract features from the signal.

One limitation of frequency-domain analysis is its inability to handle non-stationary waveform signals, which are very common when machinery faults occur.

In several PMSM applications, torque and speed are not constant (i.e. aeronautical and traction applications) and usually operate under variable operational conditions.

Generally, frequencies related with fault diagnosis have a mathematical relationship with the fundamental one (commonly referred as orders). The order spectrum represents the amplitude of a signal as a function of the harmonic order instead of the absolute frequency [31]. Order or harmonic tracking (OT) is the process for recovering a particular order waveform in the time domain from a given waveform, which usually contains multiple harmonics and noise [32].

Time-frequency distributions such as wavelet-based analysis [33] or methods based on the Cohen's class [34] among others may also be applied to track harmonic frequencies. However, in order to improve the resolution, some of the methods based on time-frequency transforms require filtering the analyzed signal to remove the fundamental harmonic frequency because its amplitude is often much greater than that of the harmonic of interest. Additionally, most of them calculate the whole or at least a broad band of the spectrum at each time interval prior to obtain a fault indicator index.

In this work, the Vold-Kalman Filtering Order Tracking (VKF-OT) method is introduced to track selected harmonics for fault diagnosis proposes. Its advantage is that VKF-OT only extracts the harmonic frequency of interest (but not the whole spectrum) by applying an adaptive band-pass filter centered on that frequency. When tracking a very small number of harmonics, VKF-OT is a compact solution since it includes the harmonic extraction and tracking steps. Hence, the VKF-OT algorithm allows minimizing the data structure of the problem, and therefore its computational burden.

2.3.3 Fault diagnosis

Machine fault diagnostics is the process in which the information obtained in the detection or signal processing step is analyzed with the aim of determining the type, magnitude and location of the most probable fault [30], and their expected impact.

Conventionally, fault diagnosis is done manually by experts in an off-line analysis with auxiliary graphical tools such as spectrum graph, spectrogram, wavelets spectrogram, etc. Therefore highly qualified and skilled technicians are needed to perform this task.

Automatic fault diagnosis is highly attractive. This can be achieved on-line by means of the classification of signals based on the features extracted from the raw signals and combined with computational technologies. Fig. 2.1 summarizes the fault diagnosis methods [35].

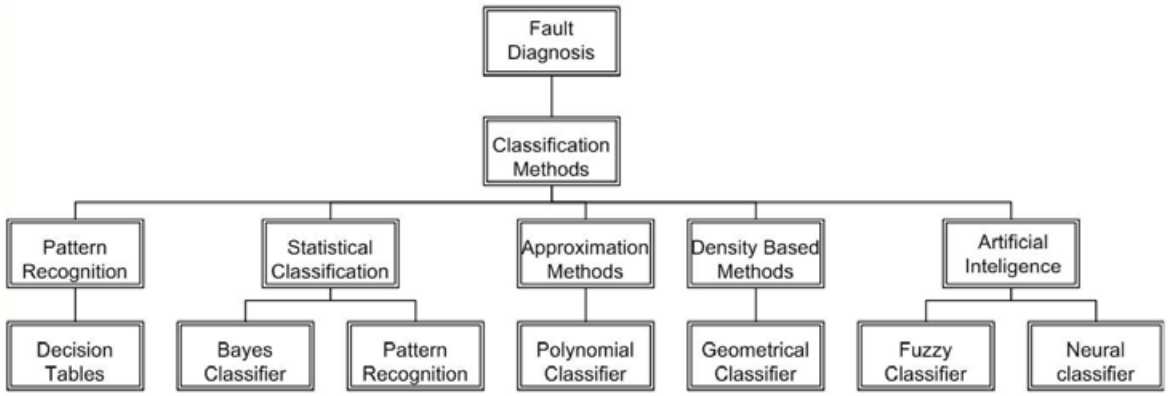

Fig. 2.1. Fault Diagnosis Methods

2.4 PMSM faults

A first step to incorporate PMSMs in a condition monitoring program is the study of their failures modes. Faults in PMSMs are classified into three groups: electrical, magnetic, and mechanical faults as summarized in Fig.2.2 [12].

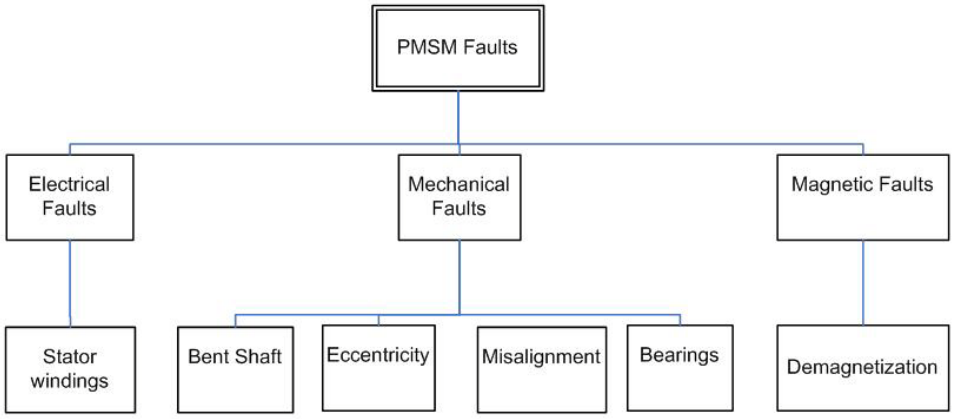

Fig.2.2. Faults classification in PMSMs

Electrical faults involve abnormal connection of the stator windings, stator open-turns and stator short-circuited turns. Inter-turn short-circuits are one of most usual three-phase motors failures types [36] which are related to stator winding insulation degradation. In the case of PMSMs, inter-turn short-circuits may result in stator over currents that create a magnetic flux opposed to the natural flux of the permanent magnets, which in turn may lead to a demagnetization of the rotor magnets [14]. Mechanical faults involve bearing and eccentricity faults. Eccentricity faults consist of static eccentricity, dynamic eccentricity, and mixed eccentricity. They occur due to manufacturing imprecision such as unbalanced mass, shaft bow, and bearing tolerance. Eccentricity may cause magnetic and dynamic problems with

additional vibrations, noise emissions and torque pulsations [12]; magnetic faults consist on partial or total demagnetization of the rotor magnets. This work is focused on the fault detection and diagnosis of electrical and magnetic faults as shown in Fig. 2.3.

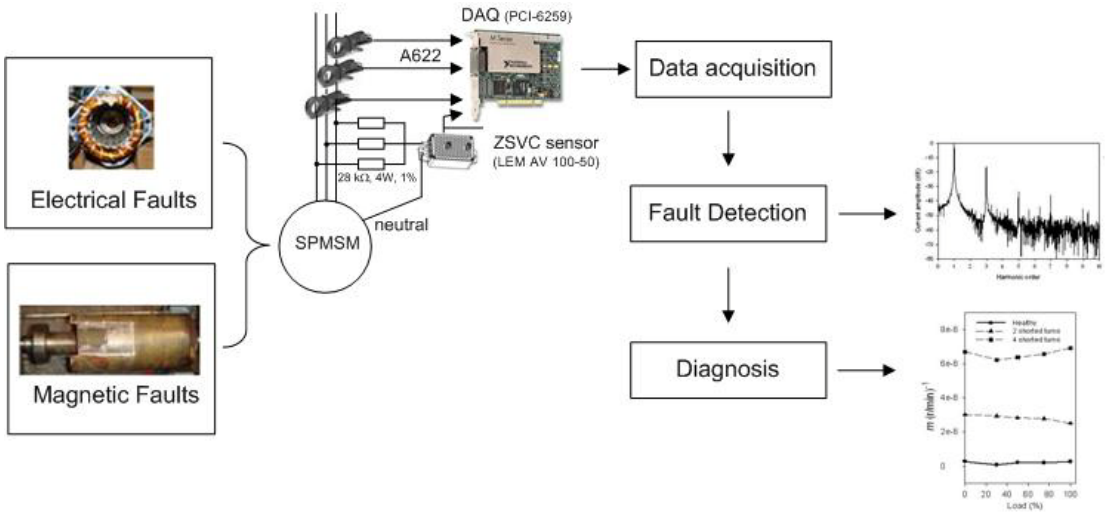

Fig. 2.3. Summary of the scope of this work: detection and diagnosis of magnetic and electrical faults in PMSMs

2.4.1 Rotor magnets demagnetization

Permanent-magnet machines are designed to remain magnetized when operating under normal working conditions. The operating point of the magnet (or its portion) may slip below the knee of demagnetization at extreme temperatures or fault currents (such as short-circuit currents produced by the inverter or stator faults) and under heavy loads.

The demagnetization curve shown in Fig. 2.4 displays the operation point of a PMSM for healthy conditions and with 4 and 8 shorted-turns at 120°C. The operational point is determined by the intersection of the demagnetization curve with a straight line representing the permeability of the external magnetic circuit.

It should be noted that a temperature increment may displace the demagnetization curve towards the right side, thus approaching the demagnetization point *k* to the straight line and increasing the risk of permanent or irreversible demagnetization [37].

If the failure causes the operating point to fall off the lower end of a recoil line, there will be an irreversible flux loss [38].

As a consequence of demagnetization, the distributed magneto motive force (MMF) is not sinusoidal. If demagnetization exists, the frequency components appear[5]:

$$f_{dmg} = f_s \left|1 \pm k / p\right| \quad k = 1, 2, 3...n \tag{2.1}$$

Where f_s is the supply frequency, p is the pole pairs and k is an integer.

A more extended study of demagnetization faults is found in chapter 4.

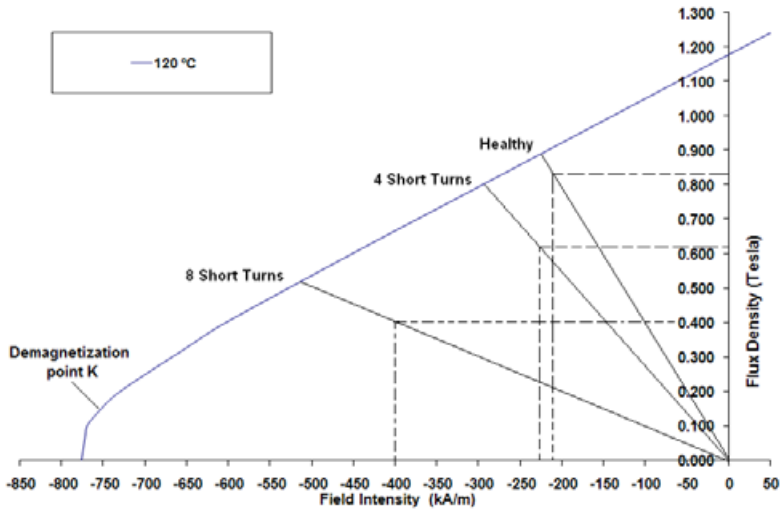

Fig. 2.4. Operation points of permanent magnets for a PMSM

2.4.2 Inter-turn short-circuits

Inter-turn short-circuits are one of most usual failures in PMSM; these kinds of failures are generated by problems in stator winding insulation (modeled as R_f in Fig. 2.5). The no detection of such faults may produce other problems in the machine, i.e. permanent magnets demagnetization [14].

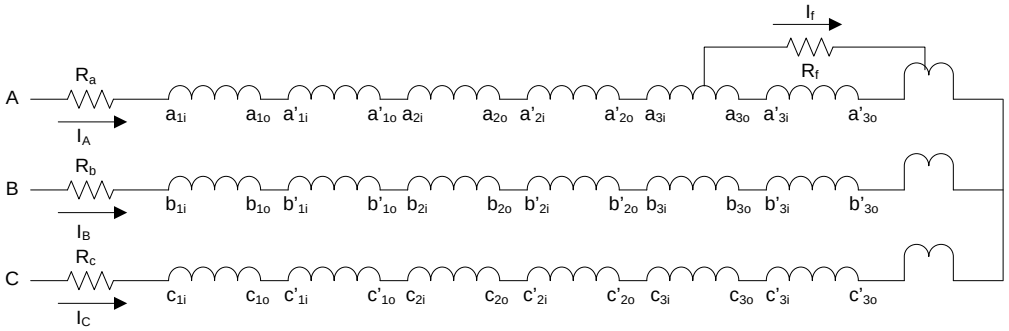

Fig. 2.5. PMSM stator with inter-turns short-circuits

The distribution of the stator MMF in the air gap will be affected by the current i_f that circulates through the short-circuited turns. The fault of the shorted turns in the stator phase winding leads to three main effects on the machine flux. First, the injured phase winding has less effective turns and, therefore,

generates less MMF. Moreover, the shorted turns lead to an increase of the local leakage flux, particularly slot leakage; this changes the local saturation conditions of the teeth. Thus, there is a change in flux density near the short-circuit point. Second, the short-circuited turns will create their own MMF but with a phase that is in opposition to that of the damaged windings. Then, currents induced in the shorted coils oppose the establishment of the main air-gap flux, reducing the corresponding main flux along the winding axis of the shorted coil [39]. Third, the current through the shorted turns increases the heat and can further deteriorate the insulation.

Among the serious consequences of inter-turn short-circuits, the loss of stator symmetry leads to the appearance of third harmonic components in the stator currents, as well as an amplitude change of the integer harmonics. This information may be used for fault diagnosis.

On the other hand, for a wye-connected electrical machine without any asymmetry, the ZSVC of the stator voltages is zero, regardless of the unbalance in the supply voltages. A stator winding turn-fault detection scheme based on monitoring the zero-sequence voltage component has been proposed in [19] for wye-connected electrical machines. The method requires an access to the neutral point of the stator winding.

Inter-turn short-circuit faults are studied in detail in chapter 5.

2.4.3 Eccentricity

Eccentricity faults constitute a considerable portion of the faults related to electric motors. Machine eccentricity is the condition of unequal air gap that exists between the stator and rotor [28]. There are two types of air-gap eccentricity: the static air-gap eccentricity and the dynamic air-gap eccentricity. In the case of the static air-gap eccentricity, the position of the minimal radial air-gap length is fixed in space. Dynamic eccentricity occurs when the center of the rotor is not at the center of the rotation and the position of minimum air-gap rotates with the rotor [40]. In reality, static and dynamic eccentricities tend to coexist. An inherent level of static eccentricity exists in healthy machines.

Fault harmonic frequencies due to dynamic eccentricity can be localized according to the following expression [41]:

$$f_e = f_s\left(1 \pm \frac{2k-1}{p}\right) \tag{2.2}$$

Where f_e are the fault frequencies in the stator currents.

2.4.4 Bearing damage

The majority of the electrical machines use ball or rolling element bearings. Each of these bearings consists of two rings, inner and outer respectively. A set of balls or rolling elements placed in raceways

rotate inside these rings. Even under normal operating conditions with balanced load and good alignment, fatigue failures may take place. Flaking or spilling of bearings might occur when fatigue causes small pieces to break loose from the bearing. Apart from normal internal operating stresses, other causes of bearing damages due to vibration, inherent eccentricity, and bearing currents due to solid state drives appear as well [42].

Sometimes bearing faults might manifest themselves as rotor asymmetry faults [28], which are usually covered under the category of eccentricity-related faults. Otherwise, the ball bearing related defects can be categorized as outer bearing race defects, inner bearing race defects, ball defects, and train defects. All these mechanical defects cause distortions in flux distribution inside the machine, which in turns leads to new current harmonics in the stator currents.

The characteristic fault frequencies are the result of the absolute motion (vibration) of the machine [43]. The stator current is not affected by the absolute motion of the machine, but rather by a relative motion between the stator and rotor (i.e., changes in the air gap). When a bearing fault occurs, the characteristic fault frequencies are essentially modulated by the electrical supply frequency.

The mechanical displacement resulting from a damaged bearing causes the machine air gap to vary in a manner that can be described by a combination of rotating eccentricities moving in both directions. As with the air-gap eccentricity, these variations generate stator currents harmonics at frequencies given by [44].

$$f_{bng} = \left| f_s \pm k f_{i,o} \right| \tag{2.3}$$

$$f_{i,o} = \frac{n_b}{2} f_r \left[1 \pm \frac{bd}{pd} \cos\beta \right] \tag{2.4}$$

Where n_b is the number of bearing balls, $f_{i,o}$ are the characteristic vibration frequencies, f_r is the mechanical rotor speed, bd is the ball diameter, pd is the bearing pitch diameter, and β is the contact angle of the balls on the races.

2.5 Conclusion

The aim of this chapter is to present a brief introduction and description of maintenance and condition monitoring methods in order to contextualize the study of fault diagnosis in PMSMs. As discussed before, the reasons and justification behind the implementation of any of the maintenance techniques presented is a tradeoff between financial and technical aspects. Advantages and disadvantages of machine condition monitoring should be considered in the decision of selecting the best technique for a specified situation. Potential advantages of machine condition monitoring include improved machine availability and reliability, extended operational time, increased efficiency, and improved safety. However, some of the

disadvantages of condition monitoring include increase in equipment costs, operational costs and training costs.

Additionally, in this chapter the fundamentals of faults in PMSMs are described, among them electrical and magnetic faults that are presented in deep in the following chapters

3. HEALTHY SPMSM

It is important the study of the healthy machine state in order to formulate an accurate interpretation of changes in the behavior of a faulty SPMSM. In this chapter the healthy condition of SPMSMs is studied.
The motor can produce constant torque only if the magnetic flux through the stator windings due to the rotor field has a pure sine-wave distribution. Although it is easy to design electrical machines with accurate back-EMF frequency and amplitude, it is more difficult to produce a pure sinusoidal back-EMF waveform without presence of harmonics different from the fundamental [45]. This harmonic content has a negative influence on the torque generated by the machine. Furthermore, the induced back-EMF depends on the stator winding distribution and the air-gap flux, which in turn depends on the permanent magnets geometry and winding configuration. Consequently, manufacturers take corrective actions for minimizing the flux harmonic content.

3.1 Winding distribution

One of the usual measures to ensure a smooth torque consists on an appropriate stator winding distribution because it has a significant influence on the cogging torque [46]. A proper winding distribution leads to a reduction of the MMF harmonics generated by the permanent magnets of the rotor with a small reduction of the fundamental harmonic.
In low power PMSMs the stator winding is typically concentrated, being the number q of stator slots per pole and per phase equal to one. Contrarily, high power machines usually have distributed stator windings, where q is greater than one.
The MMF reduction factor k_M due to the stator and rotor configuration can be expressed as:

$$k_M = k_d k_p k_s \tag{3.1}$$

Where k_d, k_p and k_s are the distribution windings, short pitching and skewed reduction factors respectively.
The MMF reduction factor k_d due to a distributed winding can be expressed as [47]:

$$k_d = \frac{\sin\frac{\upsilon\pi}{2m}}{q\sin\frac{\upsilon\pi}{2mq}} \tag{3.2}$$

Where υ is the harmonic order and m is the number of phases. TABLE 3.1 summarizes the MMF reduction factors for different distributed windings. Note that the higher the term q, the more sinusoidal the MMF of the motor is.

TABLE 3.1.Harmonic Reduction factors for different distributed windings

	Number of slots per pole and per phase *q*				
Harmonic order	**2**	**3**	**4**	**5**	**6**
1	0.966	0.960	0.958	0.957	0.956
3	0.707	0.667	0.653	0.647	0.644
5	0.259	0.218	0.205	0.200	0.197
7	-0.259	-0.177	-0.158	-0.149	-0.145
9	-0.707	-0.333	-0.271	-0.247	-0.236
11	-0.966	-0.177	-0.126	-0.109	-0.102
13	-0.966	0.218	0.126	0.102	0.092
15	-0.707	0.667	0.271	0.200	0.173
17	-0.259	0.960	0.158	0.102	0.084

3.2 Short pitching

In AC windings and important parameter is the pole pitch *y* and can be defined as:

$$y = \frac{Z}{2p} \tag{3.3}$$

Where *Z* is the number of stator slots and *p* the number of poles pairs.

When the distance between two coil sides is equal to a pole pitch, the winding is defined as a full pitched. If coils are slightly less spaced than a pole pitch, the winding is defined as short pitched. Coils are generally shorted by one or two slots. The equation for the reduction MMF factor k_p due to a short-pitched winding can be expressed as follows [47]:

$$k_p = sin\left(\nu \frac{\pi y}{2 y_p}\right) \tag{3.4}$$

Where y_p is the coil pitch.

Like in the case of winding distribution, short pitching reduces and in some cases eliminates high frequency harmonics.

3.3 Skewed magnets

Another measure taken in the industry for minimizing the flux harmonic content is the step skewing of permanent magnets in the rotor, due to ease of manufacturing and cost reduction [48].

The cogging torque is an undesirable phenomenon that results from the interaction between stator winding MMF force and angular variations of rotor magnetic reluctance. It can be greatly reduced by skewing the rotor magnets with an appropriate angle θ_{skew} specific of the rotor configuration [49]:

$$\theta_{skew} = \frac{2\pi}{Z_1 N_{period}} \tag{3.5}$$

Where N_{period} is given by,

$$N_{period} = \frac{2p}{HCF(Z,2p)} \tag{3.6}$$

Being *HCF* the highest common factor.

The net flux per pole Φ_T for a skewed rotor with n_s magnet segments having radial magnetization can be calculated as:

$$\phi_T = \sum_{k=1}^{n} \phi_k = \sum_{k=1}^{n} \frac{B_r r l}{n_s} \left[\tau' - \frac{2\theta_{skew}(k-1)}{n_s - 1} \right] \tag{3.7}$$

Being B_r the remanent flux density, τ' is the magnet arc in radians, r is the radius of the magnet and l is the axial length of the rotor. Since the following identity is true:

$$\sum_{k=1}^{n_s} (k-1) = \frac{n_s(n_s-1)}{2} \tag{3.8}$$

the total flux per pole can be expressed as:

$$\phi_T = B_r l r (\tau' - \theta_{skew}) \tag{3.9}$$

From the above equation it is deduced that the effect of the skew consists on a reduction of the permanent magnets effective width by a factor of $r\theta_{skew}$. The reduction MMF factor k_s due to a skewed rotor is:

$$k_s = \frac{sin(\nu\theta_{skew})}{n sin\left(\frac{\nu\theta_{skew}}{2n_s}\right)} \tag{3.10}$$

3.4 Finite elements model (FEM) of healthy SPMSM

Nowadays, finite elements based methods (FEM) are being commonly applied in the design and analysis of electrical machines. Among the most interesting capacities of FEM packages it must be noted the ability to deal with highly non-linear problems, being the case of rotating electrical machines due to the characteristics of magnetic materials. FEM based analysis is an excellent tool that fits with the strictest

design requirements of electrical industry. High reliability, minimum power losses, maximum power and torque density and low production costs among others, are requirements demanded by rotating electrical machines designers. Therefore, it is crucial to dispose software packages specially conceived for designing and analyzing the rotating electrical machine in detail, from which a near-optimum design may be obtained. It is in this area where FEM packages offer an integrated powerful solution. They are currently being applied instead of the classical analytical and experimental methods, which require expensive and nonflexible prototyping.

As explained in 3.3, when considering the effects of rotor permanent magnets skew, a simplified modeling of the SPMSM by means of a 2D FEM model is not possible since 2D models suppose symmetry of the machine along the shaft axis. However, when dealing with skewed machines, the axial magnetic field distribution varies. Researchers have checked different alternatives for solving this problem. One possibility is performing a full 3D FEM analysis. Although different 3D FEM packages are available, 3D modeling of SPMSMs with skewed rotor is not easy yet due to the complex geometry, demanding computational burden [50] as well as required resources [51]. For these reasons this approach is inappropriate for everyday design, especially for medium and large machines where a large number of nodes are required. Consequently, other alternatives are preferred.

A common used approach is the multi-slice FEM method [52-53]. Under this approach, the base 2D surface mesh –which is perpendicular to the shaft axis- is duplicated *n* times along the shaft axis direction to produce a total of *n* slices. The slices are coupled by means of the electric circuit. The 2D rotor is rotated in each slice according a well-defined skew angle. Each slice is represented by a flat disk having a thickness *1/n*. However, a considerable number of slices may be necessary to properly represent skewed magnets [51]. Additionally, the number of unknowns of the equations system to be solved simultaneously increases with the number of slices. When compared with a 2D FEM analysis, the multi-slice methodology increases simulation time and costs considerably [54-55]. Moreover, not all the available electromagnetic FEM packages allow performing a multi-slice simulation.

There exist also other techniques to deal with skewed machines. For example, in [50] a 2D FEM analysis consisting on separated 2-D models of rotor and stator, which are coupled by floating boundary conditions in dependence with skewing and angular rotor position, is carried out.

Faults disturb the normal operation of SPMSMs and shorten their useful life. Therefore, a simple but accurate analysis of the faulty machines with skewed rotor magnets becomes essential to study such faults [45].

In this work, it is proposed an alternative for analyzing SPMSMs with skewed rotor magnets, which is based on generating an equivalent non-skewed permanent magnet distribution which accounts for the skewed motor [56].

An appealing feature of this method is that it can be easily performed in any 2D electromagnetic FEM package. Attributes of the equivalent geometry include simplicity, high accuracy and low computational

burden and high simulation speed compared to 3D and 2D multi-slice FEM analysis. Moreover, in case of dealing with a faulty motor, in which the symmetry is frequently lost, it is not possible to take advantage of the symmetry of the machine being not feasible to simulate only a fraction of the machine.

The equivalent geometry deals with a *n*-step skewed SPMSM. For better understanding Fig. 3.1 shows a scheme of a four-step skewed rotor.

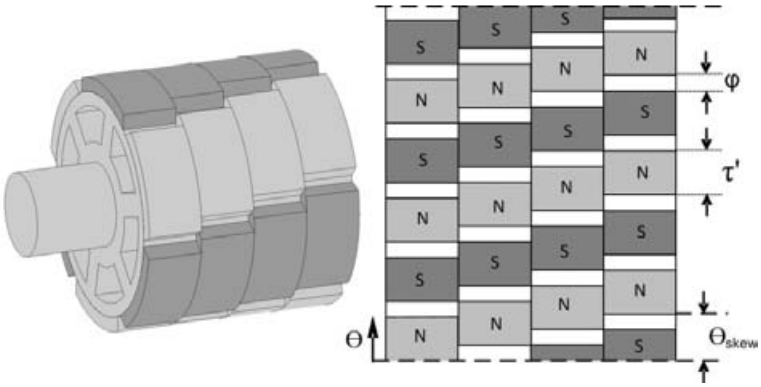

Fig. 3.1. Rotor scheme of a SPMSM with three poles pairs and four-step magnets

The magnetic flux density B_k of each one of the n_s magnet segments of length $1/n_s$ shown in Fig. 3.2 can be expressed as a function of the mechanical angle θ and the angular displacement φ of the magnets as,

$$B_1 = \begin{cases} B_r & 0 \le \theta \le \tau' \\ 0 & \tau' \le \theta \le \tau'+\varphi \\ -B_r & \tau'+\varphi \le \theta \le 2\tau'+\varphi \end{cases} \tag{3.11}$$

$$B_2 = \begin{cases} B_r & +\theta_{skew}/n_s \le \theta \le \tau'+\theta_{skew}/n_s \\ 0 & \tau'+\theta_{skew}/n_s \le \theta \le \tau'+\theta_{skew}/n_s+\varphi \\ -B_r & \tau'+\theta_{skew}/n_s+\varphi \le \theta \le 2\tau'+\theta_{skew}/n_s+\varphi \end{cases} \tag{3.12}$$

$$B_k = \begin{cases} B_r & +(k-1)\theta_{skew}/n_s \le \theta \le \tau'+(k-1)\theta_{skew}/n_s \\ 0 & \tau'+(k-1)\theta_{skew}/n_s \le \theta \le \tau'+(k-1)\theta_{skew}/n_s+\varphi \\ -B_r & \tau'+(k-1)\theta_{skew}/n_s+\varphi \le \theta \le 2\tau'+(k-1)\theta_{skew}/n_s+\varphi \end{cases} \tag{3.13}$$

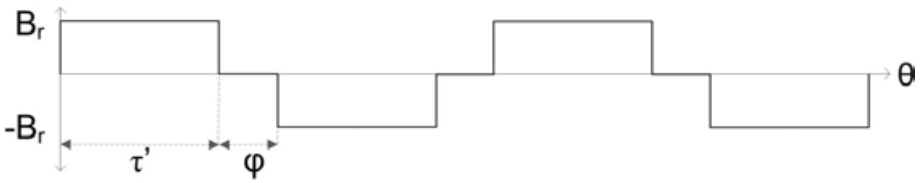

Fig. 3.2. Magnetic flux density for a magnet segment

It is assumed a rotor having n_s magnets. All the magnets are supposed to have length l and remanence B_r/n_s. The magnetic flux density distribution is as shown in Fig. 3.2. The resultant distribution of the magnetic flux density in the air-gap is equivalent to that produced by a set of fictitious equivalent magnets with different remanence values. This new geometry allows dealing with an equivalent 2D axis-symmetric distribution of the rotor magnets as shown in Fig.3.3. Consequently, the new geometry allows the researcher to deal with a simplified 2D FEM model that accounts for the skew of the rotor magnets. This system allows avoiding a full 3D FEM geometry as well as the 2D multi-slice FEM geometry, thus minimizing the computational burden of the problem. In the example illustrated in Fig.3.3 for a four poles rotor with two magnet segments, the equivalent fictitious magnet of each pole is divided into three segments. Each segment has its own magnetic flux density strength.

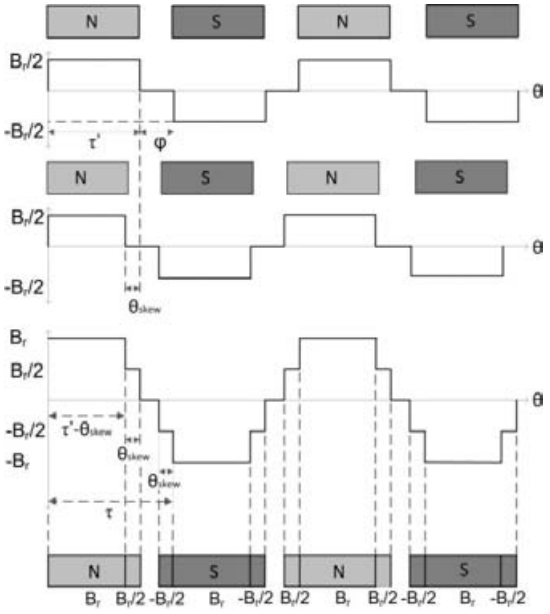

Fig.3.3. Magnetic flux density for a two magnet segments (n = 2) and its equivalent magnet geometry

3.5 The studied SPMSM

Experimental data have been acquired from a 380 Vac SPMSM with 3 poles pairs, 18 slots, rated torque of 2.3 Nm, rated current of 3 A, and rated speed of 6000 r/min manufactured by ABB. The motor was driven by an ABB power converter model DGV 700. The drive control is a vector control, with $i_d = 0$ and a PID speed control loop. The motor is loaded by an additional SPMSM driven by a torque controller. A constant load is imposed during experiments. The geometry of this SPMSM has been used to carry out FEM simulations. A detailed explanation of the experimental test bench is in Appendix A. The SPMSM studied in this work has a skewed rotor with six rows containing four permanent magnets each, this is to say, n = 4 magnets/pole, as shown in Fig. 3.4.

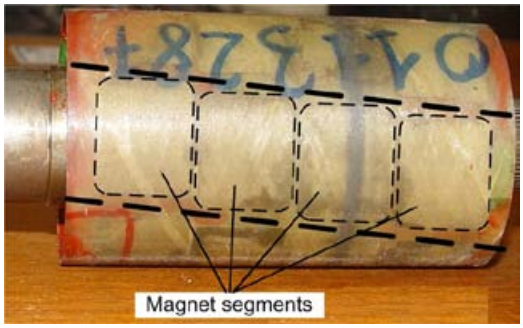

Fig. 3.4.Skewed rotor of the SPMSM used in experiments

The resultant magnetic flux density distribution for the studied rotor and the resultant magnet geometry is shown in Fig.3.5.

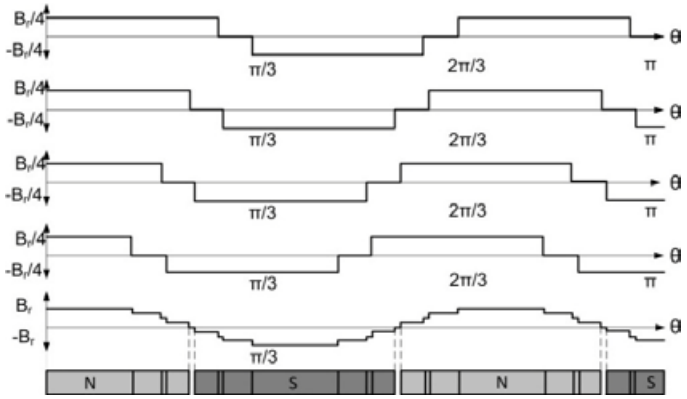

Fig.3.5. Magnetic flux density distribution for the skewed rotor with six poles (*p* = 3) and four magnet segments (*n* = 4) studied in this work.

Fig.3.6 shows the classical magnet geometry and the new geometry proposed in this work in the way they are introduced in the FEM simulation environment. While in the classical geometry each magnetic pole is defined by a whole magnet piece, in the new geometry each magnetic pole is divided into seven segments as detailed in Fig.3.6. According to Fig.3.5, each segment has its own remanence.

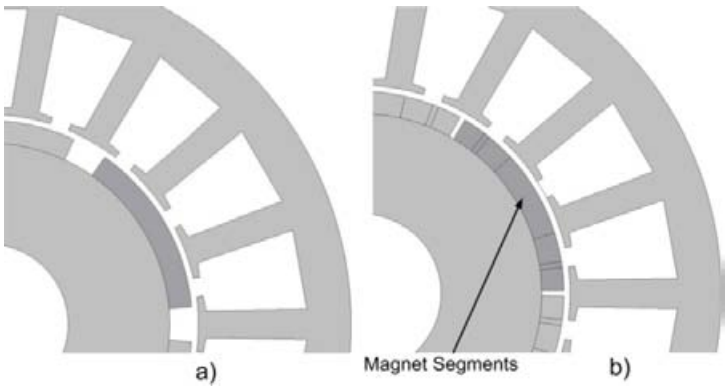

Fig.3.6. a) Classical 2D magnet geometry. b) New equivalent skewed 2D magnet geometry

3.6 Experimental and simulations results

In this section experimental data and FEM simulation results obtained from the classical 2D FEM analysis, the 2D multi-slice FEM analysis and the new proposed 2D FEM analysis are analyzed and compared. Fig.3.7 shows the magnetic flux in each phase winding obtained from FEM simulations by applying the three discussed FEM methods.

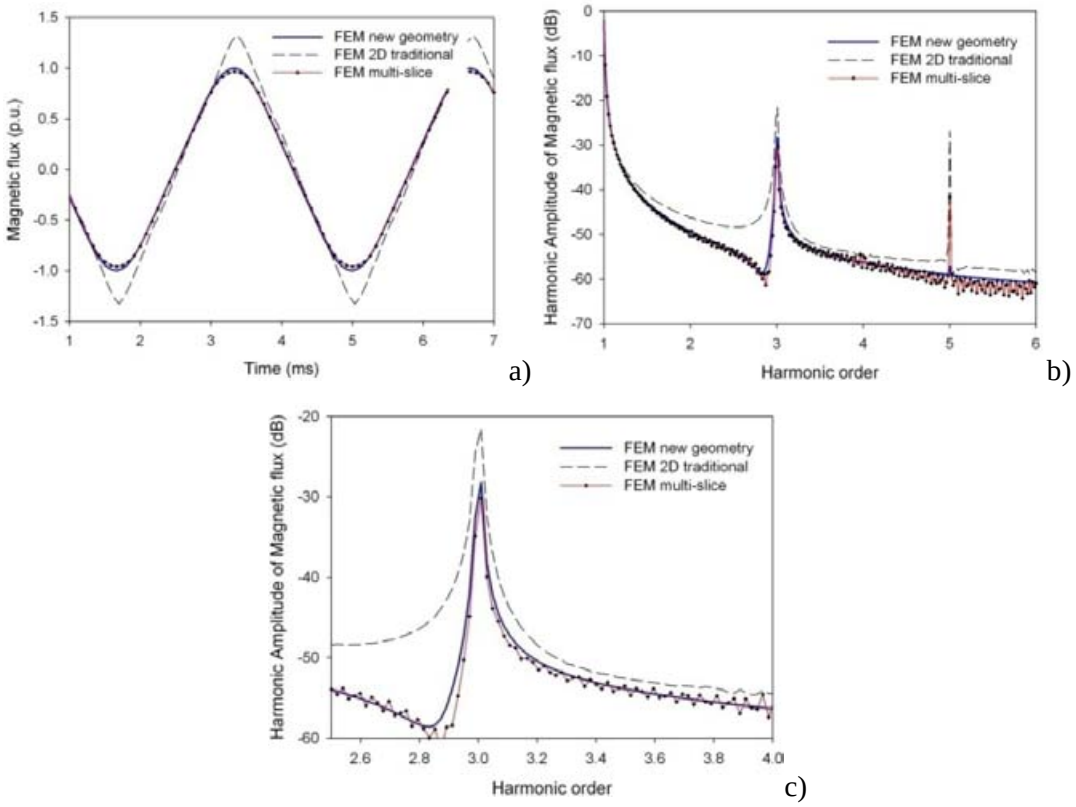

Fig.3.7.Magnetic flux in phase A when operating at 6000 r/min under no-load conditions. a) Magnetic flux in p.u. versus time. b) Magnetic flux amplitude in dB versus frequency. c) Detail of b.

Fig.3.7 clearly indicates that results obtained from the new proposed 2D FEM analysis are very close to those obtained by the multi-slice 2D FEM analysis. Fig.3.8 shows the experimental back-EMF in phase A and the results obtained from FEM simulations by applying the three FEM methods. Note that the experimental back-EMF has been obtained by measuring the voltage induced in the open-circuited stator windings of the studied SPMSM at 6000 r/min.

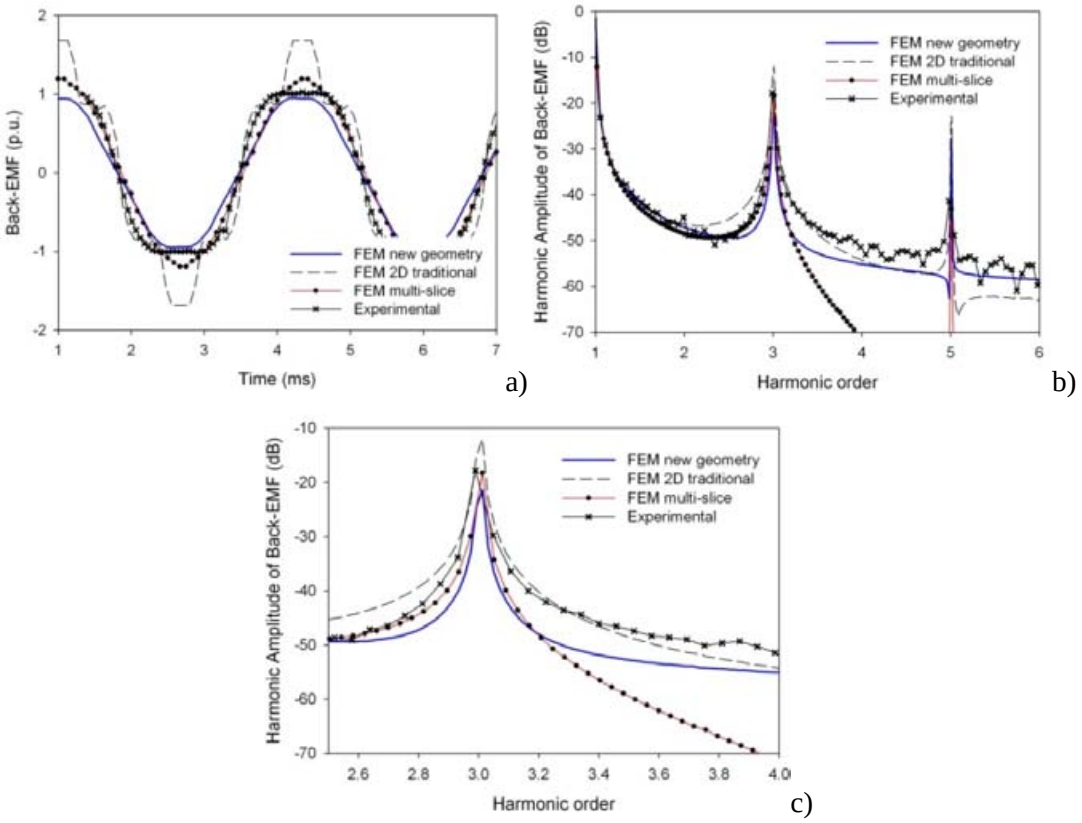

Fig.3.8. Back-EMF when operating at 6000 r/min. a) Back-EMF in p.u. versus time. b) Back-EMF amplitude in dB versus frequency. c) Detail of b.

Once again, Fig.3.8 indicates that results obtained from the new proposed 2D FEM analysis are very close to those obtained by the multi-slice 2D FEM analysis.

Fig. 3.9 shows the experimental current in phase A when the motor operates at 6000 pm under rated current as well as the results obtained from FEM simulations by applying the three analyzed FEM methods.

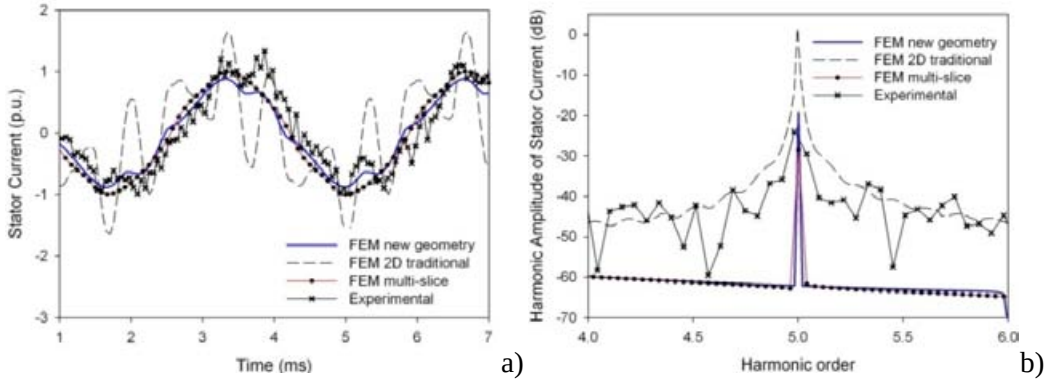

Fig. 3.9. Current when operating at 6000 r/min under rated load. a) Current in p.u. versus time. b) Current amplitude in dB versus frequency.

Once again, results shown in Fig. 3.9 indicate the excellent behavior of the proposed 2D FEM analysis.

TABLE 3.2 compares the calculation times, the number of nodes and the number of elements of the 2D FEM method proposed in this work compared with the 2D multi-slice FEM method and the 3D FEM method. Comparisons have been performed through FEM simulations with similar mesh resolutions for all the analyzed models by modeling one sixth of the full geometry.

TABLE 3.2. Comparison between the applied fem methods

FEM method	Number of nodes	Number of elements*	Relative computational burden
Proposed 2D	873	2203	100%
2D multi-slice	3515	8812	263%
3D	27415	78084	963%

*Includes line, surface and volume elements

Results from TABLE 3.2 clearly indicate that the proposed 2D FEM method allows reducing the computational burden and the resources required when compared with 2D multi-slice and 3D FEM modeling.

3.7 Comparative with different winding configurations

In order to study how different winding types influence the fault diagnosis, four additional machines are investigated by means of FEM simulations, they are $q < 1$, $q > 1$ with fractional winding, $q > 1$ integral and $q > 1$ integral with short-pitching.

TABLE 3.3 summarizes the main parameters of the studied SPMSMs. More details are Appendix B. The SPMSMs models include skewed rotor magnets.

TABLE 3.3. Parameters of SPMSMs with different windings configurations

	Analyzed PMSMs			
	Motor 1	Motor 2	Motor 3	Motor 4
Slots	24	30	36	36
Poles	16	8	4	4
q	1/2	1+1/4	3	3 (Short pitching)
Rated current	20	2,5	7.5	7.5

In this section the results of FEM simulations at rated load which were carried out considering the PMSMs operating under healthy conditions are presented in TABLE 3.3.

In simulations, the electrical frequency was 50 Hz, which is equivalent to 375 r/min in motor 1, 750 r/min in motor 2 and 1500 r/min in motors 3 and 4. Fig.3.10 shows the current spectrum of the studied SPMSMs from simulations results.

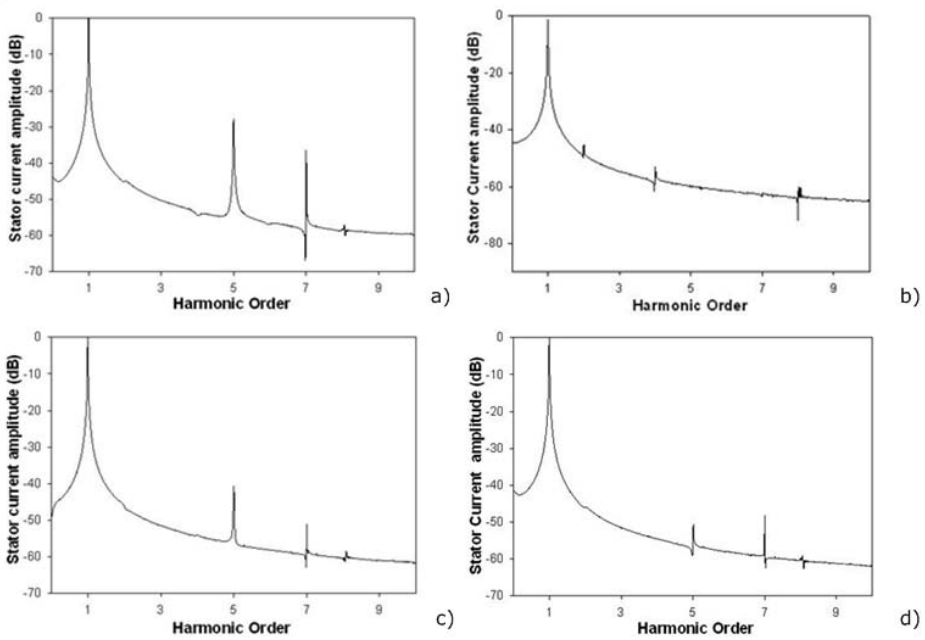

Fig.3.10. Current spectra of SPMSMs with different winding configurations. a) q = 1/2. b) q = 1+1/4. c) q = 3. d) q = 3 with short pitching.

TABLE 3.4 and TABLE 3.5 summarize the amplitude of the back-emf and stator currents harmonics, respectively. Note that the motor with q = 1+1/4 can eliminate the most relevant odd harmonics in the current spectrum.

TABLE 3.4. Back-emf harmonics for different windings configurations

	Back-emf amplitude (dB)					
q	3th	5th	7th	9th	11th	13th
1/2	< Noise	-21.3	-53.97	< Noise	-33.03	-41.77
1+1/4	-23.03	<Noise	-51.21	-56.33	-56.52	-47.92
3	-26.01	-38.75	-46.55	-35.97	-40.38	-40.42
3 (Short pitching)	-31.27	-53.88	-48.04	-35.12	-41.9	-39.39

TABLE 3.5. Stator current harmonics for different windings configurations

	Stator current amplitude (dB)			
q	5th	7th	11th	13th
1/2	-29.28	-36.7	-44.88	-44.57
1+1/4	<Noise	<Noise	<Noise	<Noise
3	-41.35	-51.18	-54.39	-59.32
3 (Short pitching)	-50.59	-48.2	-58.64	-59.61

3.8 Conclusion

In this chapter the back-emf and current spectrum of a healthy machine are analyzed. To acquire Knowledge about the healthy state is an initial point of any faults study in SPMSMs.

In healthy SPMSMs, the most relevant harmonics in the back-emf spectrum and as a consequence, in the stator currents spectrum, are the odd harmonics, which amplitudes are principally influenced by machine constructive aspects such as winding configuration, short-pitching and skewed magnets.

Additionally, in this chapter it is presented a novel 2D FEM-based system for analyzing SPMSMs with skewed rotor magnets. The proposed system requires making a simple change in the geometry of the magnets, thus being very simple its application. One of the main advantages of this method is that both required computer resources and computational burden are almost the same as required by traditional 2D FEM modeling. The proposed methodology is based on generating an equivalent non-skewed permanent magnet distribution which accounts for the skewed distribution of the magnets in a practical rotor.

Both FEM simulations and experimental results show that the proposed FEM system is able to properly predict the features and the behavior of a healthy SPMSM with step-skewed magnets with an accuracy degree equal or superior than the attained with the 2D multi-slice FEM modeling.

4. DEMAGNETIZATION FAULTS IN SPMSMS

In this chapter a theoretical an experimental study of demagnetization faults is presented. The reference motor is analyzed and the results are compared with those obtained by considering different winding configurations. Furthermore, the mechanical effects arising as a consequence of demagnetization faults are studied.

Demagnetization of rotor magnets may reduce significantly the output torque of the SPMSM, thus deteriorating motor characteristics severely [14]. Once the partial demagnetization occurs, a higher than the rated current flows into the stator windings to generate the same output torque. Consequently, demagnetization causes an increase of copper losses, thus increasing the temperature of the SPMSM. This, in turn, causes more demagnetization which again increases the current [15]. Additionally, the electrical current of the stator winding produce an inverse magnetic field that opposes the remanent induction of the permanent magnets [57]. This repeated phenomenon may enhance the demagnetization of permanent magnets [5, 58]. Moreover, inter-turn short-circuits generate over currents, which in turn may lead to a demagnetization of the rotor magnets [14].

In the technical literature [59] it is well documented that partial demagnetization leads to harmonic frequencies in the stator currents according to:

$$f_{dmg} = f_s \left|1 \pm k / p\right| \quad k = 1, 2, 3...n \tag{4.1}$$

Stator currents diagnostic by means of monitoring and analyzing the stator currents harmonic spectrum has been applied to detect this type of faults [6, 60]. However, as stated in [60], depending on the stator windings configuration and the type of demagnetization, in some cases no new harmonic or sub-harmonic frequencies different than those already present in a healthy machine appear due to demagnetization faults. Hence, in these cases, demagnetization faults can only be detected by analyzing other machine variables. Additionally, it is also known that other types of rotor defects such as dynamic eccentricity can be detected by studying the same characteristic fault frequencies in the stator currents [40]. Consequently in some cases the diagnostic method based on analyzing the stator currents spectrum does not allow to distinguish between demagnetization and other types of rotor faults.

In this work a surface mounted permanent magnet synchronous motor (SPMSM) with symmetrical series-connected concentrated stator windings is analyzed (Appendix A). It is shown that when analyzing a single stator slot, partial demagnetization induces harmonic frequencies in the spectrum of the back-emf since the flux linking the stator windings is no longer symmetrical. However, when analyzing the resultant back-emf voltage in all the slots of a phase winding the fault harmonic frequencies are cancelled. It means that in practical machines similar to the one studied where the back-emf is not available it is not feasible to measure the fault harmonics due to demagnetization. For this reason, in this work it is

proposed the diagnostic of incipient rotor demagnetization faults in SPMSMs with concentrated windings by means of an on-line monitoring of ZSVC instead of applying the classical stator currents diagnostic based on analyzing the three-phase stator currents[23]. An accessible neutral point of the stator windings is need to measure the ZSCV, just as required in fault tolerant schemes. They usually add an extra inverter leg which, in fault mode, is connected to the neutral point of the SPMSM, thus replacing the faulty phase [39, 61]. Hence, the drawback that supposes the accessibility of the neutral point may be offset because the system is able to detect incipient demagnetization faults, thus making the whole system more reliable.

4.1 Demagnetization Harmonics induced in the back-emf

In this section the effects of partial demagnetization faults in the back-emf voltage on both a single slot and the resultant effect on all the slots of a phase stator winding (series-connected) is analyzed. Results presented in this section are based on healthy and a partially demagnetized three-phase SPMSM. The faulty SPMSM has two 25% partially demagnetized poles. For the analyzed winding configuration it is equivalent to a 50% partially demagnetized pole. For this purpose some magnets have been removed (see Section 4.4).

4.1.1 Induced back-emf voltage in a single slot

The permanent magnets placed in the rotor induce a back-emf in the stator windings which amplitude increases nearly linearly with the rotor speed. A healthy machine induces a regular and periodic back-emf voltage in each slot of the stator windings. Conversely, when dealing with a partially demagnetized machine, the back-emf induced in a single slot is not regular, as shown below. It is so because the damaged or removed magnets have a reduced contribution in the back-emf, thus producing a gap or asymmetry in its waveform whenever a removed magnet passes in front of the analyzed slot. Thus, such a behavior is not difficult to model.

Neglecting the effects of the geometric disposition of the rotor magnets, the back-emf voltage in a single slot e_{slot} of a healthy machine has a sinusoidal shape as shown in Fig.4.1. However, supposing a faulty machine with a 50% demagnetized pole, whenever this pole passes in front of the analyzed slot, the back-emf induced in this slot is halved. This effect can be modeled by subtracting the waveform $y(t)$ from the sinusoidal waveform $e_{slot}(t)$ shown in Fig.4.1.

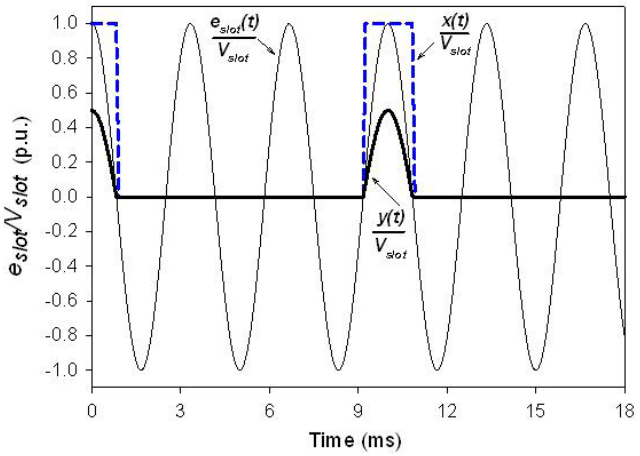

Fig.4.1. Waveforms used to develop the proposed model

Mathematically, the wave *y(t)* can be obtained by multiplying a fundamental sinusoidal wave by the square wave *x(t)* in Fig.4.1, which has a frequency f_s/p and a duty cycle $d = 1/2p$. This square wave can be expressed by means of the Fourier series:

$$x(t) = \frac{1}{2p} + \sum_{k=1}^{\infty} \frac{2}{k\pi} sin(\pi k d) cos\left(\frac{2k\pi f_s t}{p}\right) \tag{4.2}$$

The wave *y(t)* shown in Fig.4.1 is obtained by performing the product between the square wave and the sinusoidal one, resulting in:

$$y(t) = cos(2\pi f_e t)\left[\frac{1}{2p} + \sum_{k=1}^{\infty} \frac{2}{k\pi} sin(\pi k d) cos\left(\frac{2k\pi f_s t}{p}\right)\right] \tag{4.3}$$

After some algebraic operations it leads to:

$$y(t) = \frac{1}{2p} cos(2\pi f_s t) + \sum_{k=1}^{\infty} \frac{1}{k\pi} sin\left(\frac{k\pi}{2p}\right) cos\left[2\pi f_s t\left(1 \pm \frac{k}{p}\right)\right] \tag{4.4}$$

The equation of the induced voltage in the first slot of phase “a” of the analyzed faulty SPMSM can be expressed as:

$$\frac{d\lambda_{slot}(t)}{dt} = V_{slot}\, cos(2\pi f_e t) - V_{slot} K_{dem} y(t) \tag{4.5}$$

Being V_{slot} the amplitude of the back-emf induced in a single slot and K_{dem} the ratio between the remanent flux density of a demagnetized pole and a healthy one.

By substituting equation (4.4) in (4.5), the induced back-emf voltage in the first slot of phase “a” results in:

$$e_{slot,1}(t)=\frac{d\lambda_{slot}(t)}{dt}=V_{slot}\left(1-\frac{K_{dem}}{2p}\right)cos(2\pi f_s t)-V_{slot}K_{dem}\sum_{k=1}^{\infty}\frac{1}{k\pi}sin\left(\frac{k\pi}{2p}\right)cos\left[2\pi f_s t\left(1\pm\frac{k}{p}\right)\right] \quad (4.6)$$

The factor $1-K_{dem}/2p$ in the first part of above equation is the reduction of the fundamental harmonic amplitude of the back-emf voltage due to the fault. It is worth noticing that in the second part of this equation, the harmonic frequencies owing to the demagnetization fault are the same than in equation (4.1) which agrees with the technical literature [59-60]. This is a validation of the usefulness of this simple model.

Additionally, the predicted amplitudes of these fault harmonics are as follows:

$$A_{dem}=\frac{V_{slot}K_{dem}}{k\pi}sin\left(\frac{k\pi}{2p}\right) \quad (4.7)$$

Fig.4.2 shows comparative results of the back-emf induced in a single slot obtained by means of FEM simulations and from the model proposed in equation (4.6). It is supposed a faulty SPMSM operating at 6000 r/min with a 50% demagnetized pole.

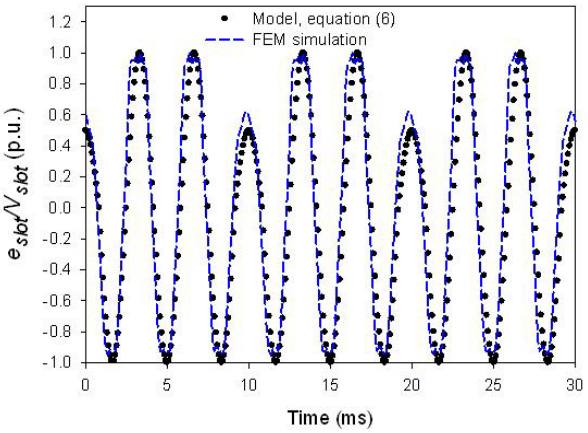

Fig.4.2. Normalized back-emf voltage (e_{slot}/V_{slot}) induced in a single slot of a faulty SPMSM with a 50% demagnetized pole when running at 6000 r/min.

Simulation results shown in Fig.4.2 clearly indicate that the effect of 50% demagnetization in a pole is a 50% decrease in the back-emf amplitude whenever the demagnetized pole passes in front of the analyzed stator slot. Thus, these results evidence the significant effect of this fault on the back-emf voltage in a single slot. Additionally Fig.4.2 illustrates that results obtained from the simple model explained here are in close agreement with FEM simulation results.

In a concentrated winding (q=1), the electric angle between two adjacent slots of the same phase is π rad. Therefore, the back-emf voltage induced in any slot of phase "a" can be computed by extending equation (4.6) as:

$$e_{slot}(t)=\frac{d\lambda_{slot}(t)}{dt}=(-1)^{m-1}V_{slot}\left(1-\frac{K_{dem}}{2p}\right)cos[2\pi f_s t-\pi(m-1)]- \\ (-1)^{m-1}V_{slot}K_{dem}\sum_{k=1}^{\infty}\frac{1}{k\pi}sin\left(\frac{k\pi}{2p}\right)cos\left[2\pi f_s t\left(1\pm\frac{k}{p}\right)-\pi(m-1)\left(1\pm\frac{k}{p}\right)\right] \quad (4.8)$$

Where $m = 1,2,\ldots 2p$ is the pole number of the slot where the back-emf is calculated.

The factor $(-1)^{m-1}$ is positive in slots where the conductors are entering and negative in slots where conductors are leaving. Note that the equation above may be extended to all winding configurations, e.g. changing the angle between two adjacent slots in the same phase in a short pitched coil (which is different from π rad).

The magnetic flux in any slot of phase "a" is obtained by integrating the back-emf voltage induced in it.

$$\lambda_{slot}(t)=\int e_{slot}(t)dt \quad (4.9)$$

By substituting equation (4.8) into (4.9) it results,

$$\lambda_{slot}(t)=(-1)^{m-1}N\lambda_1\left(1-\frac{K_{dem}}{2p}\right)sin[2\pi f_s t-\pi(m-1)]- \\ (-1)^{m-1}N\lambda_1 K_{dem}\sum_{k=1,k\neq p}^{\infty}\frac{p}{k\pi(p\pm k)}sin\left(\frac{k\pi}{2p}\right)sin\left[2\pi f_s t\left(1\pm\frac{k}{p}\right)-\pi(m-1)\left(1\pm\frac{k}{p}\right)\right] \quad (4.10)$$

Being $N\lambda_1 = V_{slot}/(2\pi fe)$.

Fig.4.3 shows the magnetic flux induced in a single slot of phase a when dealing with a faulty SPMSM running at 6000 r/min having a 50% demagnetized pole. Note that the harmonic order is an integer or a fractional multiple number of the fundamental supply frequency.

Results from Fig.4.3 clearly show the close similitude between the magnetic flux obtained from FEM simulations and from equation (4.10). Additionally, the harmonic content obtained from FEM simulations and detailed in part b is in close agreement with equation (4.10), since the fractional harmonics appear in both cases, being their amplitudes very similar. Note that equation (4.10) has been deduced by only taking into account the effects of the fundamental harmonic, thus ignoring the effects of constructive harmonics really present in the back-emf due to the own geometry of the machine.

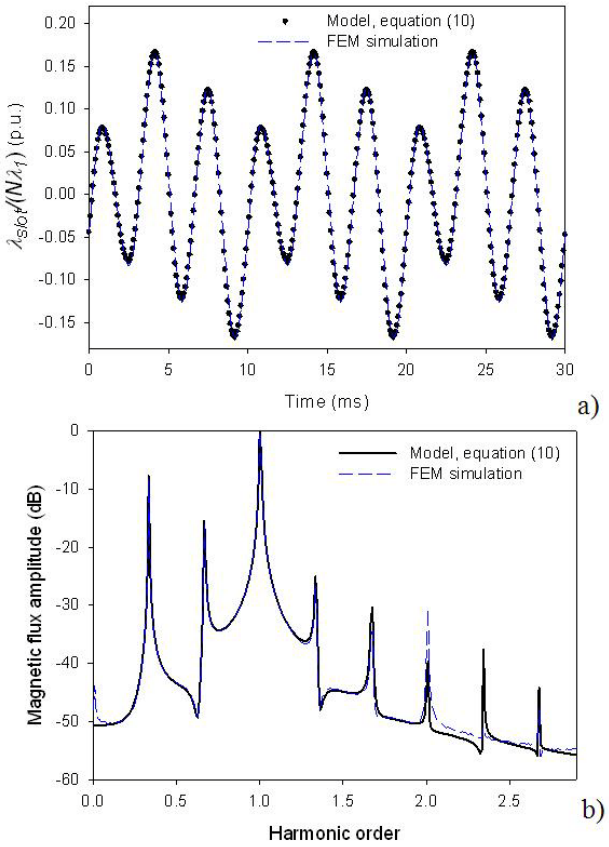

Fig.4.3. a) Normalized magnetic flux in a single slot ($\lambda_{slot}/N\lambda_1$) of a faulty SPMSM obtained by means of FEM simulations and from equation (4.10). b) Magnetic flux spectrum.

4.1.2 Back-emf induced in all slots of a phase series-connected winding

In a serial concentrated winding with q = 1, the back-emf voltage in phase A can be calculated as:

$$e_{phase}(t)=\sum_{m=1}^{2p} e_{slot,m}(t)=\frac{d\lambda_{phase}(t)}{dt} \tag{4.11}$$

By substituting equation (4.8) into (4.11) it results:

$$\begin{aligned} e_{phase}(t)=&\,2\pi f N\lambda_1\left(1-\frac{K_{dem}}{2p}\right)\sum_{m=1}^{2p}(-1)^{m-1}\cos\left[2\pi f_s t-\pi(m-1)\right]- \\ &2\pi f N\lambda_1 K_{dem}\sum_{m=1}^{2p}(-1)^{m-1}\sum_{k=1}^{\infty}\frac{1}{k\pi}\sin\left(\frac{k\pi}{2p}\right)\cos\left[2\pi f_s t\left(1\pm\frac{k}{p}\right)-\pi(m-1)\left(1\pm\frac{k}{p}\right)\right] \end{aligned} \tag{4.12}$$

Changing the sum order in the second part of (4.12) it results:

$$e_{phase}(t) = 2\pi f N\lambda_1\left(1-\frac{K_{dem}}{2p}\right)\sum_{m=1}^{2p}(-1)^{m-1}\cos\left[2\pi f_s t-\pi(m-1)\right]- \\ 2\pi f N\lambda_1 K_{dem}\sum_{k=1}^{\infty}\frac{1}{k\pi}\sin\left(\frac{k\pi}{2p}\right)\sum_{m=1}^{2p}(-1)^{m-1}\cos\left[2\pi f_s t\left(1\pm\frac{k}{p}\right)-\pi(m-1)\left(1\pm\frac{k}{p}\right)\right] \quad (4.13)$$

It can be demonstrated that the first term in the above equation results in:

$$\sum_{m=1}^{2p}(-1)^{m-1}\cos\left[2\pi f_s t-\pi(m-1)\right]=2p\cos(2\pi f_s t) \quad (4.14)$$

Additionally, it can also be verified that the second term is null:

$$\sum_{m=1}^{2p}(-1)^{m-1}\cos\left[2\pi f_s t\left(1\pm\frac{k}{p}\right)-\pi(m-1)\left(1\pm\frac{k}{p}\right)\right]=0 \quad (4.15)$$

Hence, from equations (4.13), (4.14) and (4.15) the back-emf induced phase a can be rewritten as:

$$e_{phase}(t)=\frac{d\lambda_{phase}(t)}{dt}=4p\pi f_s N\lambda_1\left(1-\frac{K_{dem}}{2p}\right)\cos(2\pi f_s t) \quad (4.16)$$

The above equation shows that the effect of the partial demagnetization of one pole of the machine is a reduction in the back-emf voltage in a factor $1 - K_{dem}/2p$. However, unlike the back-emf induced in a single slot, in the resultant back-emf induced in a phase there is no trace of harmonics different from the fundamental one. Thus, the effects due to demagnetization faults cannot be measured through the back-emf harmonics induced in a phase of the stator winding. Similar results are obtained when dealing with other types of symmetric windings [60].

By integrating equation (4.16) it results the following expression for the magnetic flux of phase "a":

$$\lambda_{phase}(t)=2pN\lambda_1\left(1-\frac{K_{dem}}{2p}\right)\sin(2\pi f_s t) \quad (4.17)$$

The back-emf induced in each of the phases of a healthy SPMSM –including the effects of the constructive harmonics– may be calculated as follows:

$$e_a(t)=\frac{d\lambda_a(t)}{dt}=4\pi f_s Np\left[\lambda_1\cos(2\pi f_s t)+\sum_{\nu=2k+1}\lambda_\nu\cos(2\pi f_s t\nu-\phi_\nu)\right] \\ e_b(t)=\frac{d\lambda b_B(t)}{dt}=4\pi f_s Np\left[\lambda_1\cos\left(2\pi f_s t-\frac{2\pi}{3}\right)+\sum_{\nu=2k+1}\lambda_\nu\cos\left(2\pi f_s t\nu-\phi_\nu-2\nu\frac{\pi}{3}\right)\right] \quad (4.18) \\ e_c(t)=\frac{d\lambda_c(t)}{dt}=4\pi f_s Np\left[\lambda_1\cos\left(2\pi f_s t+\frac{2\pi}{3}\right)+\sum_{\nu=2k+1}\lambda_\nu\cos\left(2\pi f_s t\nu-\phi_\nu+2\nu\frac{\pi}{3}\right)\right]$$

In case of a partially demagnetized SPMSM, the back-emf induced in each of the three phases is:

$$e_a(t)=\frac{d\lambda_{a,f}(t)}{dt}=\left(1-\frac{K_{dem}}{2p}\right)\frac{d\lambda_a(t)}{dt}$$
$$e_b(t)=\frac{d\lambda_{b,f}(t)}{dt}=\left(1-\frac{K_{dem}}{2p}\right)\frac{d\lambda_b(t)}{dt} \quad (4.19)$$
$$e_c(t)=\frac{d\lambda_{c,f}(t)}{dt}=\left(1-\frac{K_{dem}}{2p}\right)\frac{d\lambda_c(t)}{dt}$$

Fig.4.4 shows the back-emf induced in phase "a" obtained by means of FEM simulations when dealing with healthy and a faulty SPMSM –having a 50% demagnetized pole– running at 6000 r/min.

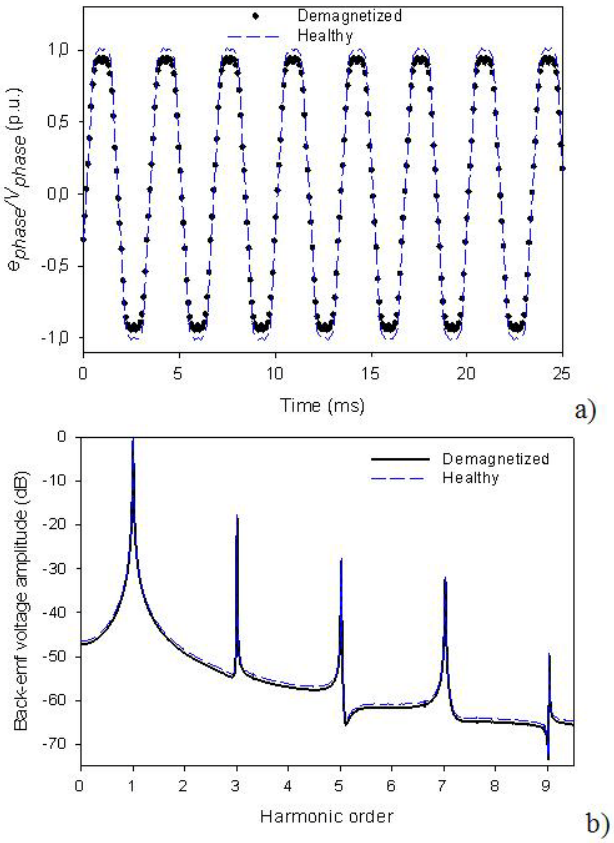

Fig.4.4. a) FEM simulations of the normalized back-emf voltage (e_{phase}/V_{phase}) induced in phase "*a*". b) Back-emf spectrum.

Fig.4.4 corroborates that when analyzing the back-emf induced in a phase of the SPMSM –supposing symmetrical concentrated stator windings connected in series– it is not possible to measure harmonic frequencies due to demagnetization faults.

Fig.4.5 shows the current spectrum of phase "a" of healthy and partially demagnetized SPMSM.

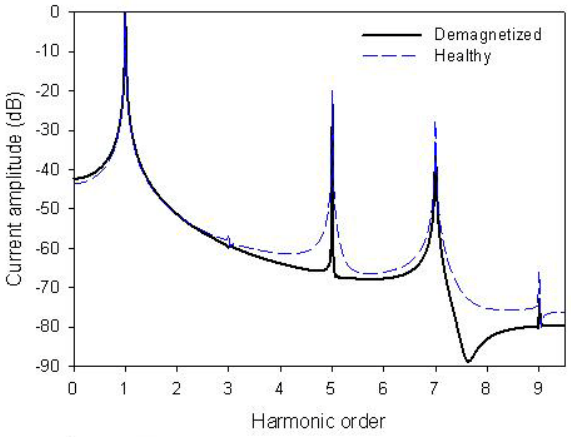

Fig.4.5. FEM simulated current spectrum of phase "*a*" –faulty and healthy machine- when the SPMSM operates at 6000 r/min.

Results from Fig.4.5 show no presence of fractional harmonics in the stator current spectrum, corroborating the results of equation (4.16). Thus, in the analyzed motor type, it is difficult to diagnose demagnetization faults from the stator current spectrum data.

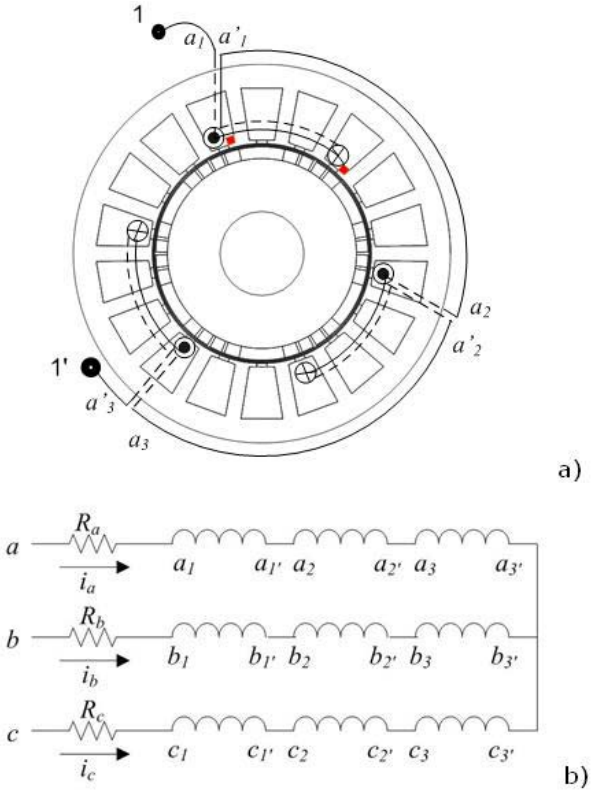

Fig.4.6. a) SPMSM geometry. b) Stator windings connection diagram.

The elimination of the fractional harmonics through the entire coil can be explained in a quantitative manner as follows. As the demagnetized pole is passing in front of the first coil of phase "a" (coil a1-a1' in Fig.4.6), the induced back-emf is quite similar to the other coils back-emf, but with a lower amplitude.

While the demagnetized pole faces the second coil (coil a2-a2') its induced back-emf is once more lowered. As a result, the back-emf induced in each coil is lowered. On the other hand, as the phase back-emf voltage is the sum of the all coils voltages (serial connected winding), the entire back-emf induced in phase "a" has reduced amplitude but it does not contain fractional harmonics. In order to illustrate this phenomenon, a FEM simulation using the reference motor was carried out with a full pole removed [62]. These results are shown in Fig.4.8, which proves that the entire back-emf induced in phase "a" has lower amplitude (compared with a healthy machine) but it does not contain fractional harmonics.

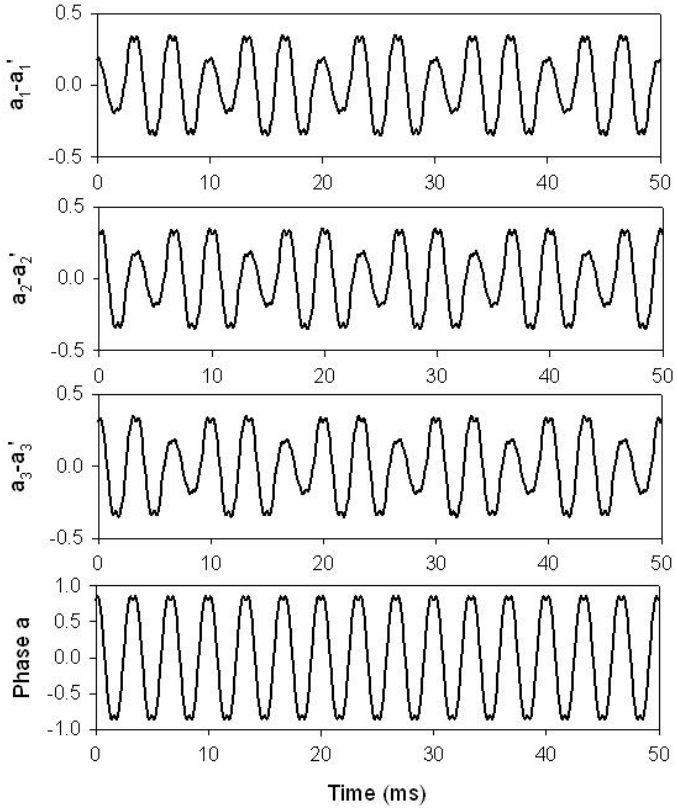

Fig.4.7. Back-emf voltage –normalized with respect to phase voltage–induced in a series-connected winding obtained by means of FEM simulations supposing a full pole removed.

4.2 Expression of the ZSVC for healthy and partially demagnetized SPMSMS

In this section the equation of the V0 ZSVC is derived for both healthy and partially demagnetized machines.

4.2.1 Healthy SPMSM

As stated in [39], when dealing with a healthy symmetrical SPMSM, the stator equations in abc reference frame can be expressed as follows:

$$[V_{s,abc}] = [R_{sh}]\cdot[i_{s,abc}] + [L_{sh}]\cdot\frac{d}{dt}[i_{s,abc}] + \frac{d}{dt}[\lambda_{PM,abc}] + [V_0] \tag{4.20}$$

Where the $[V_0] = V_0[1\ 1\ 1]^t$ term is due to the voltage difference between the center point of the stator windings and the neutral point of the three-phase voltage-source. This term is zero when neglecting the effects of constructive harmonics.

The induced back-emf voltage matrix due to the permanent magnets can be written as:

$$\frac{d}{dt}[\lambda_{PM,abc}] = \left[\frac{d\lambda_a}{dt}\ \frac{d\lambda_b}{dt}\ \frac{d\lambda_c}{dt}\right] \tag{4.21}$$

With wye-connected windings it results:

$$i_a + i_b + i_c = 0 \tag{4.22}$$

By adding the rows in (4.20) and having into account the above equation, the expression of the ZSVC V_0 is obtained as follows:

$$V_0 = \frac{1}{3}(V_a + V_b + V_c) - \frac{d\lambda_{PM,0}}{dt} \tag{4.23}$$

Where $\frac{d\lambda_{PM,0}}{dt} = \frac{1}{3}\left(\frac{d\lambda_a}{dt} + \frac{d\lambda_b}{dt} + \frac{d\lambda_c}{dt}\right)$

4.2.2 Partially demagnetized SPMSM

Including equation (4.19) in (4.20) it results:

$$[V_{s,abc}] = [R_{sh}]\cdot[i_{s,abc}] + [L_{sh}]\cdot\frac{d}{dt}[i_{s,abc}] + \left(1 - \frac{K_{dem}}{2p}\right)\frac{d}{dt}[\lambda_{PM,abc}] + [V_0] \tag{4.24}$$

By adding the rows of the above equation and having into account (4.22) it results the expression of the ZSVC V_0:

$$V_0 = \frac{1}{3}(V_a + V_b + V_c) - \left(1 - \frac{K_{dem}}{2p}\right)\frac{d\lambda_{PM,0}}{dt} \tag{4.25}$$

In order to validate the accuracy of the above equation, two type of demagnetization faults are analyzed by means of FEM simulations. Demagnetization type I assumes a SPMSM with a 50% partially demagnetized pole. To obtain this demagnetization some magnets have been removed as detailed in Section 4.4. Contrarily, demagnetization type II supposes a lateral demagnetization in which each one of the 6 rotor poles (each pole has 4 magnets) have a 33.33% demagnetized magnet. Both conditions are equivalent to a pair of poles 25% demagnetized, or a 50% demagnetized pole, respectively. Possibly, a real demagnetization is more likely to happen in the same region of all the magnet poles because a large and localized short circuit stator current may demagnetize all these magnets each time they pass near this region.

Fig.4.8 shows the simulated ZSVC V_0 spectra for both healthy and demagnetized SPMSMs (demagnetization types I and II).

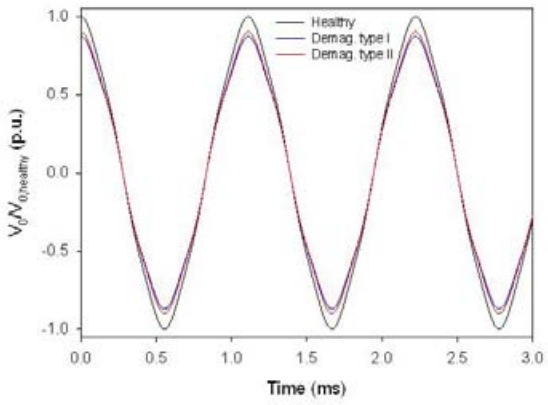

Fig.4.8. FEM simulations of ZSVC V_0 voltage for healthy and two types of partially demagnetized machines.

Results from Fig.4.8 prove that both type of demagnetization faults lead to similar results. From these results the obtained values of the factor $1 - K_{dem}/2p$ in equation (4.25) are 0.877 for demagnetization type I and 0.901 for demagnetization type II, whereas its theoretical value is 0.917.

4.3 Detection of demagnetization faults in inverter-fed SPMSMs

This section sets the bases of ZSVC method proposed in this work to detect demagnetization faults when dealing with inverter-fed SPMSMs. Due to geometric effects, the magnetic flux spectrum in a real SPMSM has a third harmonic component and their multiples [63]. Consequently, the air-gap flux has an important third harmonic component [64]. This in turn induces a third harmonic voltage in the stator windings. However, if the SPMSM is wye-connected, no zero sequence components will exist in the stator currents.

Commercial SPMSMs are usually fed by electronic inverters; hence the line-to-neutral voltages are not available. Additionally, the inverter injects ZSVC in the SPMSM. Similarly as in [65], Fig.4.9 shows an inverter-fed SPMSM and a three-phase balanced resistor network used to measure the ZSVC.

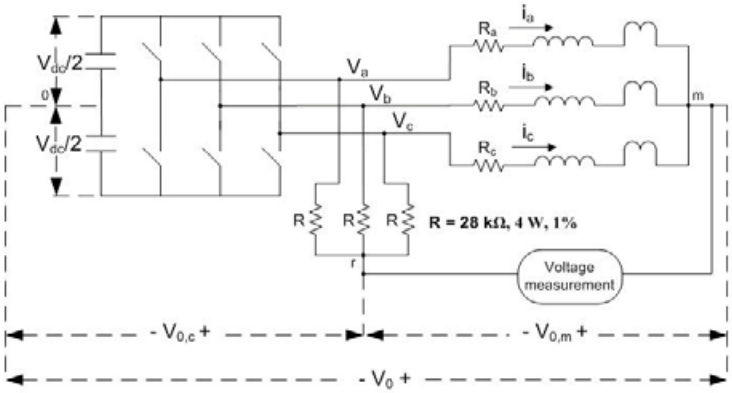

Fig.4.9.Scheme diagram of SPMSM connection with the inverter, the stator windings and the resistor network used to generate an artificial neutral point.

PWM inverters usually inject zero-sequence voltages in the machine, which influence V_0. According to [65] the zero-sequence voltage injected by the inverter can be divided into components that are intrinsic to PWM –independent of the modulation method–, components that depend on the modulation method and components caused by switching transients. ZSVC intrinsic to PWM have a frequency content greater than or equal to the inverter switching frequency, and therefore far from the fault-related frequencies of interest [66]. ZSVC generated by the inverter modulation method are almost totally removed by using a three-phase balanced resistor network. Additionally, components produced by switching transients have typically frequencies above 100 kHz. Due to this spectral separation, these components do not cause interference in the diagnostics of the machine.

According to Fig.4.9, the sum of currents through the three branches of the balanced resistor network is zero, resulting in:

$$\frac{V_a - V_{0,c}}{R} + \frac{V_b - V_{0,c}}{R} + \frac{V_c - V_{0,c}}{R} = 0 \tag{4.26}$$

From (4.26) it results:

$$V_{0,c} = \frac{1}{3}(V_a + V_b + V_c) \tag{4.27}$$

$$V_0 = V_{0,c} + V_{0,m} \tag{4.28}$$

In case of phase-to-neutral voltages containing ZSVC –it is the case of inverter-fed machines– the balanced three-phase resistor network allows removing them from the neutral voltage of the machine. Thus the voltage $V_{0,m}$ is only influenced by the own harmonics of the machine [65]. Also when the SPMSM operates under fault condition, the study of $V_{0,m}$ instead of V_0 has the benefit that the acquisition

system can be scaled according to the zero-sequence voltage magnitude which is usually much lower than the phase-to-neutral voltages $V_{a,m}$, $V_{b,m}$ and $V_{c,m}$ [65].

When including the three-phase balanced resistor network equations (4.23) and (4.25) can be expressed as:

$$V_{0,m} = -\frac{d\lambda_{PM,0}}{dt} \tag{4.29}$$

$$V_{0,m} = -\left(1 - \frac{K_{dem}}{2p}\right)\frac{d\lambda_{PM,0}}{dt} \tag{4.30}$$

The value of $1 - K_{dem}/2p$ depends on the analyzed type of demagnetization. However it is worth noting that all the demagnetization types reduce the $V_{0,m}$ ZSVC value. Therefore this reduction may be used as a fault severity index which informs about the equivalent demagnetization degree.

4.4 Experimental results

Experiments were carried out by means of healthy and faulty machines (reference SPMSMs, Appendix A). A SPMSM was modified to carry out the experimental part which neutral point of the stator winding was made accessible as well as the two terminals of a pair of poles of phase A. Additionally, two rotor magnets were removed to obtain a faulty SPMSM with a 50% partially demagnetized pole (demagnetization type I), as illustrated in Fig.4.10.

Fig.4.10. Rotor of the analyzed partially demagnetized SPMSM. It has 6 rows with 4 magnets/row

The two removed magnets are in opposite poles in order to balance the magnetic forces on the rotor, thus avoiding mechanical effects, which are studied in section 4.6. Afterwards the rotor mass was balanced.

Fig.4.11.a shows the acquired back-emf induced in one out of the three pair of slots of phase A. Note that it had been normalized with respect to phase-to-neutral back-emf. Back-emf voltage was obtained experimentally with the machine operating as a generator. It can be clearly appreciated that whenever the removed magnets pass in front of analyzed slots, they produce a gap in its waveform.

Fig.4.11.b shows the spectrum corresponding to Fig.4.11.a, which confirms the presence of fractional harmonics.

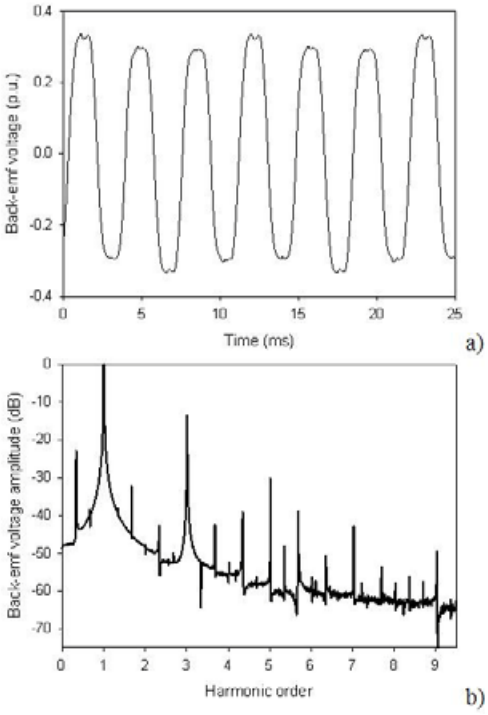

Fig.4.11.a) Experimental back-emf induced in a pair of poles of the stator winding of a partially demagnetized SPMSM when operating at 6000 r/min. b) Spectrum of part a.

Fig.4.12 shows the experimental back-emf induced in phase A (normalized with respect to phase-neutral voltage) for both healthy and partially demagnetized SPMSMs. The amplitude reduction in case of faulty SPMSM, agrees with equation (4.16). While the theoretical value of the reduction in the back-emf is given by $1 - K_{dem}/2p = 1 - 0.5/6 = 0.917$, the experimental values are 0.940 and 0.926 for the amplitudes of the first and third harmonics, respectively. It is important to highlight that there are not additional harmonics in the back-emf voltage of a partially demagnetized SPMSM different than those of a healthy machine.

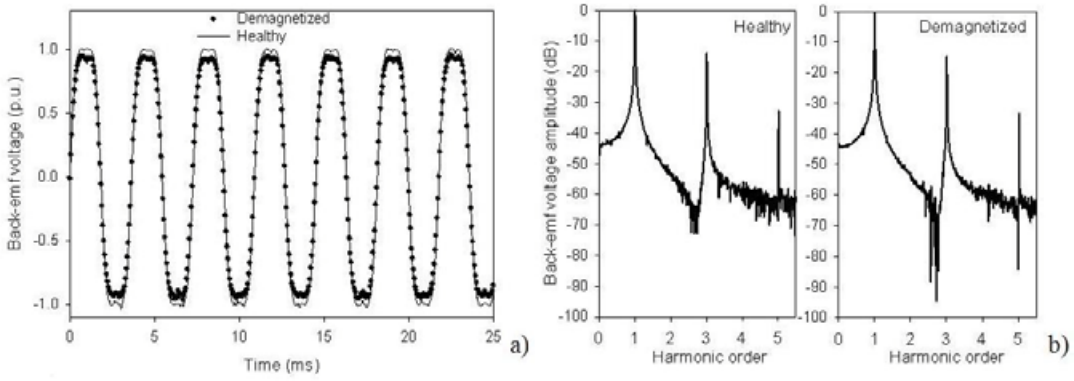

Fig.4.12.a) Measured back-emf induced in phase A when the SPMSM operates at 6000 r/min. b) Back-emf healthy and faulty spectrum.

Fig.4.13.shows the experimental $V_{0,m}$ ZSVC of a healthy and a partially demagnetized SPMSM, normalized with respect to phase-neutral back-emf.

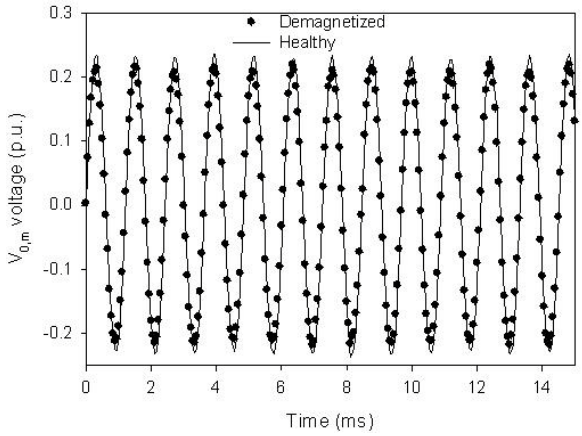

Fig.4.13.Experimental ZSVC voltage of healthy and partially demagnetized SPMSM operating at 6000 r/min.

Results from Fig.4.13 are an experimental validation of equation (4.30) since the experimental third harmonic amplitude reduction factor $1 - K_{dem}/2p$ is 0.922, which is in close agreement with its theoretical value of 0.917. Thus, the third harmonic amplitude reduction factor of the $V_{0,m}$ ZSVC (K_{dem}) may be adopted as a fault severity index which may be very useful to design an on-line fault diagnosis scheme.

4.4.1 ZSVC under different operating conditions

In order to validate the usefulness of the ZSVC-based method to diagnose demagnetization faults, a healthy and a new partially demagnetized SPMSMs modified according to Fig.4.14 (equivalent to 2 poles 50% demagnetized) were tested under different operating conditions.

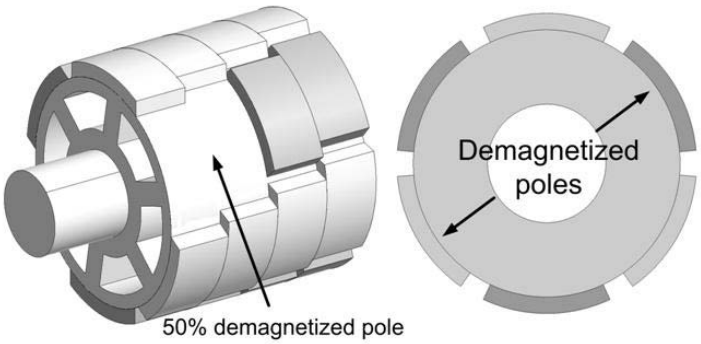

Fig.4.14. Rotor of the analyzed partially demagnetized SPMSM (2 poles, 50% demagnetized)

Fig.4.15 shows the fundamental harmonic amplitude of $V_{0,m}$ ZSVC (third harmonic of the supply frequency) for healthy and partially demagnetized SPMSMs.

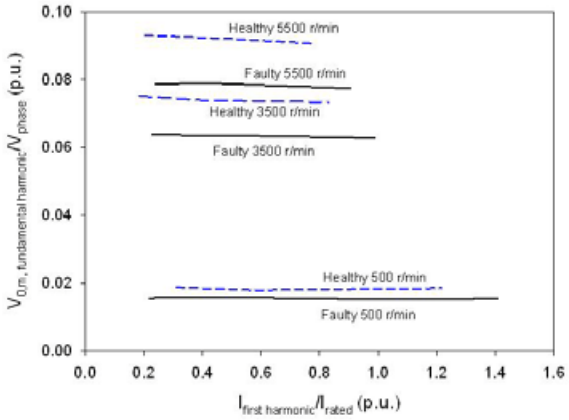

Fig.4.15. 1th harmonic amplitude of $V_{0,m}$ZSVC in healthy and faulty SPMSM operating under different speeds and load conditions (different currents).

Results shown in Fig.4.15 indicate that for a given speed, the amplitude of the fundamental harmonic of the $V_{0,m}$ ZSVC is almost constant regardless of the load level.

Fig.4.16 plots the experimental relation between the fundamental harmonic amplitude of the $V_{0,m}$ ZSVC and the speed when the motor operates under rated load. Results shown in Fig.4.16. indicate that for a given load level, the amplitude of the fundamental harmonic of the $V_{0,m}$ ZSVC increases with the speed. Note that it is not difficult to fit the response curve of the healthy machine by means of a 2nd order polynomial. Hence, the $V_{0,m}$ ZSVC of a practical machine may be compared with the value obtained by the adjusted polynomial.

TABLE 4.1 summarizes the experimental results of the fault severity index 1-K_{dem}.

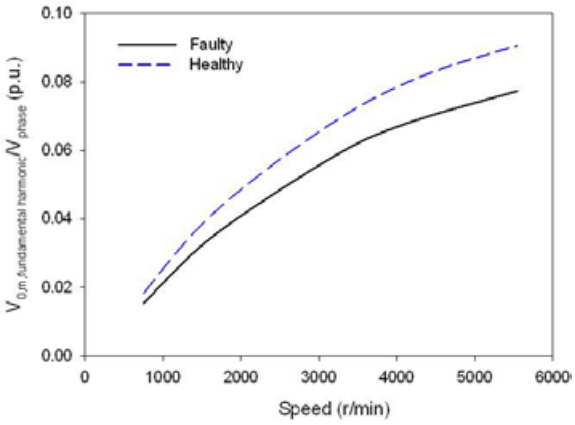

Fig.4.16. 1th harmonic amplitude of $V_{0,m}$ZSVC in healthy and faulty SPMSM operating at different speeds under rated load.

TABLE 4.1. Fault severity index 1-k_{dem} under rated load and different speeds.

Speed (r/min)	Fault indicator 1-k_{dem}
500	0.837
1500	0.841
2500	0.845
3500	0.855
4500	0.848
5500	0.854
Mean 1-k_{dem}	**0.847**
Theoretical 1-k_{dem}	**0.833**

4.5 Comparative results when analyzing different windings configurations

To analyze the influence of the winding configuration on the harmonic content of the stator currents and the ZSVC, a total of five configurations are analyzed different from the reference motor, whose main parameters are detailed in TABLE 4.2.

The analyzed machines include fractional and integral stator slot windings, overlapping and non-overlapping, single- and double-layer, full- and short-pitch and series- and parallel-connected windings. The work is focused on determining the influence of the number of slots per pole per phase (q) on the harmonic content of the stator currents and the ZSVC.

The stator currents harmonics are analyzed for each machine when operating under healthy and partially demagnetized conditions. To facilitate the comparison, all the analyzed faulty PMSMs have the same demagnetization degree.

All the results presented are based on FEM simulations carried out under stationary load and speed conditions. Although the different analyzed machines have different active dimensions and consequently, different rated power, it has no influence on the results. It is so because the spectra of the stator currents for each analyzed SPMSM are plotted normalized with respect to the fundamental harmonic of the same motor when operating under healthy conditions.

TABLE 4.2. Parameters of demagnetized SPMSMs

Features	m1	m2	m3	m4	m5
Slots/pole/phase (*q*)	1/2	1+1/4	1+1/4	3	3
Poles (2*p*)	16	8	8	4	4
Slots number	24	30	30	36	36
Turns per slot	96	40	40	24	24
Layer type	Double	Double	Single	Single	Double
Short pitch	No	Yes	No	No	Yes
Variable pitch	No	No	Yes	No	No
Parallel-branches	8	2	-	2	2
Symmetric winding	Yes	Yes	No	Yes	Yes
Equivalent removed poles	2.66	1.33	1.33	0.66	0.66

4.5.1 Serial connected windings

Fig. 4.17 shows the stator currents spectra for the five analyzed series-connected winding configurations shown in TABLE 4.2

Results clearly indicate that the winding configurations have a profound impact on the harmonic content of the stator currents. A summary of these results is as follows:

- m1 (q = 1/2, double layer): the amplitudes of the constructive harmonics (5-th and 7-th) increase slightly in a partially demagnetized machine and there are new even harmonics (2-nd and 4-th) but not fractional harmonics appear in the currents spectrum.
- m2 (q = 1+1/4, constant-pitch): in the case of a partially demagnetized SPMSM the amplitudes of the constructive harmonics (5-th and 7-th) increase significantly and new harmonic components (0.5-th, 3.5-th, 5.5-th and 6.5-th among others) appear in the currents spectrum. These are the fractional harmonics predicted by (4.1).
- m3 (q = 1+1/4, variable-pitch): when a demagnetization fault occurs, the constructive harmonics amplitudes (5-th and 7-th) change slightly. The currents spectrum of a partially demagnetized SPMSM contains new harmonic components (0.25-th, 0.5-th, 1.25-th, 1.75-th and 2.5-th among others) as predicted by (4.1).
- m4 (q = 3, full-pitch): when dealing with a partially demagnetized machine, the amplitudes of the constructive harmonics (5-th and 7-th) decrease moderately. No new harmonics appear in the stator currents spectrum due to demagnetization faults.

- m5 (q = 3, short-pitch): in the case of a partially demagnetized machine, the amplitudes of the constructive harmonics (5-th and 7-th) decrease moderately and no new harmonics appear in the stator currents spectrum.

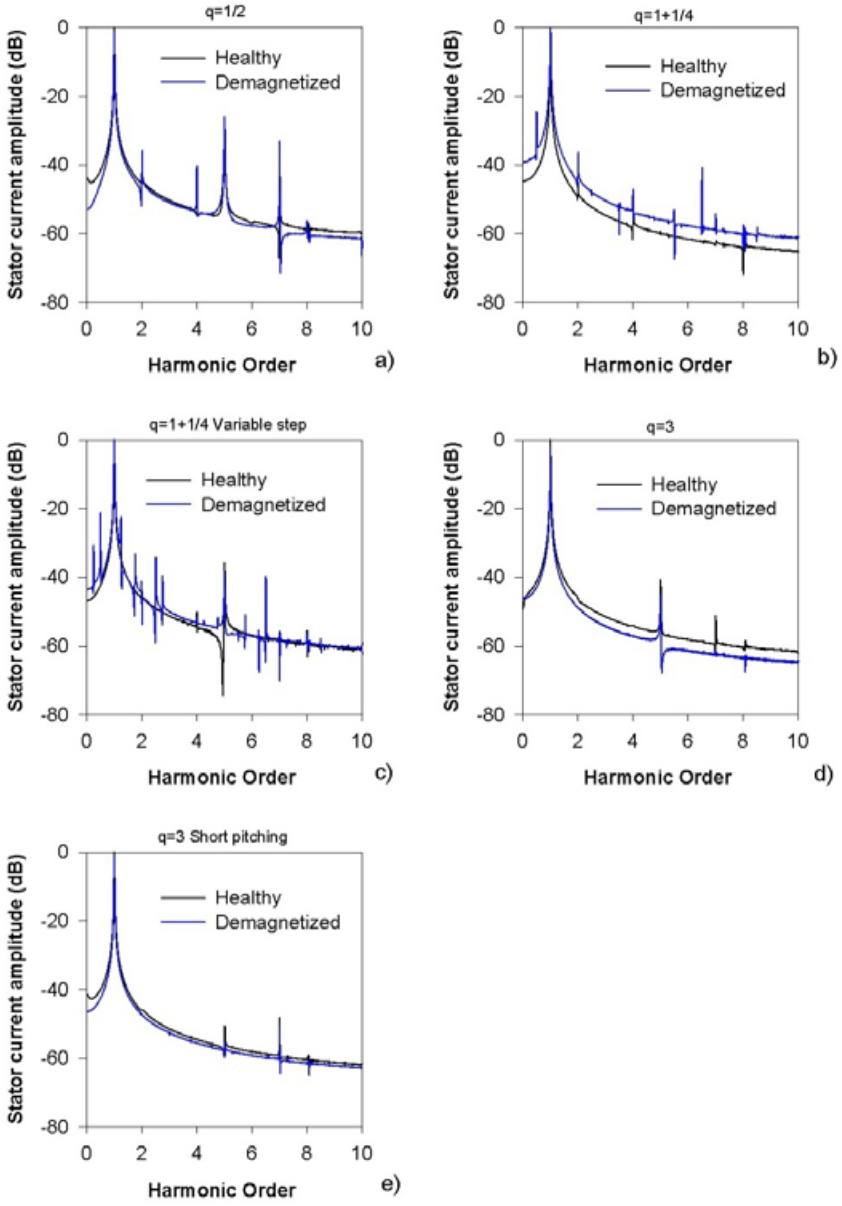

Fig. 4.17. Currents spectra for healthy and demagnetized SPMSMs. a) q=1/2 b) q=1+1/4 c) q=1+1/4 with variable step d) q=3 e) q=3 with short pitching

Results from Fig. 4.18 show the influence of the winding configurations on the harmonic content of the ZSVC.

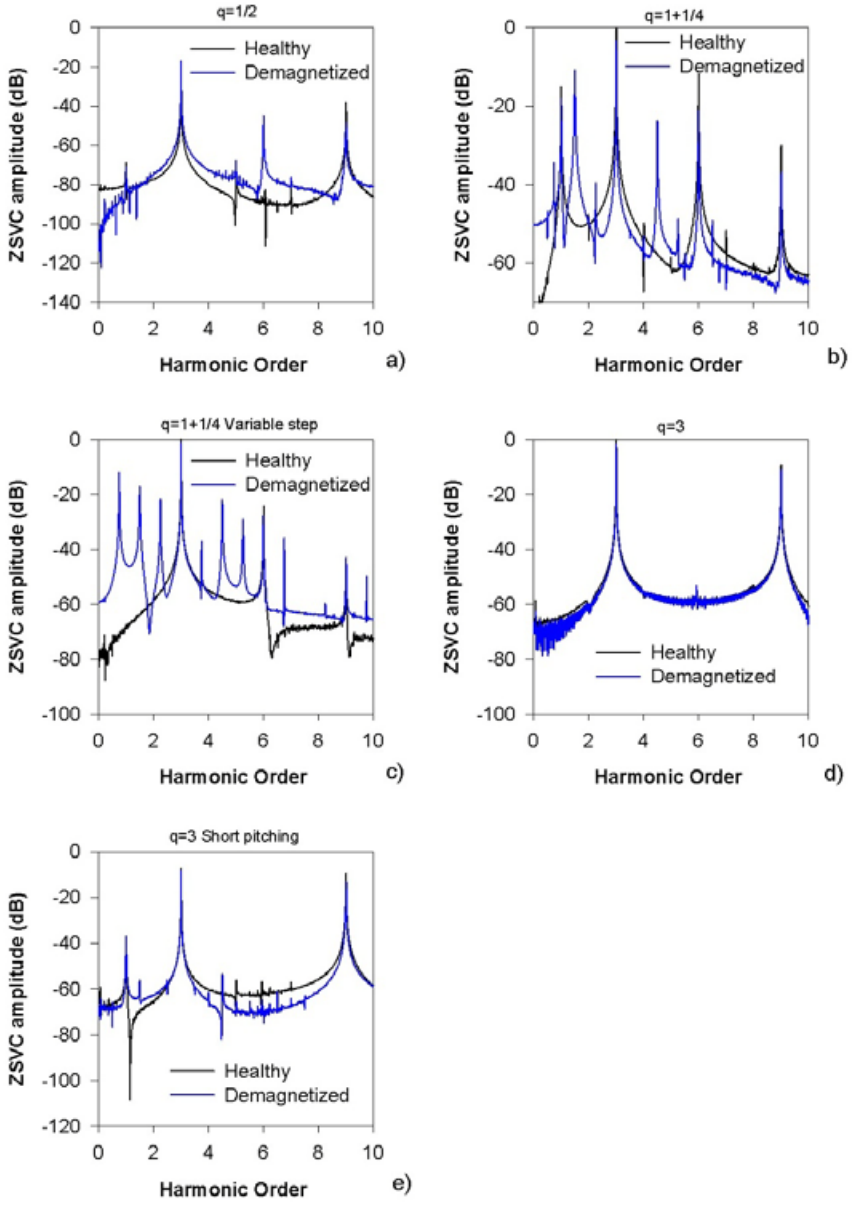

Fig. 4.18. ZSVC spectra for healthy and demagnetized SPMSMs. a) q=1/2 b) q=1+1/4 c) q=1+1/4 with variable step d) q=3 e) q=3 with short pitching

A summary of the results presented in Fig. 4.18 is as follows:

- m1 (q = 1/2, double layer): the amplitudes of the ZSVC constructive harmonics (3-th and 9-th) change significantly in the case of partially demagnetized SPMSM and an important 6-th harmonic component appears in the ZSVC spectrum.
- m2 (q = 1+1/4, constant-pitch): in the case of a partially demagnetized SPMSM, the amplitudes of constructive harmonics (3-th, 6-th and 9-th) decrease significantly. Additionally, new harmonic components appear in the ZSVC spectrum (1.5-th and 4.5-th).

- m3 (q = 1+1/4, variable-pitch): the constructive harmonics amplitudes (3-th, 6-th and 9-th) decrease slightly in the case of partially demagnetized SPMSM and new harmonic components (0.75-th, 1.5-th, 2.25-th, 3.75-th and 4.5-th among others) appear in the ZSVC spectrum.
- m4 (q = 3, full-pitch): when dealing with a partially demagnetized machine, the constructive harmonics amplitudes (3-th and 9-th) decrease slightly. No new harmonic components appear in the ZSVC spectrum due to demagnetization faults.
- m5 (q = 3, short-pitch): in the case of a partially demagnetized machine, the amplitudes of the constructive harmonics (3-th and 9-th) decrease slightly. The ZSVC spectrum of a partially demagnetized SPMSM contains new fractional harmonic components (1.5-th and 4.5-th).

4.5.2 Parallel connected windings

Fig. 4.19 shows the stator currents spectra for the analyzed winding configurations except for m3 (because of its asymmetry it cannot have parallel-connected windings).
Similarly as in the case of series-connected windings, results from Fig. 4.19 prove that the stator configuration greatly influences the current spectrum composition. A summary of these results is presented as follows:

- m1 (q = 1/2, double layer): in the case of a demagnetization fault, the constructive harmonics amplitudes (5-th and 7-th) decrease slightly and the spectrum has new even harmonics (2-nd and 4-th). However, the stator currents spectra do not have fractional harmonics.
- m2 (q = 1+1/4, constant-pitch): in the case of a faulty SPMSM, the constructive harmonics amplitudes (5-th and 7-th) change slightly and new fractional harmonic components (0.5-th, 3.5-th, 5.5-th and 6.5-th among others) appear in the currents spectrum.
- m4 (q = 3): when dealing with a partially demagnetized machine, the amplitudes of the constructive harmonics (5-th and 7-th) decrease slightly. No new harmonic components appear in the current spectrum.
- m5 (q = 3, short-pitch): in the case of a partially demagnetized machine, the amplitudes of the constructive harmonics (5-th and 7-th) remain almost constant. No new harmonics appear in the stator current spectrum due to demagnetization faults.

Fig.4.20 shows that stator currents spectra in parallel branches of a demagnetized motor contain fractional harmonics which do not appear in the line currents. As a consequence there are circulating currents, which can increase joule losses and may lead to more demagnetization.

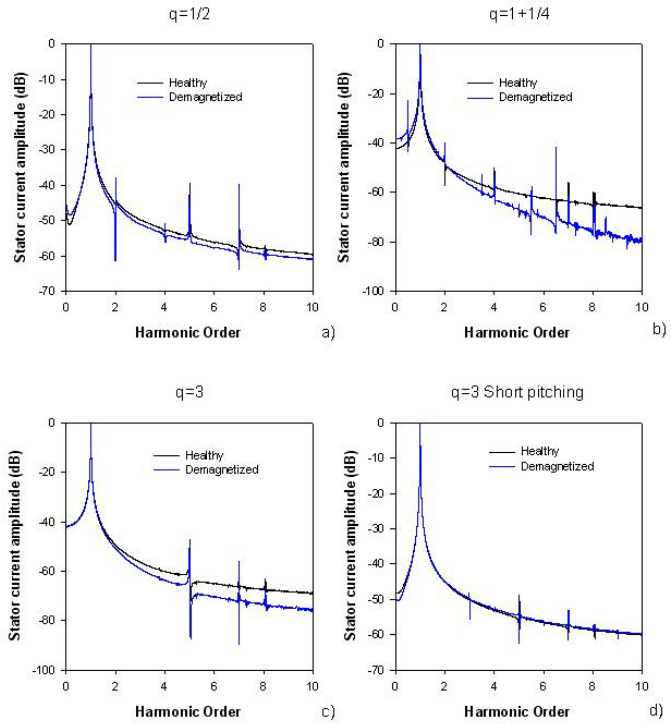

Fig. 4.19. Currents spectra for healthy and demagnetized SPMSMs with parallel connections. a) q=1/2 b) q=1+1/4 c) q=3 d) q=3 with short pitching

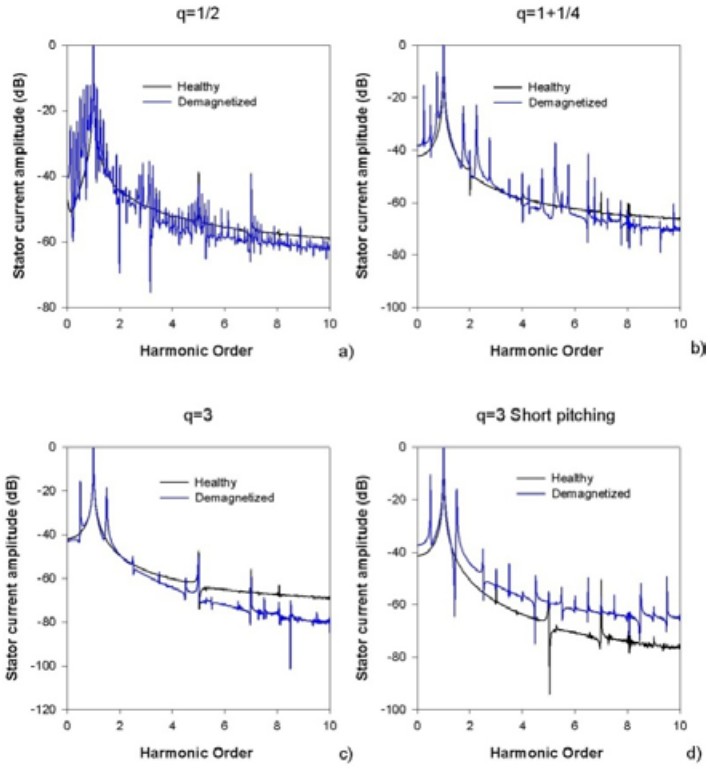

Fig.4.20. Currents spectra in parallel branches for healthy and demagnetized SPMSMs. a) q=1/2 b) q=1+1/4 c) q=3 d) q=3 with short pitching

Fig. 4.21 shows the windings configurations influence on the ZSVC harmonic content. A summary of these results is presented as follows:

- m1 (q = 1/2, double layer): in the case of a faulty machine, the constructive harmonics amplitudes (3-th and 9-th) decrease moderately and a new 6-th harmonic component appears in the ZSVC spectrum.
- m2 (q = 1+1/4, constant-pitch): in a partially demagnetized SPMSM the 3-th, 6-th and 9-th constructive harmonics amplitudes decrease slightly and new fractional harmonic components appear in the ZSVC spectrum (0.5-th, 0.75-th, 1.5-th, 2.25-th and 4.5-th among others).
- m4 (q = 3): in the case of the partially demagnetized SPMSM, constructive harmonics amplitudes (3-th and 9-th) present a very slight change and a new 6-th harmonic component appears in the ZSVC spectrum.
- m5 (q = 3, short-pitch): in the case of partially demagnetized machine, the 3-th and 9-th constructive harmonics amplitudes decrease slightly but the 5-th experiments a sharp increase. Additionally, the ZSVC spectrum of partially demagnetized SPMSM contains new fractional harmonic components (0.5-th, 1.5-th, 2-th, 3.5-th and 4.5-th among others).

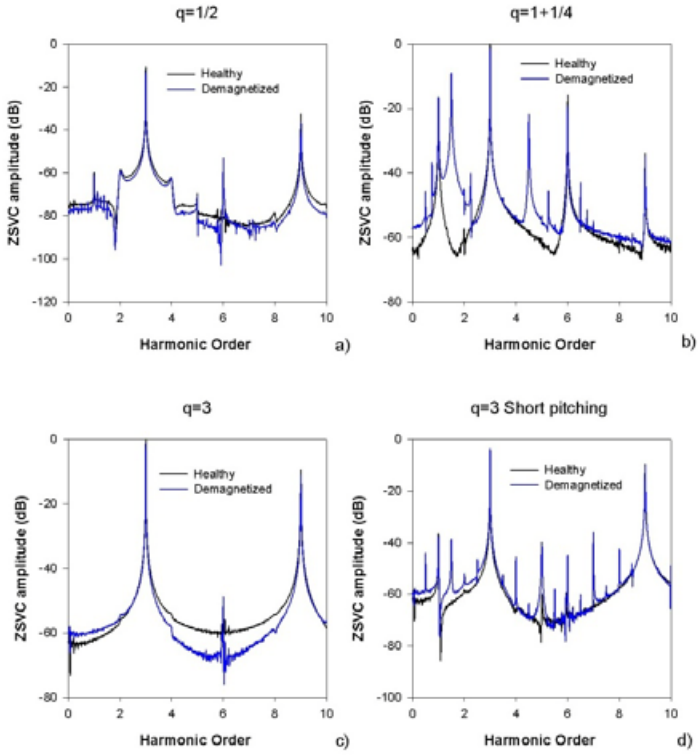

Fig. 4.21. ZSVC spectra for healthy and demagnetized SPMSMs with parallel connections. a) q=1/2 b) q=1+1/4 c) q=3 d) q=3 with short pitching

4.6 Mechanical effects of demagnetization faults

In this section it is proved that demagnetization faults in PMSMs lead unavoidably to the generation of unbalanced magnetic forces which in turn may generate a deviation of the rotor trajectory. The evidences presented in this section are from both FEM simulations and a direct measurement of the motor shaft displacement in X and Y axes by means of self-mixing interferometry using two laser diodes to support this hypothesis.

4.6.1 Magnetic analysis of unbalance demagnetization

In section 4.4 is analyzed a balanced demagnetization in two SPMSMs with removed magnets in opposite poles in order to avoid magnetic forces on the rotor. In an actual rotor fault, a feasible demagnetization fault may occur when only one or two adjacent poles are partially demagnetized. As a consequence of an unbalance fault, non-equilibrated magnetic forces may appear on the rotor.

In this section the effects of unbalanced demagnetization faults are analyzed by means of FEM simulations and experimental results. To conduct an experimental study with an unbalance demagnetized SPMSM, six rotor magnets placed in consecutive poles were removed in the reference machine (Appendix A), as shown in Fig.4.22. This demagnetization pattern is equivalent to a 75% partially demagnetized SPMSM. As in section 4.4, the rotor mass was balanced.

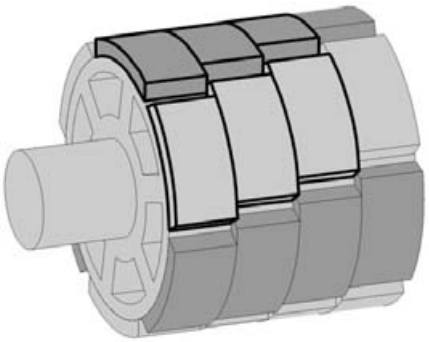

Fig.4.22. Type of demagnetization analyzed in this work. The removed magnets are dashed in solid black line.

Fig.4.23 shows the results obtained by means of FEM simulations of the stator currents of both healthy and partially demagnetized machines. These simulations suppose the motor shaft rotating perfectly around its symmetry axis.

In section 4.1.2 it is demonstrated that integral slot windings tend to remove from the stator currents spectrum the effects of periodic changes of parameters that may modify the magnetic flux. Results presented in Fig.4.23 clearly show that the simulated current spectrum does not contain additional harmonics in the case of an unbalanced partially demagnetized SPMSM. It is due to the particular windings configuration of the analyzed motor, an integral slot winding with q = 1 slots per pole per phase.

Note that the main difference between both spectra (healthy and partially demagnetized motor) is that the amplitude of the odd harmonics is lower for the partially demagnetized motor.

Fig.4.24 shows the spectrum of experimental currents, for both healthy and faulty SPMSM running at 1500 r/min under rated load.

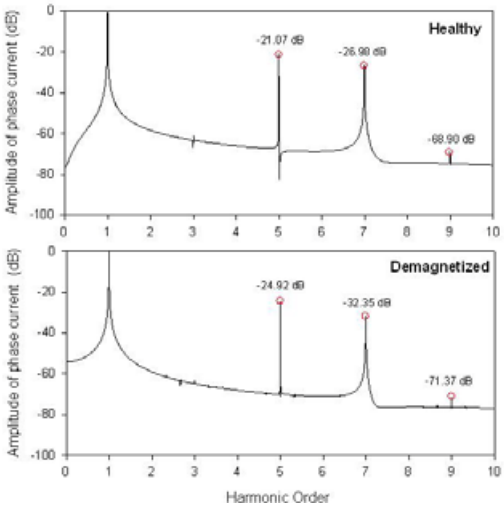

Fig.4.23. Stator currents spectra of healthy and partially demagnetized SPMSM operating at 1500 r/min under rated load. FEM simulation results.

Experimental spectra shown in Fig.4.24 are more complex than those obtained from FEM simulations since the former shows the presence of fractional and even harmonics for both healthy and partially demagnetized machines. FEM simulations suppose the SPMSM fed by ideal sources, whereas it is well known that the motor controller may injects harmonics [59]. Additionally, the fractional harmonics may be also due to mechanical causes such as inherent rotor misalignments and eccentricities [56].

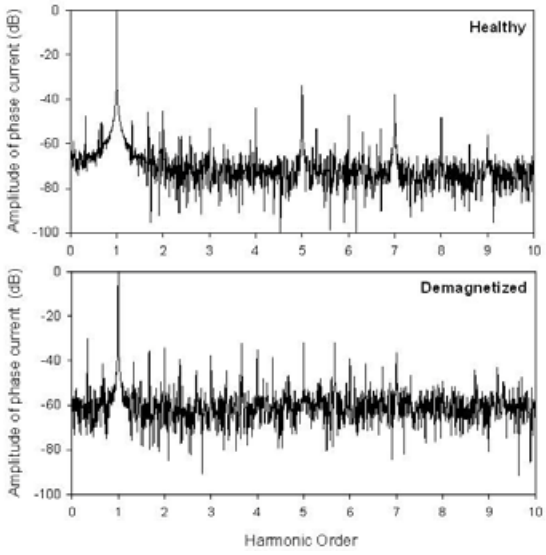

Fig.4.24. Stator currents spectra of a healthy and a partially demagnetized SPMSM operating at 1500 r/min under rated load. Experimental results.

To explain the presence of fractional harmonics, this study must be extended to analyze possible mechanical effects arising from demagnetization faults. It is well known that there is a magnetic attraction force between the ferromagnetic stator core and the rotor magnets. These radial forces may be obtained from FEM simulations, as shown in Fig.4.25.

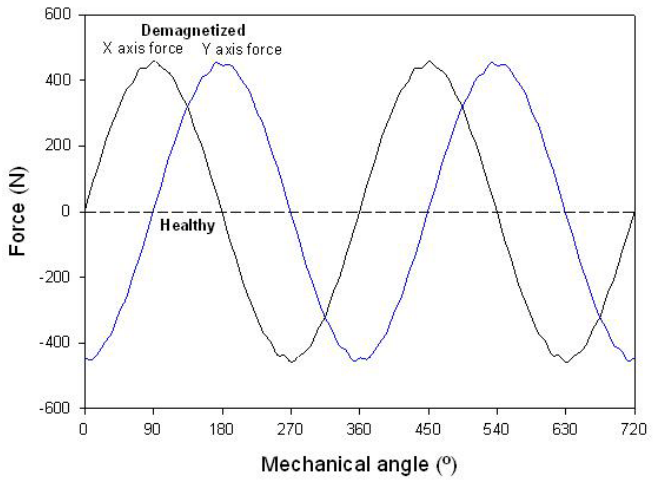

Fig.4.25. Radial magnetic forces on the shaft of a healthy and a partially demagnetized SPMSM when operating at 1500 r/min under rated load. FEM simulation results.

Simulation results from Fig.4.25 show that in the case of a healthy SPMSM, these radial forces are equilibrated. However, in case of a partially demagnetized SPMSM, there is a non-zero resultant radial force which must generate mechanical effects.

Fig.4.26 plots the Y axis force against the X axis force, which have been obtained from FEM simulations of a partially demagnetized SPMSM. It clearly shows 18 lobules corresponding to the 18 stator slots.

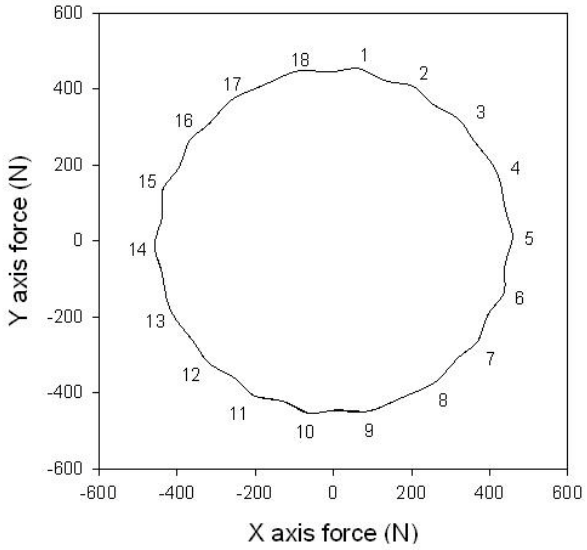

Fig.4.26.Y axis force against X axis force for partially demagnetized SPMSM operating at 1500 r/min under rated load. FEM Simulation results.

The influence of the stator currents on the radial forces was analyzed. To this end, two simulations were performed. In the first one the SPMSM was simulated when operating at rated load (rated current) while in the second it was analyzed under no load conditions, as depicted in Fig.4.27.

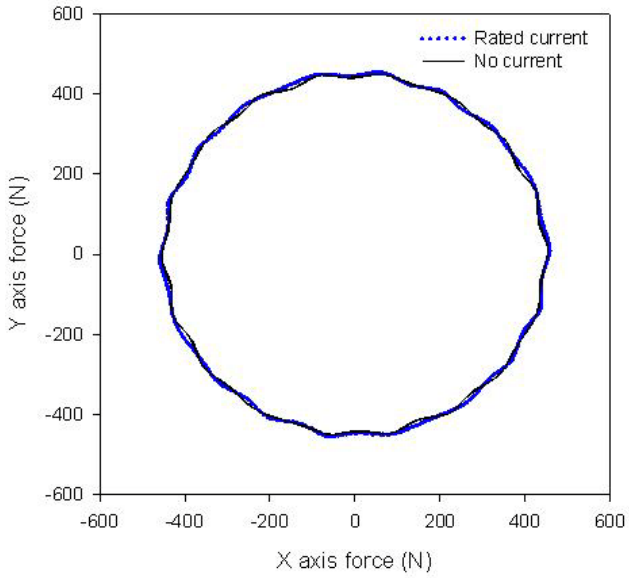

Fig.4.27. Y-axis force against X-axis force for partially demagnetized SPMSM operating at 1500 r/min under rated load and no load conditions. FEM Simulation results.

Results from Fig.4.27 show that stator the currents have nearly no contribution to the resultant radial force. Consequently, it can be assumed that this force is only due to the magnetic interaction between the ferromagnetic stator core and the rotor magnets.

4.6.2 Mechanical effects analysis by means of laser interferometry

In this section the shaft trajectory of healthy and partially demagnetized SPMSMs is measured experimentally. As deduced from Fig.4.25 to Fig.4.27, it seems feasible that the unbalanced magnetic forces already present in a partially demagnetized machine may induce small displacements of the motor shaft. Therefore, to analyze in detail the effects of such forces, it is required an exhaustive combined electromagnetic and mechanical FEM model of the machine, which must include the bearings behavior. However, that is not an easy solution. Fortunately, the shaft displacement may be measured experimentally. In practice, and in order not to affect measurement, optimally shaft displacement should be observed using some non-contact measurement system. In this work the system has been measured using a double self-mixing interferometry (SMI) setup, depicted in Fig.4.28. The setup contains two self-mixing laser diodes (SMLDs) and associate electronics placed perpendicular to each other pointing towards the rotating shaft, to sample its 2D displacement along the X and Y axes.

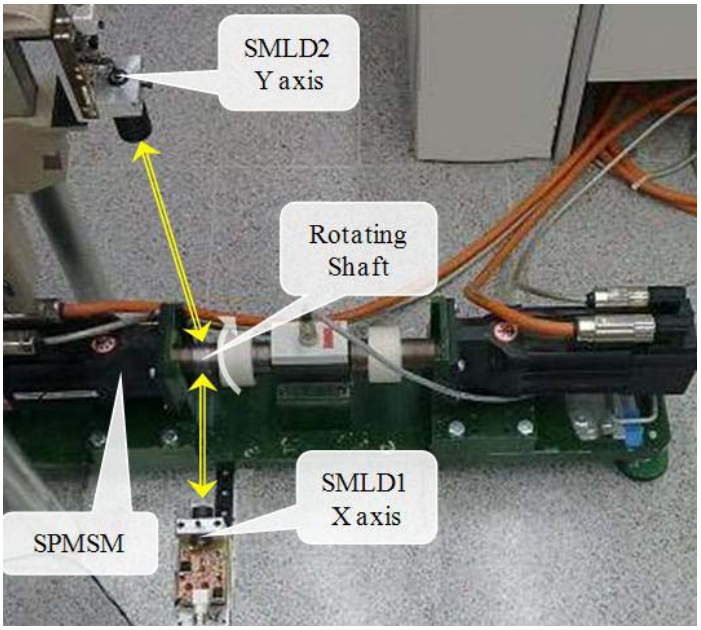

Fig.4.28. Experimental setup used to measure the shaft trajectory of analyzed SPMSMs.

SMI is an experimental technique which has been extensively used for displacement, vibration and velocity sensing during the past decades [67-69]. It is based on measuring the beat arising from the interference of a portion of laser beam back-reflected into the laser cavity by a moving target (the motor shaft in this case), and the standing wave inside the cavity. Since the SMI configuration is compact, self-aligned, robust and cheap in comparison with conventional interferometers, it is especially attractive from the industrial application viewpoint.

As there are a number of different types of noise sources in the measuring environment, such as structural vibrations or shaft surface roughness and shape deviations, a low-pass filter is applied to the acquired self-mixing signal. Afterwards, a transition detection algorithm [70] is used as the signal processing method, yielding a resolution of half the wavelength of the laser (392 nm) in the technique. However, due to different error sources in the measurement setup (mainly shaft surface waviness and structural vibrations, among others), the experiment performed had its accuracy limited to 6 μm. The two orthogonal SMLD configurations allow direct measurements of the motor shaft displacement since data of both laser diodes were acquired simultaneously. Two Hitachi HL7851G Fabry-Perot laser diodes with a maximum output power of 50 mW, emitting at the wavelength of 785 nm were used in the experiment.

Hence, by comparing measures obtained from healthy and partially demagnetized motors, mechanical effects of demagnetization faults become visible. Fig. 4.29 and Fig.4.30 show the trajectories of the target point of the motor shaft where both laser beams were pointing to.

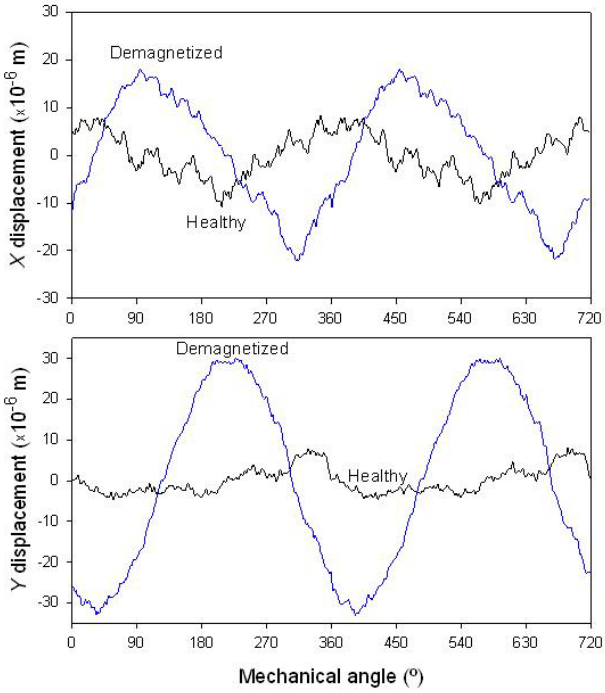

Fig. 4.29. Displacement of the motor shaft as measured by the two SMLDs placed in the X and Y axes. Healthy and partially demagnetized SPMSM were measured when running at 1500 r/min under no load conditions.

As proved in Fig. 4.29 and Fig.4.30, both healthy and faulty SPMSMs have a certain degree of eccentricity, but it becomes significantly higher in the latter. Therefore, these results are a consistent proof that demagnetization faults may increase significantly the amplitude of shaft displacement. Concretely, results presented in Fig.4.30 show a measured displacement of about ± 30 μm (± 5% of the air gap) for the partially demagnetized SPMSM.

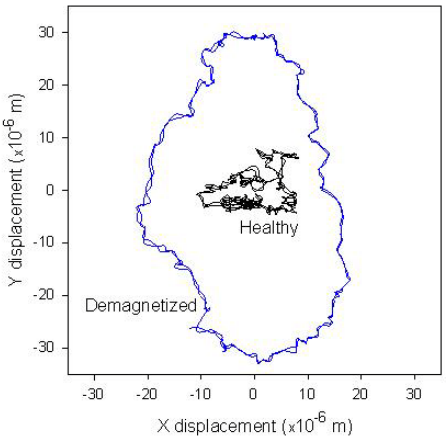

Fig.4.30.Trajectory of the measured target point of the motor shaft in the X-Y plane. Healthy and partially demagnetized SPMSM were measured when running at 1500 r/min under no load conditions.

4.6.3 Analysis of joint mechanical and magnetic effects

In section 4.6.1 it has been shown that results from conventional FEM models of SPMSMs which do not include the shaft displacement are not in close agreement with experimental results. Therefore, in this section, the experimental displacement of the motor shaft is included in FEM simulations. As it will be proved, this procedure allows performing more realistic results.

Experimental results presented in Fig. 4.29 and Fig.4.30 for both, healthy and partially demagnetized motors will be used to adjust the FEM model, which takes into account the displacement of the motor shaft. It will allow explaining the mechanical effects due to demagnetization faults.

Fig.4.31 and Fig.4.32 show changes in the self-inductance L and the mutual inductance M between two phases as a consequence of the demagnetization fault. They have been obtained by introducing experimental displacements (X,Y) of the motor shaft shown in Fig.4.30 in the FEM model.

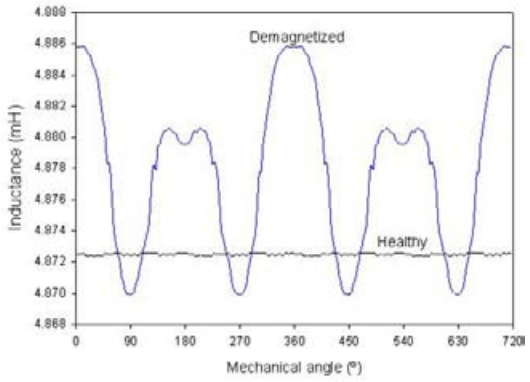

Fig.4.31. Self-inductance L considering the measured displacements of the shaft. Both motors operate under rated load at 1500 r/min. FEM simulation results.

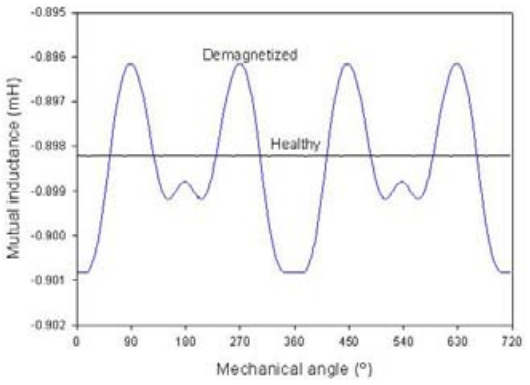

Fig.4.32. Mutual inductance M considering the measured displacements of the shaft. Both motors operate under rated load at 1500 r/min. FEM simulation results.

As shown in Fig.4.31 and Fig.4.32, in the case of a healthy motor, both L and M inductances remain nearly constant regardless the rotor position. Contrarily, when dealing with a partially demagnetized

SPMSM, their values change with the rotor angular position. It is so because of the reluctance change due to the motor shaft displacement (change in air gap distance), which is due to the radial forces.

Changes in inductances generate fluctuations in the magnetic flux generated by them. Additionally, due to the shaft displacement, the permanent magnets magnetic flux is also altered. Hence, these combined effects are traduced in stator flux variations, which are reflected and amplified (due to the time derivative) in the back-emf spectrum, as shown in Fig.4.33.

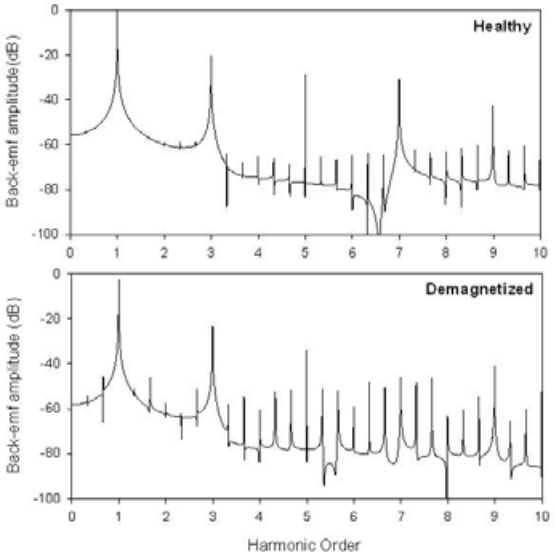

Fig.4.33. Back-emf spectra of healthy and partially demagnetized SPMSMs operating at 1500 r/min under rated load. Simulations obtained by introducing measured motor shaft displacements in the FEM model.

Results from Fig.4.33 show that when considering a FEM model including both the effects of demagnetization and eccentricity, the back-emf spectrum contains fractional harmonics.

Fig. 4.34 shows the simulated spectrum of the stator current when taking into account the shaft displacement.

Results from Fig. 4.34 show the presence of fractional harmonics. It should be pointed out that when considering the demagnetization effects but not the shaft displacement there is no presence of fractional harmonics in the stator currents spectrum. Hence, these results show that demagnetization faults may amplify the amplitude of shaft displacement already present in any healthy motor, which in turn may induce fractional harmonics in the current spectrum.

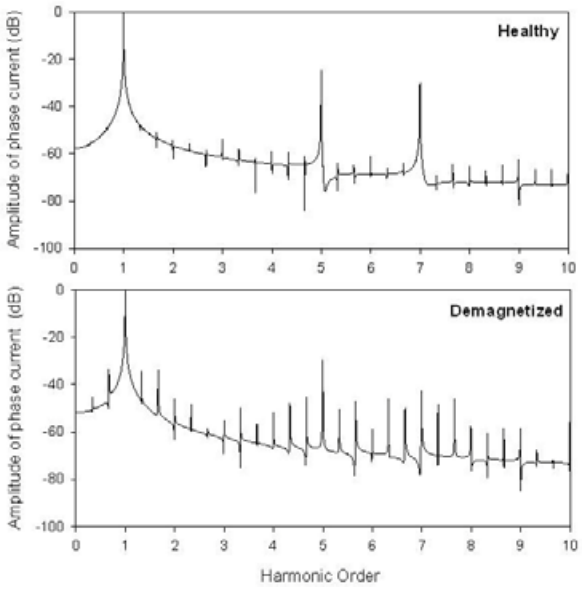

Fig. 4.34. Phase currents spectra of healthy and partially demagnetized SPMSMs operating at 1500 r/min under rated load. Simulations obtained by introducing the measured motor shaft displacements in the FEM model.

4.7 Conclusion

In SPMSMs with integral windings the result of a partial demagnetization over a phase is a decrease in the back-emf voltage in a factor $1 - K_{dem}/2p$. However there no appear frequencies different from those of the constructive harmonics. As a consequence, since the current is mainly influenced by the back-emf, it is difficult to identify demagnetization from stator current spectrum data.

In this chapter is studied demagnetization faults in SPMSMs and an on-line diagnosis method based on the ZSVC is proposed, their theoretical foundations are established and results from experiments and simulations are compared taking into account equations obtained in this work.

Although PWM inverters usually generate frequency components which can influence the ZSVC, these components can be removed by a low cost three-phase balanced resistor network. Thus ZSVC measurements between the motor neutral point and the neutral point of the resistor network are decoupled from the motor source and are only influenced by the machine harmonics. Simulation and experimental results show the efficacy of the ZSVC-based method

Both simulation and experimental results show that the amplitude of the ZSVC provides reliable information about the condition of the SPMSM. Moreover, this methodology provides an easy-to-calculate fault indicator or severity index which value depends on the severity of the fault. The proposed fault indicator is obtained and discussed with experimental test with healthy and faulty SPMSMs running at different load and speed operation points.

5. ELECTRICAL FAULTS IN SPMSM

Electrical SPMSMs faults can be divided in abnormal connection of the stator windings, stator short-circuited turns and phase-to-phase or phase-to-neutral short-circuits. The first two are analyzed in this chapter.

Inter-turns short-circuits are one of the most usual three-phase motors failures, which are related to stator winding insulation degradation, being one of the most difficult failures to identify and the initial step of a more severe fault (e.g. phase-phase short-circuit) [21]. In the case of PMSMs, inter-turn short-circuits may result in stator over currents that create a magnetic flux opposed to the natural flux of the permanent magnets, which in turn may lead to a demagnetization of the rotor magnets [22].

Stator inter-turn short-circuit faults have been analyzed in dc machines [71] as well as in induction motors using reference frame transformation theory [72-73]] or by adding an external sensor for measuring the dispersion flux for inter-turn short-circuit detection [74]. In the case of SPMSMs, references [75] and [14] propose a model whose parameters -inductances and back electromotive force, emf- were calculated from a finite elements simulation of the machine when running under the same operating conditions. In [76] a SPMSM parametric model is presented when single and double phase internal fault occurs, but no information about harmonic fault content is presented. Additionally, in [39] a parametric model to study stator inter-turn short circuit faults in a SPMSM is presented by using classical two-axis theory. However, this reference does not take into account the effects of spatial harmonics such as those due to the geometrical distribution of the rotor permanent magnets or non-sinusoidal stator windings configuration, although the last ones have a lower influence. Additionally, other researchers have made efforts for identifying stator short-circuit faults from the acquired spectrum of the stator currents with no aim to generate a fault model [66].

Thus, from the abovementioned references it is not possible to obtain a model able to localize the stator current harmonics due to short-circuit faults when dealing with SPMSMs with spatial harmonics. As a result, there is a clear lack of mathematical and physical foundations of stator short-circuit inter-turn faults in SPMSMs -especially when dealing with machine models that take into account spatial harmonics- and their effects in the harmonic content of stator currents.

In this chapter it is presented a rigorous mathematical study of both stator short-circuit inter-turns and unbalance resistive faults in SPMSMs. To meet this objective, a set of consistent equations that allow modeling both healthy and faulty SPMSMs have been developed and simulated and compared with experimental test. From the models results, two fault detection methods are proposed; the first one is based on the analysis of the amplitude of the third harmonic of the stator currents for different operating points of the SPMSM, whereas the second one is based on the analysis of the first harmonic of the ZSVC.

5.1 Model of the SPMSM with resistive unbalance and inter-turns faults

In this section the model of a healthy and faulty SPMSM with resistive unbalance and stator windings inter-turn faults is derived. Modeling of SPMSMs operating under these types of faults is the first stage to understand their effects and to develop fault detection methods.

Several models have been created to describe an ac machine with inter-turn short-circuit faults [19, 58] but they do not take into account the effects of spatial harmonics.

Fig.5.1 shows a wye-connected stator with n short-circuited inter-turns out of N total turns in phase A.

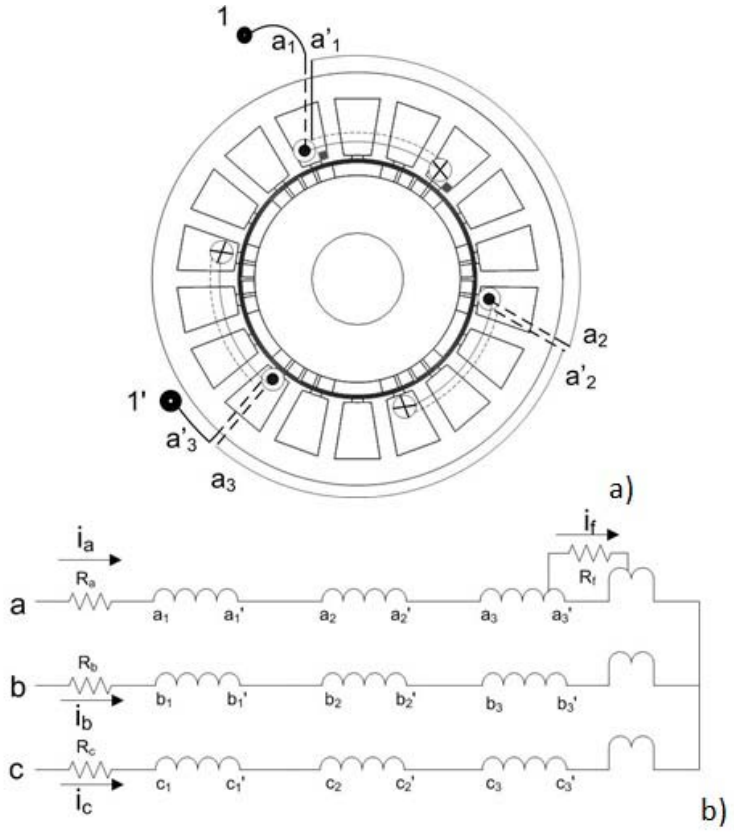

Fig.5.1. a) Diagram of the three poles pairs studied SPMSM with stator inter-turn short-circuit faults. b) Stator windings connections diagram.

In the case of an inter-turn short-circuit fault, both the actual speed of the SPMSM and the ratio $\upsilon = n/N$, between the number n short-circuited inter-turns and the total number of turns N in a certain phase, greatly affects the severity of the fault. The current through the n short-circuited turns is designated as i_f while R_f is a resistance whose value depends on the fault severity. Lower values of R_f indicate severest inter-turn short-circuit conditions.

The electrical equations of a faulty SPMSM – subscript *f* – with resistive unbalance in phase A and inter-turn faults in phase B expressed in abc reference may be calculated similarly to [19, 39]:

$$[V_{sf,abc}] = [R_{sf}] \cdot [i_{sf,abc}] + [\lambda'_{sf,abc}] + [V_0] \quad (5.1)$$

Where the symbol ´ indicates the time derivative and:

$[\lambda_{sf,abc}] = [L_{sf}][i_{sf,abc}] + [\lambda_{PM,f,abc}]$

$[\lambda_{PMf,abc}] = [\lambda_{PM,a}\ \lambda_{PM,b}\ \lambda_{PM,c}\ \lambda_{PM,f}]^t$, $\lambda_{PM,f} = \upsilon\lambda_{PM,b}$, $[V_{sf,abc}] = [V_a\ V_b\ V_c\ 0]^t$, $[i_{sf,abc}] = [i_a\ i_b\ i_c\ i_f]^t$, $[V_0] = V_0[1\ 1\ 1\ 0]^t$,

$$[L_{sf}] = \begin{bmatrix} L & M & M & -\upsilon M \\ M & L & M & -\upsilon L \\ M & M & L & -\upsilon M \\ \upsilon M & \upsilon L & \upsilon M & -\upsilon^2 L \end{bmatrix}$$

where the resistance matrix $[R_{sf}]$ has been adapted according to the unbalanced term $R_{s,a} = kR_s$, being k a multiplying factor that modifies the resistance in phase A. Hence, the resistance matrix results in:

$$[R_{sf}] = \begin{bmatrix} kR_s & 0 & 0 & 0 \\ 0 & R_s & 0 & -\upsilon R_s \\ 0 & 0 & R_s & 0 \\ 0 & \upsilon R_s & 0 & -\upsilon R_s - R_f \end{bmatrix} \quad (5.2)$$

The flux linkage $[\lambda_{PM,abc}]$ expressed in abc reference due to the permanent magnets taking into account the spatial harmonics (owing to the geometrical configuration of rotor magnets or non-sinusoidal stator windings configuration) is as follows [39]:

$$\begin{cases} \lambda_{PM,a} = \lambda_{PM,1}\cos(\theta) + \sum_{h=1,3,5...} \lambda_{PM,h}\cos(h\theta - \theta_v) \\ \lambda_{PM,b} = \lambda_{PM,1}\cos\left(\theta - 2\frac{\pi}{3}\right) + \sum_{h=1,3,5,...} \lambda_{\mathrm{PM,h}}\cos\left(h\theta - \theta_v - 2h\frac{\pi}{3}\right) \\ \lambda_{\mathrm{PM,c}} = \lambda_{PM,1}\cos\left(\theta + 2\frac{\pi}{3}\right) + \sum_{h=1,3,5,...} \lambda_{\mathrm{PM,h}}\cos\left(h\theta - \theta_v + 2h\frac{\pi}{3}\right) \end{cases} \quad (5.3)$$

Where h is the harmonic order.

Equation above increases the accuracy of the model, because the spectrum of the current flowing through the faulty turns is directly influenced by spatial harmonics.

Adding the first three rows of equation (5.1) and having into account equation (5.3), the expression of the ZSVC measured between the center of the stator windings and the dc mid-point of the inverter is obtained as follows:

$$V_0 = \frac{1}{3}(V_a + V_b + V_c) - \frac{1}{3}R_s(k-1)i_a + \frac{1}{3}\upsilon R_s i_f + \frac{1}{3}\upsilon(L+2M)i'_f - \lambda'_{PM,0} \quad (5.4)$$

Where

$$\lambda_{PM,0} = \frac{1}{3}(\lambda_{PM,a} + \lambda_{PM,b} + \lambda_{PM,c})$$

The ZSVC measured as in equation (5.4) is not decoupled from the motor source effects. These influences are almost totally removed by measuring the ZSVC between the neutral point of the stator

windings and the central point of a three-phase balanced resistor network connected between the inverter and the motor as detailed in section 4.3 thus resulting in

$$V_{0,measured} = -\frac{1}{3}R_s(k-1)i_a + \frac{1}{3}\upsilon R_s i_f + \frac{1}{3}\upsilon(L+2M)i'_f - \lambda'_{PM,0} \tag{5.5}$$

The first three terms in equation above are mainly influenced by the first harmonic of the supply frequency. Contrarily, the last term which is not related to the studied faults, primarily depends on the third harmonic component due to the permanent magnets particular geometry [39]. Hence, from the study of the first harmonic of ZSVC it is possible to detect both resistive unbalance and inter-turn faults.

5.2 SPMSM with resistive unbalance and inter-turn faults including saturation

It is well known that core saturation generates harmonic frequencies in the air gap flux distribution. Hence, saturation effects lead to odd harmonics in the experimental current spectrum [71]. A straightforward manner to estimate the magnetic saturation curve is by means of a polynomial approximation:

$$B = \sum_{m=1,3,5,\ldots} k_m H^m \tag{5.6}$$

Note that equation above only accounts for odd harmonics because of the odd symmetry of B-H curve. Neglecting saturation effects, the linear magnetic flux λ_L through a phase winding is as follows:

$$\lambda_L = k_{wind} B_L = \mu k_{wind} H \tag{5.7}$$

Where k_{wind} is the winding factor, which value depends on the particular type of winding and μ is the magnetic permeability of the ferromagnetic core. From equation (5.7) it results in:

$$H = \frac{\lambda_L}{\mu k_{wind}} \tag{5.8}$$

By taking into account saturation effects and equation (5.6), the expression of the saturated flux λ_{sat} through a phase winding is obtained:

$$\lambda_{sat} = k_{wind} B(H) = \mu k_{wind} \sum_{m=1,3,5,\ldots} k_m H^m \tag{5.9}$$

From (5.8) and (5.9) it results in:

$$\lambda_{sat} = \sum_{m=1,3,5,\ldots} k_{\lambda m} \lambda_L^m \tag{5.10}$$

Where

$$k_{\lambda m} = \frac{k_m}{\mu^m k_{wind}^{m-1}}.$$

By including (5.5) in (5.1), the expression of phase fluxes under faulty conditions is obtained as:

$$\begin{cases} \lambda_a = Li_a + Mi_b + Mi_c + \frac{1}{3}\upsilon(L-M)i_f + \lambda_{PM,a} - \lambda_{PM,0} \\ \lambda_b = Mi_a + Li_b + Mi_c - \frac{2}{3}\upsilon(L-M)i_f + \lambda_{PM,b} - \lambda_{PM,0} \\ \lambda_c = Mi_a + Mi_b + Li_c + \frac{1}{3}\upsilon(L-M)i_f + \lambda_{PM,c} - \lambda_{PM,0} \\ \lambda_f = \upsilon Mi_a + \upsilon Li_b + \upsilon Mi_c - \upsilon^2 Li_f + \upsilon\lambda_{PM,b} \end{cases} \quad (5.11)$$

By performing the time derivative of equation above and having into account saturation effects by means of (5.10) until grade 7 it results in:

$$\begin{cases} \lambda'_{a,sat} = \zeta_{sa}[Li'_a + Mi'_b + Mi'_c + \frac{1}{3}\upsilon(L-M)i'_f + \lambda'_{PM,a} - \lambda'_{PM,0}] \\ \lambda'_{b,sat} = \zeta_{sb}[Mi'_a + Li'_b + Mi'_c - \frac{2}{3}\upsilon(L-M)i'_f + \lambda'_{PM,b} - \lambda'_{PM,0}] \\ \lambda'_{c,sat} = \zeta_{sc}[Mi'_a + Mi'_b + Li'_c + \frac{1}{3}\upsilon(L-M)i'_f + \lambda'_{PM,c} - \lambda'_{PM,0}] \\ \lambda'_{f,sat} = \zeta_{sf}[\upsilon Mi'_a + \upsilon Li'_b + \upsilon Mi'_c - \upsilon^2 Li'_f + \upsilon\lambda'_{PM,b}] \end{cases} \quad (5.12)$$

Where

$\zeta_{s\,phase} = k_{\lambda 1} + 3k_{\lambda 3}\lambda_{phase}^2 + 5k_{\lambda 5}\lambda_{phase}^4 + 7k_{\lambda 7}\lambda_{phase}^6$ and phase states for a, b, c or f.

Note that saturation effects are neglected when $k_{\lambda 3}$, $k_{\lambda 5}$ and $k_{\lambda 7}$ are set to zero. By including (5.12) in (5.1) it results in:

$$[V_{sf,abc}] = [R_{sf,sat}]\cdot[i_{sf,abc}] + [L_{sf,sat}][i'_{sf,abc}] + [e_{sat}] \quad (5.13)$$

Note this last equation has into account saturation effects, and their matrixes are expressed as:

$$[R_{sf,sat}] = \begin{bmatrix} -\frac{R_s}{3}(2k+1) & 0 & 0 & \frac{1}{3}\upsilon R_s \\ -\frac{R_s}{3}(k-1) & R_s & 0 & -\frac{2}{3}\upsilon R_s \\ -\frac{R_s}{3}(k-1) & 0 & R_s & \frac{1}{3}\upsilon R_s \\ 0 & \upsilon R_s & 0 & -\upsilon R_s - R_f \end{bmatrix}$$

$$[L_{sf,sat}] = \begin{bmatrix} \zeta_{as}L & \zeta_{as}M & \zeta_{as}M & \frac{1}{3}\upsilon\zeta_{as}(L-M) \\ \zeta_{bs}M & \zeta_{bs}L & \zeta_{bs}M & -\frac{2}{3}\upsilon\zeta_{bs}(L-M) \\ \zeta_{cs}M & \zeta_{cs}M & \zeta_{cs}L & \frac{1}{3}\upsilon\zeta_{cs}(L-M) \\ \upsilon\zeta_{fs}M & \upsilon\zeta_{fs}L & \upsilon\zeta_{fs}M & -\upsilon^2\zeta_{fs}L \end{bmatrix}$$

$$[e_{sat}] = \begin{bmatrix} \lambda'_{PM,a}\zeta_{as} - \lambda'_{PM,0}\zeta_{as} \\ \lambda'_{PM,b}\zeta_{bs} - \lambda'_{PM,0}\zeta_{bs} \\ \lambda'_{PM,c}\zeta_{cs} - \lambda'_{PM,0}\zeta_{cs} \\ \upsilon\lambda'_{PM,b}\zeta_{fs} \end{bmatrix}$$

According to (5.13), resistive unbalance faults generate negative-sequence components due to the loss of symmetry in $[R_{sf,sat}]$. In a faulty machine the abovementioned conditions may result in third harmonic components in the current spectrum even with sinusoidal feeding. It is so because negative-sequence components may cause a phase of the machine to work instantaneously beyond the knee point of the B-H curve, thus generating saturation and third harmonic components in the current spectrum.

Shorted turns also generate negative-sequence components due to the lack of symmetry in matrixes $[R_{sf,sat}]$ and $[L_{sf,sat}]$. Additionally, the circulating current i_f has a third harmonic component which is greatly influenced by the rotor magnets geometry [39]. Equation (5.13) also predicts a link between the fault current i_f and the stator currents i_a, i_b and i_c. Hence, the stator currents spectrum must present a third harmonic component originated by the shorted-turns which is not due to saturation effects since i_f has a demagnetizing effect [39].

In case of analyzing third harmonic current components, they may be influenced by the motor source, thus making difficult the fault diagnosis.

Summarizing, the first harmonic of the ZSVC and the third one of the stator currents are proposed in this work to detect and discriminate resistive unbalance and inter-turn faults.

5.3 Simulation and experimental results

Simulation and experimental results with the reference motor (Appendix A) are compared in this section. Simulations have been carried out according to equations derived in Section 5.2, which have been implemented by means of Matlab/Simulink. Input data required to perform simulations (flux harmonics, saturation curve, etc.) are obtained from the FEM model detailed in [39, 56].

The reference motors (Appendix A) were especially modified to deal with the studied faults. The adapted SPMSM allows adjusting the shorted turns number. The stator resistances of the healthy motor were balanced to 1.50 Ω A 1 Ωresistance was connected in series with phase A of the unbalanced SPMSM. To decouple measurements from the motor source, the ZSVC was measured by using a three-phase wye-connected balanced resistive network as detailed in 4.3. The ZSVC was measured between the neutral point of the stator windings and the central point of the three-phase balanced resistor network.

5.3.1 Fault current

Inter-turns short-circuit simulations including spatial harmonics were made, with the aim to demonstrate the accuracy of proposed model.

Fig.5.2 shows simulation results of the evolution of the fault current as a function of the number of short-circuited turns. As the number of shorted-turns increases, the harmonic distortion of i_f reduces because an increase of such current implies a reduction of the flux due to the permanent magnets.

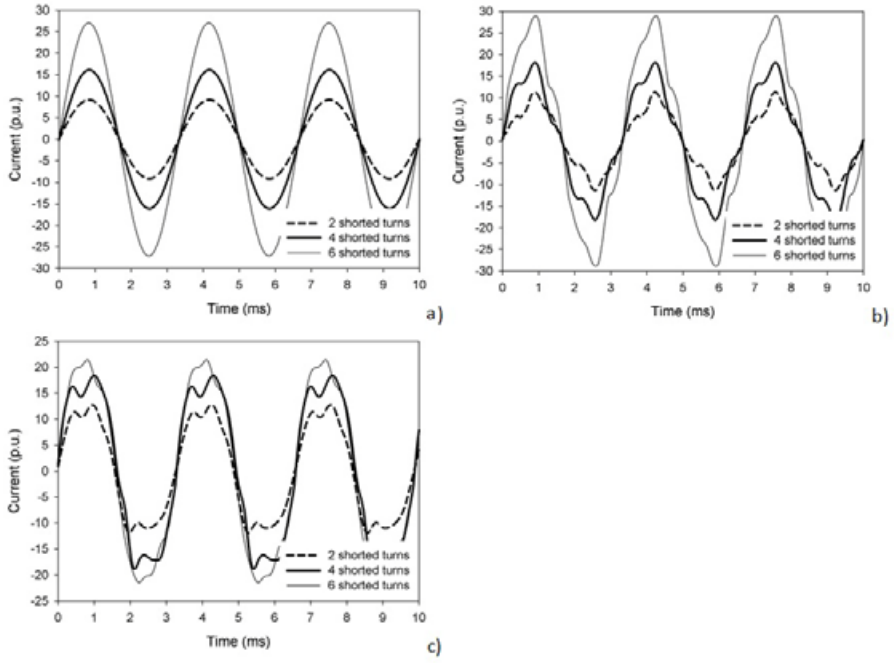

Fig.5.2. Current in the shorted turns for different fault levels at 6000 r/min and rated load. a) Model without spatial harmonics. b) New proposed model with spatial harmonics. c) Experimental.

Results from Fig.5.2 shows that the proposed model results are finer than those obtained from the simulation model that does not account for the spatial harmonics.

Once again Fig.5.3 shows a better performance of the model proposed in this work. For a given fault severity, the fault current increases with the SPMSM speed because the induced voltage due to permanent magnets flux increases linearly as well, as shown in Fig.5.3.

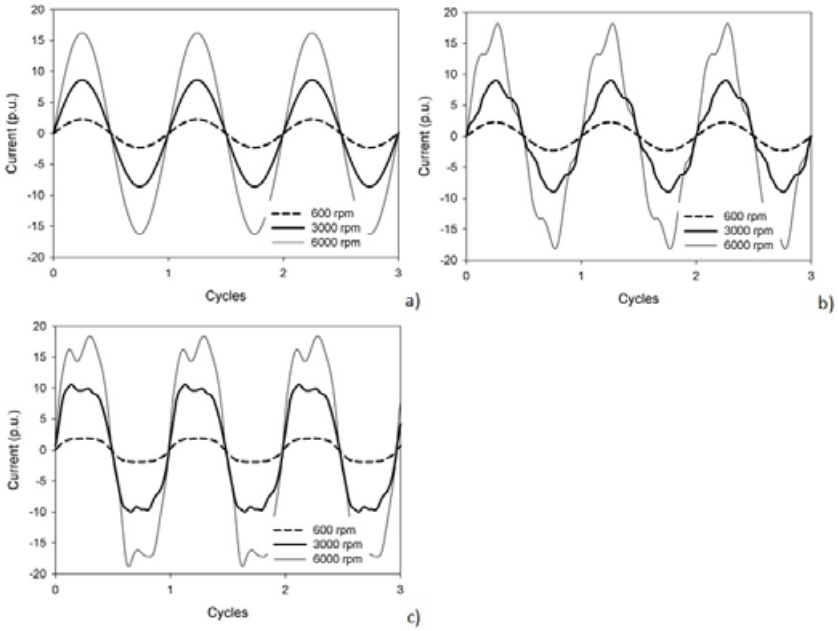

Fig.5.3. Current in four shorted turns for different speeds when running at 6000, 3000 and 600 r/min and rated load. a) Model without spatial harmonics. b) New proposed model with spatial harmonics. c) Experimental.

5.3.2 Mixed resistive unbalance and inter-turns short-circuits at low speed and different loads

Results presented in this section are based on a healthy motor (H), a motor with a resistive unbalance in phase a (RUa), a motor with four turns in short-circuit in phase A (SCb) and a motor combining both faults (RUa+SCb). The study of both types of faults is performed by analyzing the amplitude of the third harmonic of the stator currents and the first harmonic of the ZSVC.

Fig.5.4.a and Fig.5.4.b, show respectively, simulation and experimental results of the third harmonic of the stator current in phase A when the motors H, RUa, SCb and RUa+SCb are analyzed. All motors are tested under different load conditions when operating at 1500 r/min.

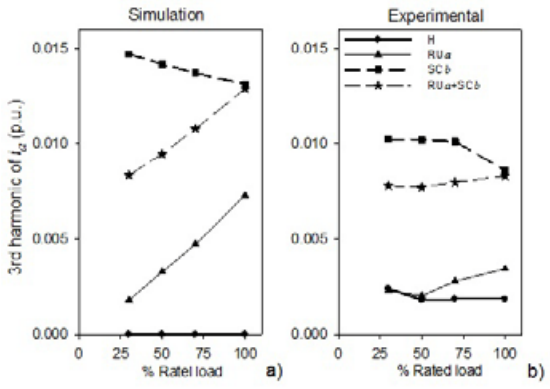

Fig.5.4. Third harmonic component of stator current in p.u. (SPMSM operating at 1500 r/min). a) Simulation results. b) Experimental results.

Fig.5.5.a and Fig.5.5.b show, respectively, simulation and experimental results of the first harmonic component of the ZSVC when the motors H, RUa, SCb and RUa+SCb operate under different load levels at 1500 r/min.

Results presented in Fig.5.4 and Fig.5.5 show a similar behavior in both the third harmonic of the currents and the first harmonic of the ZSVC. In the case of resistive unbalance, when analyzing its behavior under different load conditions, it can be approximated by a straight line intersecting the origin, as deduced from the first term in (5.5). In the case of short-circuited turns, both the third current harmonic and the first ZSVC harmonic are a consequence of the current circulating through the shorted-turns, which is greatly influenced by the actual speed of the SPMSM [39]. Hence, the behavior of these harmonics is almost not affected by the load of the motor. In the case of mixed faults (RUa+SCb), the third harmonic of the stator currents and the first one of the ZSVC have a linear behavior with respect to the load level. However, in this case the resulting straight line does not cross the origin because of the offset introduced by the short-circuit current, as explained in (5.5).

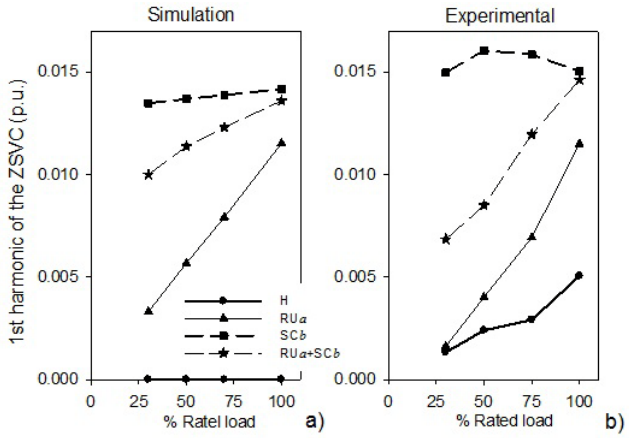

Fig.5.5. First harmonic components of the ZSVC in p.u. (SPMSM operating at 1500 r/min). a) Simulation results. b) Experimental results.

5.3.3 Mixed resistive unbalance and inter-turns short-circuits at high speed and different loads

Fig. 5.6.a. and Fig. 5.6.b show, respectively, simulation and experimental results of the third harmonic of the stator current in phase A from motors H, RUa, SCb and RUa+SCb. All motors are tested under different load levels at 5500 r/min.

Fig. 5.7.a and Fig. 5.7.b show, respectively, simulation and experimental results of the first harmonic component of the ZSVC from motors H, RUa, SCb and RUa+SCb at 5500 r/min.

Results from Fig. 5.6 and Fig. 5.7 indicate that at high speed, the resistive unbalance presents a quasi-linear behavior with respect to the load level (for both the third harmonic of the stator currents and the first one of the ZSVC), as in the case of low speed operation. When considering shorted-turns, the harmonics amplitudes are almost independent of the load level. Additionally they are higher at high speed

than at low speed operation since the circulating current i_f increases with the motor speed. When dealing with both faults simultaneously (RUa+SCb), the behavior of the harmonic frequencies is similar to that of the shorted-turns. It is so because the amplitude of the i_f harmonics prevails over the amplitude of the harmonics due to resistive unbalance.

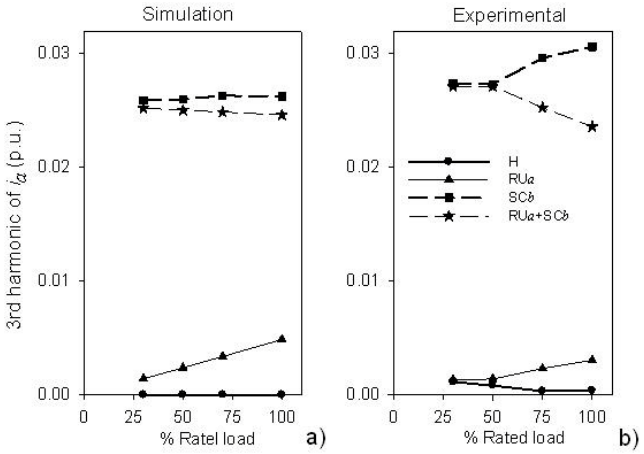

Fig. 5.6. Third harmonic components of stator current in p.u. (SPMSM operating at 5500 r/min). a) Simulation results. b) Experimental results.

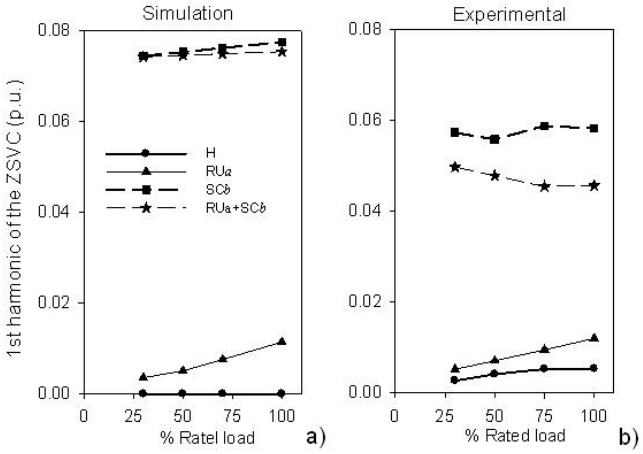

Fig. 5.7. First harmonic components of ZSVC in p.u. (SPMSMS at 5500 r/min.) a) Simulation results. b) Experimental results.

5.3.4 Mixed unbalanced and inter-turns short-circuits at rated load and different speeds

Fig. 5.8 shows simulation and experimental results of the third harmonic of the stator current in phase A from motors H, RUa, SCb and RUa+SCb. All motors are tested under different speeds at rated load.

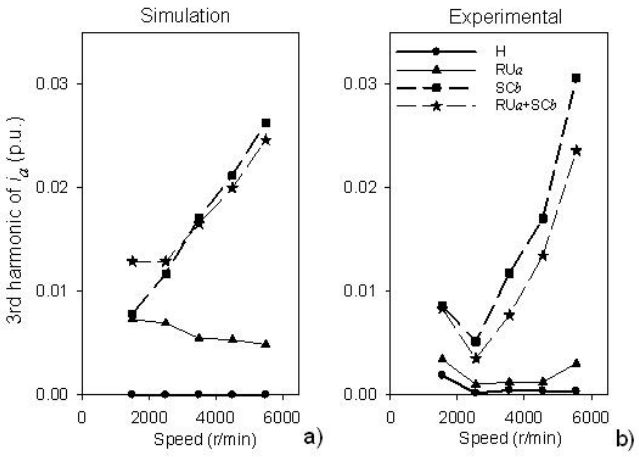

Fig. 5.8. Third harmonic component of the stator current in p.u. (SPMSM at rated load). a) Simulation results. b) Experimental results.

Fig. 5.9 show simulation and experimental results of the first harmonic of the ZSVC when the SPMSMs are tested at rated load under different speed conditions.

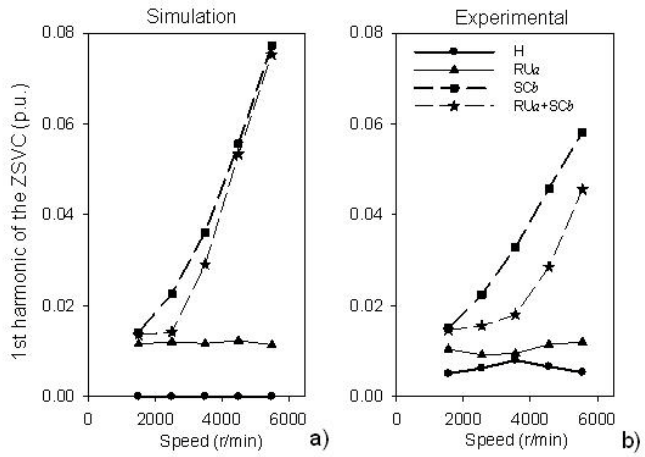

Fig. 5.9. First harmonic component of the ZSVC in p.u. (SPMSM at rated load). a) Simulation results. b) Experimental results.

From Fig. 5.8 and Fig. 5.9 it is deduced that in case of resistive unbalance the amplitudes of the first harmonic of the current and the first harmonic of the ZSVC are nearly independent of the speed. This result is corroborated by (5.5), since the mathematical expression of the ZSVC is independent of the actual speed of the SPMSM. However, in case of shorted-turns, the behavior of the analyzed harmonics is almost linear with the speed. The second and third terms in (5.5) are a function of the current i_f, whereas this last increases with the motor speed because of the induction of the rotor magnets [39]. However, when both faults occur simultaneously, the linearity between the harmonics amplitudes and the speed decreases.

According to the experimental results presented in this work, the third harmonic of the stator currents has a similar behavior than that of the first harmonic of the ZSVC.

Summarizing, the results presented in this section show that it is possible to diagnose and discriminate resistive unbalance from stator winding inter-turn faults in SPMSMs by analyzing different operating conditions. In case of a resistive unbalance the amplitude of the analyzed harmonics remains nearly constant under speed changes, but increases linearly with the load level. Contrarily, in case of short-circuit faults, the amplitude of the studied harmonics increases linearly with the motor speed but remains nearly constant under load level changes.

As explained, from the analyzed results, the experimental ZSVC first harmonic has a closer behavior when compared with simulation results than the third harmonic of current. This is so because the ZSVC is decoupled from the motor source, which may significantly influence current spectrum [59]. However, the ZSVC requires accessing to the neutral point of the stator windings as occurs in fault tolerant schemes where an extra inverter leg is added [17, 77]]. TABLE 5.1 summarizes the results of this section.

TABLE 5.1. Change in the third harmonic of the stator currents and in the ZSVC first harmonic amplitude

	RU	SC	RU+SC
Speed increase			
Low load	≈ constant	≈ linear	≈ linear
High load	≈ constant	≈ linear	non-linear
Load increase			
Low speed	≈ linear	≈ constant	≈ linear
High speed	≈ linear	≈ constant	≈ constant

RU: resistive unbalance

SC: short-circuited turns

RU+SC: resistive unbalance and short-circuited turns

5.3.5 Mixed resistive unbalance and inter-turns short-circuits generalization

From (5.5), the first harmonic amplitude of the ZSVC may be rewritten as a function of the speed and the load level as:

$$V_{0,measured}^2 = \left(-\frac{1}{3} R_s (k-1) I_a \cos\gamma + \frac{1}{3} \upsilon R_s I_f \right)^2 + \left(-\frac{1}{3} R_s (k-1) I_a \sin\gamma + \frac{1}{3} \upsilon\omega (L+2M) I_f \right)^2 \quad (5.14)$$

Where γ is the phase shift between the stator current in phase A and current i_f. Assuming that the SPMSM has unity power factor, the angular displacement γ between i_a and i_f is 120º. Fig. 5.10 shows the behavior of the first harmonic amplitude of the ZSVC as predicted by (5.14) with a SPMSM under resistive unbalance at different speeds and load conditions. It shows that the amplitude of the first harmonic is nearly independent of the speed and is proportional to the load level.

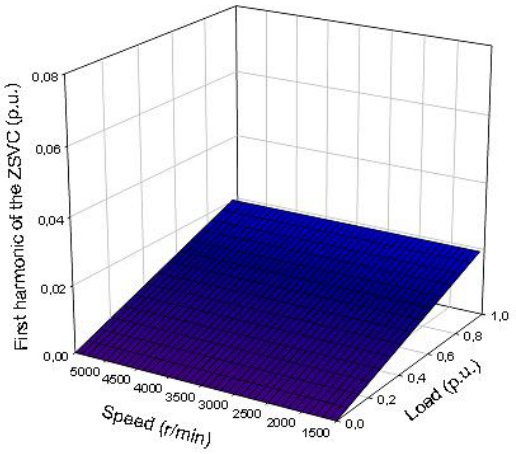

Fig. 5.10. Resistive unbalance in phase A (RU*a*). First harmonic amplitude evolution of the ZSVC at different speeds and load conditions.

Fig. 5.10 shows the evolution of the first harmonic amplitude of the ZSVC as predicted by (5.14) with the SPMSM running under fault of four shorted-turns at different speeds and load conditions. It shows that the amplitude of the first harmonic is nearly independent of the load level and increases almost linearly with speed. The deviation from the linearity is due to the inductive effect of the last term in (5.14), which becomes important at high speeds.

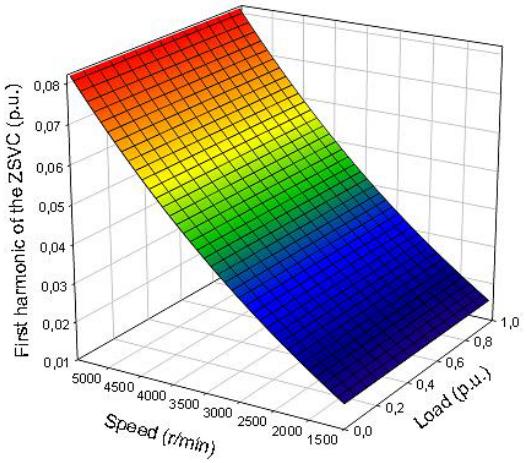

Fig. 5.11. Four short-circuited turns in phase B (SCb). First harmonic amplitude evolution of the ZSVC at different speeds and load conditions.

Fig. 5.12 plots the behavior of the first harmonic amplitude of the ZSVC with the SPMSM running with both resistive unbalance and four shorted-turns at different speeds and load conditions. It indicates that as the load increases the linearity of the response curve decreases due to the combined effects of both resistive unbalance and shorted-turns. While the resistive unbalance produces a linear increase of the

ZSVC first harmonic amplitude with the load level, shorted-turns faults produce a non-linear increase with the motor speed.

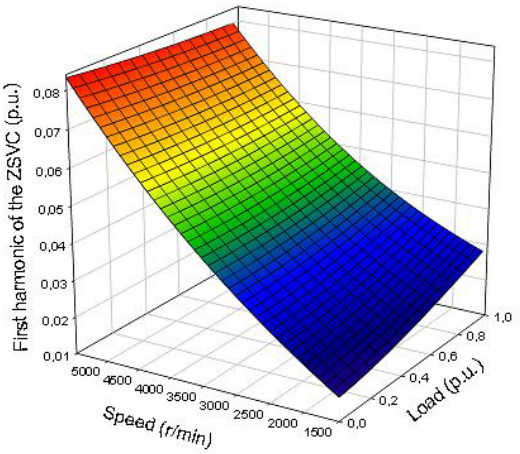

Fig. 5.12. Resistive unbalance in phase A and four short-circuited turns in phase B (RUa+SCb). First harmonic amplitude evolution of the ZSVC at different speeds and load conditions.

5.4 Comparative with different windings configurations

To analyze the influence of the winding configuration on the harmonic content of the stator currents and the ZSVC, the five motors analyzed in section 4.5 were modified to deal with inter-turns short circuits faults. All the faulty motors have the same ratio between faulty and healthy turns (TABLE 5.2). As in 4.5, FEM simulations were carried out under stationary conditions. In the case of inter-turns short-circuits faults, it is presented results only from serial connected windings because there are not significant differences when compared with the case of parallel connections.

TABLE 5.2. Parameters of SPMSMs with inter-turn short-circuits

Features	m1	m2	m3	m4	m5
Slots/pole/phase (*q*)	1/2	1+1/4	1+1/4	3	3
Poles (2*p*)	16	8	8	4	4
Slots number	24	30	30	36	36
Turns per phase	384	200	200	144	144
Layer type	Double	Double	Single	Single	Double
Short pitch	No	Yes	No	No	Yes
Variable pitch	No	No	Yes	No	No
Symmetric winding	Yes	Yes	No	Yes	Yes
Shorted turns number	8	6	6	4	4

Fig. 5.13 shows the stator currents spectra for the five series-connected winding configurations. Results indicate that in the case of SPMSM with inter-turns short-circuits; the stator configuration can change

integer harmonics amplitudes (including even harmonics in asymmetric windings). A summary of these results are as follows:

- m1 (q = 1/2, double layer): the amplitudes of the constructive harmonics (5-th and 7-th) increase significantly in the faulty motor and there appear new triplen harmonics (3-th and 9-th).
- m2 (q = 1+1/4, constant-pitch): in the case of a faulty SPMSM the constructive harmonics amplitudes (5-th and 7-th) increase significantly and new triplen harmonics components (3-th, and 6-th) appear in the currents spectrum.
- m3 (q = 1+1/4, variable-pitch): the 5-th harmonic amplitude decrease in the faulty motor, however the amplitude of 7-th harmonic increases. Furthermore, the faulty motor current spectrum contains new integer harmonics (3t-h, 4-th, 6th, etc).
- m4 (q = 3, full-pitch): when dealing with a faulty machine, the constructive harmonics amplitudes (5-th and 7-th) increase and new triplen harmonics appear in the spectrum (3-th and 9-th).
- m5 (q = 3, short-pitch): in the case of faulty machine, the amplitudes of the 5-th harmonic increases, however the amplitude of the 7-th decreases. New triplen harmonics (3-th and 9-th) appears in the spectrum of the faulty SPMSM.

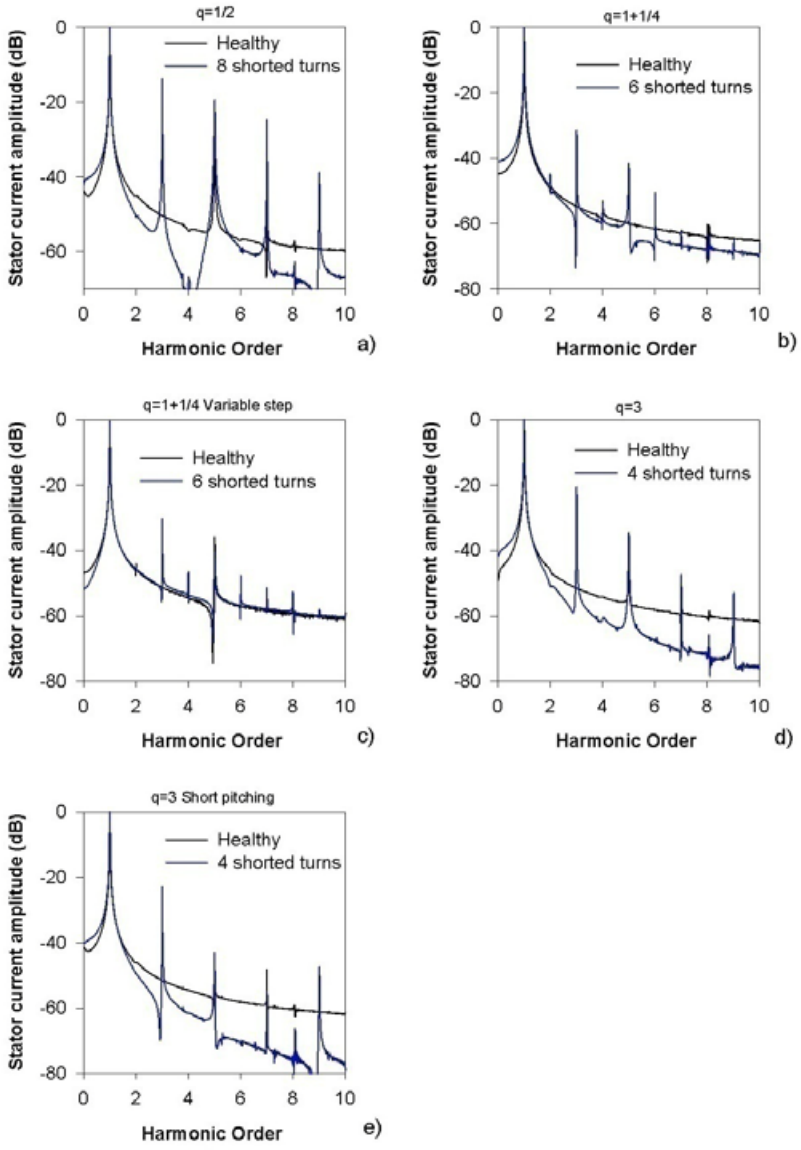

Fig. 5.13. Currents spectra for healthy and faulty SPMSMs. a) q=1/2 (8 shorted turns) b) q=1+1/4 (6 shorted turns) c) q=1+1/4 with variable step (6 shorted turns) d) q=3 (4 shorted turns) e) q=3 with short pitching (4 shorted turns)

Results from Fig. 5.14 show the influence of the winding configurations on the ZSVC spectrum. A summary of these results is as follows:

- m1 (q = 1/2, double layer): the amplitudes of the ZSVC constructive harmonics (3-th and 9-th) decrease significantly in the case of faulty SPMSM and new odd harmonics appear in the ZSVC spectrum (1-th, 5-th and 7-th).
- m2 (q = 1+1/4, constant-pitch): in the case of faulty SPMSM, amplitudes the constructive harmonics amplitudes (3-th, 6-th and 9-th) decrease slightly. Additionally, new integer harmonics appear in the ZSVC spectrum (1-th, 2-th, 4-th, 5-th, 7-th etc).

- m3 (q = 1+1/4, variable-pitch): similarly to the case of constant pitch, the constructive harmonics amplitudes decrease slightly and new integer harmonics appear in the ZSVC spectrum.
- m4 (q = 3, full-pitch): when dealing with a faulty machine, the constructive harmonics amplitudes (3-th and 9-th) decrease slightly. New odd harmonic components appear in the ZSVC spectrum (1-th, 5-th and 7-th), which have large amplitudes.
- m5 (q = 3, short-pitch): similarly to the case of a full-pitch motor, the constructive harmonics amplitudes decrease slightly. New odd harmonics components appear in the ZSVC spectrum.

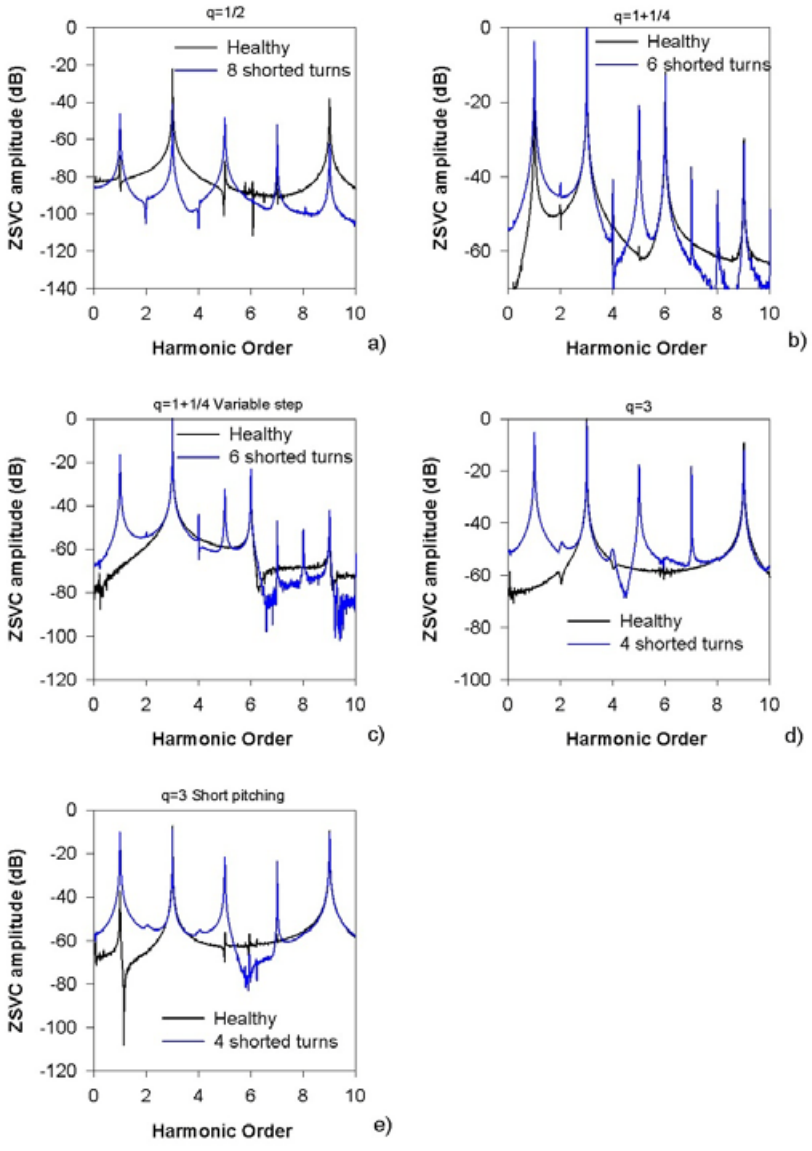

Fig. 5.14. ZSVC spectra for healthy and faulty SPMSMs. a) q=1/2 (8 shorted turns) b) q=1+1/4 (6 shorted turns) c) q=1+1/4 with variable step (6 shorted turns) d) q=3 (4 shorted turns) e) q=3 with short pitching (4 shorted turns)

Current and ZSVC harmonics due to inter-turns faults are related with the faulty current harmonics, which are a consequence of back-emf waveform. In order to investigate this phenomena, new simulations with motor m3 (q=1+1/4, variable pitch) were made, since it is the motor with the highest number of new harmonics.

Fig. 5.15 shows the back-emf spectrum from the six faulty turns When the SPMSM operates as a generator under no-load conditions. This spectrum contains odd and even harmonics because of the winding asymmetry.

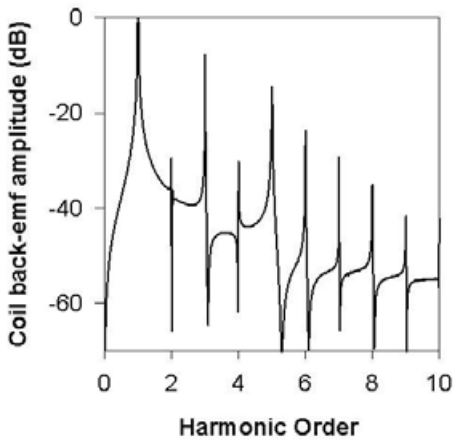

Fig. 5.15. Back-emf spectrum induced in the faulty turns. (q=1+1/4, variable pitch)

To study inter-turns short-circuit current effects, a new FEM simulation was performed by injecting a pure sine-wave current (50 A with only the fundamental harmonic) through the faulty turns as shown in Fig. 5.16.

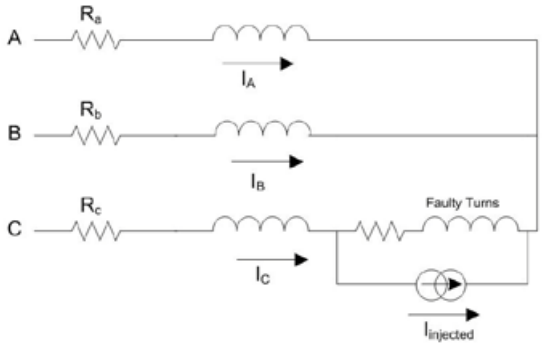

Fig. 5.16. Injected current through the faulty turns.

Fig. 5.17 shows the spectrum of the injected current and that obtained from FEM simulations with a real inter-turn short-circuit fault. An important characteristic of the short-circuit current is that it contains the same harmonics that those found in the spectrum of the faulty turns back-emf.

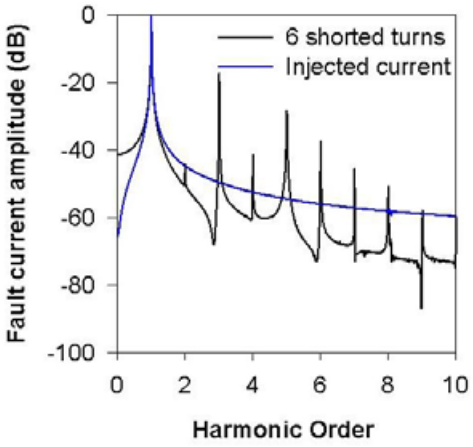

Fig. 5.17. Injected and real short-circuit current through the faulty turns.

Fig. 5.18 shows the stator current and ZSVC spectra from simulations shown in Fig. 5.17. In the case of the stator currents spectrum obtained by injecting the current in the shorted-turns (Fig. 5.18.a), in contrast with the case of the real inter-turn fault, there are not new harmonics as a result of the fault. It is important to highlight that the third harmonic disappears in the former case. Consequently, this third harmonic could be originated by the third harmonic of the short-circuit current, and not from the saturation effects of the ferromagnetic core.

As in the case of the current spectrum, the ZSVC spectrum presented in Fig. 5.18 does not contain additional harmonics besides the first harmonic.

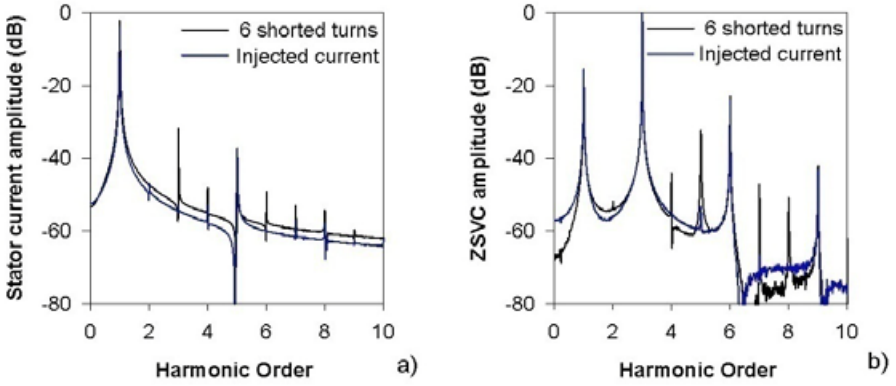

Fig. 5.18. Spectra obtained by injecting current and considering real inter-turn short-circuits (SPMSM with q=1+1/4 and variable pitch). a) Stator current spectrum. b) ZSVC spectrum

5.5 Conclusion

In this chapter resistive unbalance and stator windings inter-turns short-circuits faults in SPMSMS are analyzed. In addition, a mathematical model for the study of such faults has been developed.

Resistive unbalance faults produce negative-sequence components caused by stator asymmetry. These components may produce stator saturation which generates triplen harmonics in the current spectrum even with sinusoidal feeding.

When a motor runs with inter-turn short-circuit faults, both the SPMSM speed and the ratio between shorted and the total number of turns in the damaged phase greatly affects the fault severity. Therefore a short-circuit involving several turns at low speed can be equivalent to few shorted turns at high speed.

Resistive unbalance and inter-turns short-circuits can be diagnosed by means of the first harmonic of the ZSVC and the third one of the stator currents. The amplitude of analyzed harmonics increase linearly with the load in the case of unbalance resistance, contrarily, increase linearly with the speed under inter-turn short-circuits faults

It is demonstrated that even though the ZSVC-based method requires an accessible neutral point, its spectrum is decoupled from the motor supply influence. Contrarily, the stator current based method does not need an extra stator connection. However, the stator currents spectrum can be influenced by the converter effects, making difficult the diagnosis.

Additionally in this chapter it is studied the winding configuration influence in the inter-turns short-circuits identification by means of FEM simulations.

6. DIAGNOSIS OF SPMSMS OPERATING UNDER NON-STATIONARY CONDITIONS BY MEANS OF ORDER TRACKING FILTERING

In this chapter it is proposed a novel approach to detect demagnetization and windings inter-turn short-circuits in a SPMSM running under non-stationary speed conditions and different load levels. Additionally, the Vold-Kalman filtering order tracking (VKF-OT) method is introduced to track selected harmonics. In the automobile industry harmonic frequencies, i.e. frequencies that are integer or fractional multiples of the fundamental one are commonly referred as orders. The order spectrum represents the signal amplitude as a function of the harmonic order instead of its absolute frequency [31]. Order or harmonic tracking (OT) is a process for recovering a particular order waveform in the time domain from a given waveform which usually contains multiple harmonics and a noise signal [31]. OT is recognized as an effective instrument to deal with non-stationary vibration and noise signals whose amplitudes and frequencies are directly related with the speed of a rotating shaft [78]. One of its main appealing features is that allows identifying orders when dealing with non-stationary data, thus eliminating the influences of varying rotational speed. However, high-resolution OT-based methods require an accurate and simultaneous acquisition (at the same sampling frequency) of the machine speed and the input signal of interest [79]. One of the most suitable and promising techniques for tracking harmonic frequencies in machines running under non-stationary conditions is the Vold-Kalman filter based order tracking (VKF-OT) algorithm.

This chapter also develops and analyzes the behavior of fault indicators for detecting demagnetization and winding inter-turn short-circuits which are especially designed to deal with non-stationary speed conditions.

Time-frequency methods such as wavelet-based analysis [33] or methods based on the Cohen's class [34] among others may also be applied to track harmonic frequencies. However, in order to improve the resolution, some of the methods based on time-frequency transforms require filtering the analyzed signal in order to remove the fundamental harmonic frequency, because its amplitude is often much greater than the related fault harmonic [80]. Additionally, most of them calculate the whole or at least a broad band of the spectrum at each time prior obtaining a fault indicator index. Conversely, the VKF-OT only extracts the harmonic frequency of interest (but not the whole spectrum) by applying an adaptive band-pass filter centered on that frequency. When tracking a very small harmonics number, VKF-OT is a compact solution since it includes harmonic extraction and tracking steps. Hence, VKF-OT algorithm minimizes problem data structure and therefore its computational burden.

6.1 Vold-Kalman Order Tracking Filtering

VKF-OT provides several advantages over other OT methods. It allows extracting both the amplitude and phase of the analyzed orders at each time instant directly from the original data, working directly in the time domain [79]. Furthermore, VKF-OT allows an accurate identification of close and crossing orders over a wide speed range of the studied motor with no smearing-related problems while presenting improved order resolution compared to other OT techniques. Additionally, its tracking performance does not depend of the slew rate (rotational speed) [81].

VKF-OT is based on Kalman filtering, allowing accurate tracking of orders of known frequency from noisy signals. The VKF-OT was first developed by Havard Vold [81] to track sinusoidal waves acquired using a constant sampling period.

The VKF-OT algorithm first-generation basically consists on processing the analyzed signal through an adaptive filter whose central frequency is calculated at each time from the current motor speed, while its bandwidth is selected by applying a specific criterion. Hence, the time signal outputted by the VKF algorithm is the result of applying a band-pass filter around the analyzed order. Next, the order is extracted from this latter signal by applying an envelope detector algorithm [79]. The second-generation VKF-OT algorithm uses a different envelope detector, based on a polynomial fit. Then it is filtered by applying some particular method[81]. The selectivity of the second-generation algorithm may settled by selecting the polynomial order (number of filter poles), which usually ranges from 1 to 4, the latter being the one with the best selectivity [79]. The VKF-OT algorithm applied in this work is that found in the Vibra Tools Toolbox for Matlab.

Selection of the filter bandwidth is a key issue when applying VKF-OT technique, since a narrow bandwidth allows separating close components but with a longer response time (limited ability to follow sharp changes in the signal amplitude) and vice versa [78]. Hence, to choose a suitable bandwidth it is necessary some prior information of the analyzed signal.

Once the analyzed harmonic has been obtained from the VKF-OT, a peak detector algorithm is applied to find the amplitude envelope. The shape of this envelope is greatly influenced by the fault nature. The peak detector algorithm consists of two steps. The absolute value of the tracked harmonic waveform is calculated in the first step. Subsequently, their peaks are detected in the second step, and the tracked harmonic envelope is obtained from the whole set of peak points. Fig. 6.1 shows a diagram of the mathematical process for envelope extraction from tracked harmonic amplitude.

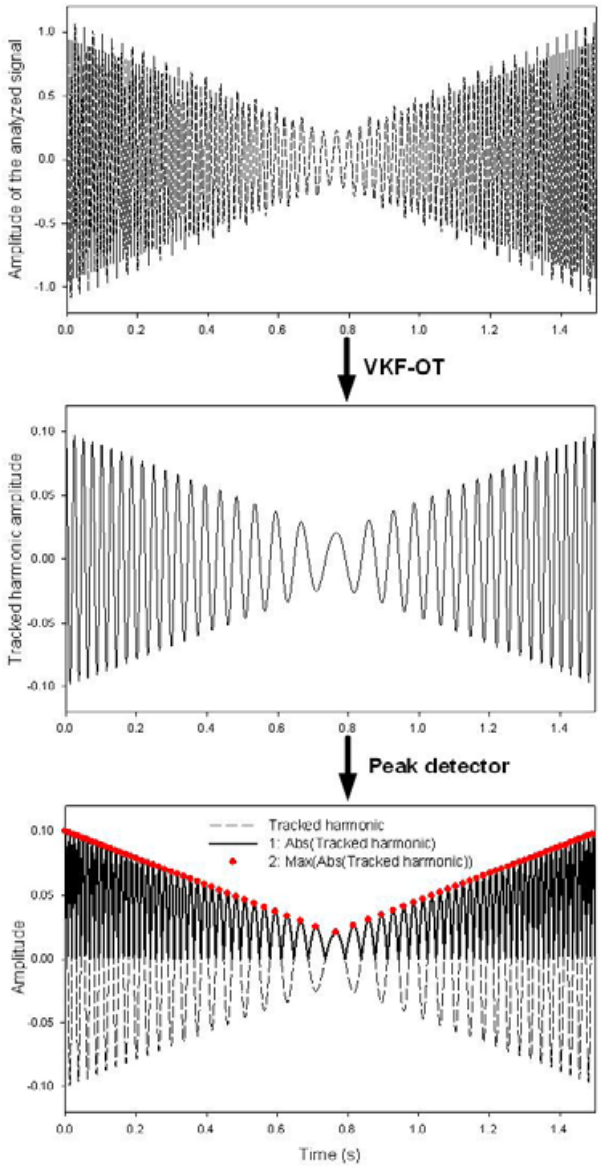

Fig. 6.1. Mathematical process for envelope extraction from the tracked harmonic amplitude.

6.2 Demagnetization harmonics tracking

According to section 4.1, when dealing with the reference motors (q = 1) (Appendix A) in the stator currents spectrum there is no presence of new fault harmonics. Hence, in order to diagnose demagnetization faults, constructive stator current harmonics must be analyzed. In section 4.4 the third harmonic of the ZSVC (fundamental harmonic of that signal) was analyzed for this purpose.

This section studies the behavior of the fifth current harmonic and the third ZSVC harmonic to diagnose demagnetization faults from experimental results. With this aim, the demagnetization index $1 - K_{dem}$, which was presented in section 4.3, is applied. The analyzed harmonics are tracked by applying the VKF-OT algorithm.

To discriminate between faulty and healthy conditions in any machine, a reference state is required. Here, that reference is obtained by performing a frequency sweep between 500 and 6000 r/min to the reference healthy machine. It is done by using a triangular speed profile as shown in Fig. 6.2 which emulates motor soft-starting and soft-stopping conditions. However, other speed profiles may be imposed since it is required data covering the whole speed range under analysis.

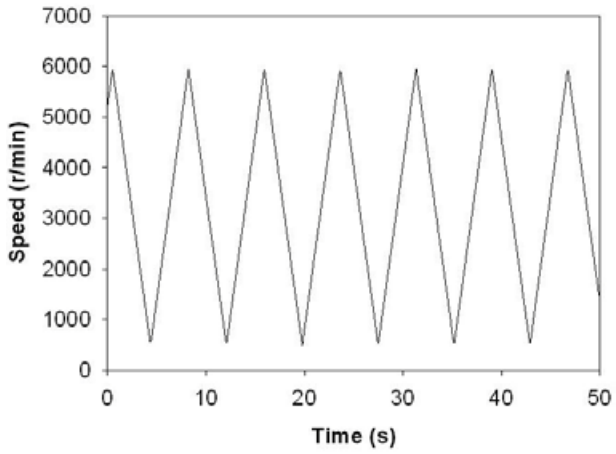

Fig. 6.2. Triangular speed profile from 500 to 6000 r/min, f=0.13 Hz

Fig. 6.3 shows the flow chart of the proposed demagnetization diagnosis method.

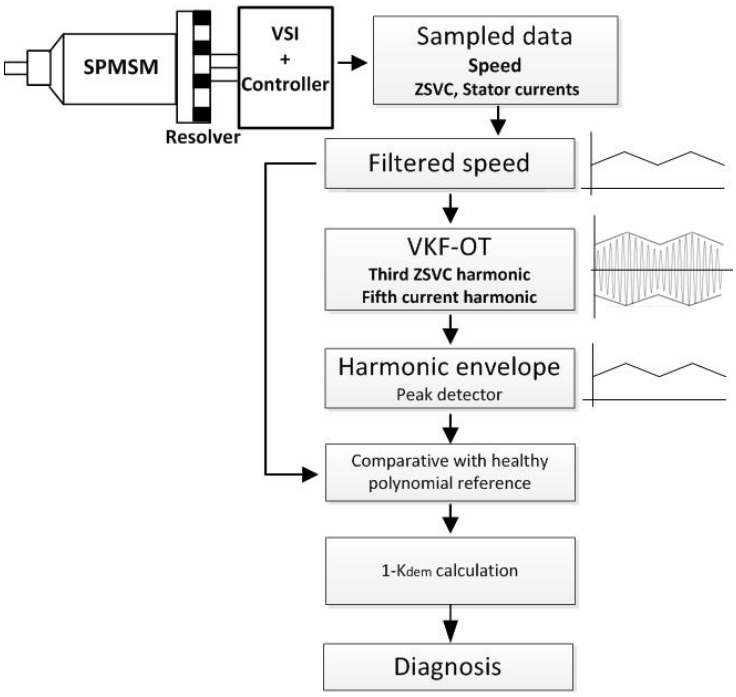

Fig. 6.3. Process chart of demagnetization diagnosis

Fig. 6.4 shows both the fifth current harmonic and the third ZSVC harmonic evolution with speed which have been tracked by applying the VKF-OT algorithm and the process detailed in Fig. 6.3.

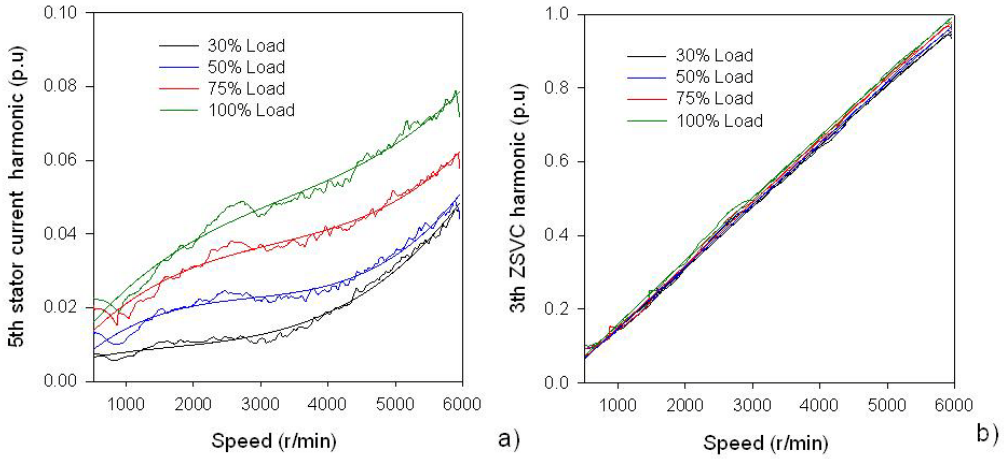

Fig. 6.4. Experimental results of a healthy SPMSM. Current and ZSVC harmonic evolution with speed (triangular speed profile, f = 0.13Hz). a) 5th current harmonic. b) 3th ZSVC harmonic

As shown in Fig. 6.4, a third-order polynomial fit of the analyzed harmonics amplitude with the speed has been applied. Results presented clearly show that load level greatly influences third current harmonic amplitude. Contrarily, the behavior of the third ZSVC harmonic is almost independent of the load conditions.

Next, a partially demagnetized SPMSM is analyzed. The faulty machine has two poles out of six 75% magnetized, leading a theoretical demagnetization index $1 - K_{dem} = 0.916$. The experimental tests carried out include a speed change between 3500 and 5500 r/min and a speed change between 500 and 2500 r/min. The triangular speed profiles frequencies are f = 0.36 Hz and f = 0.18 Hz, as detailed in Fig. 6.5.

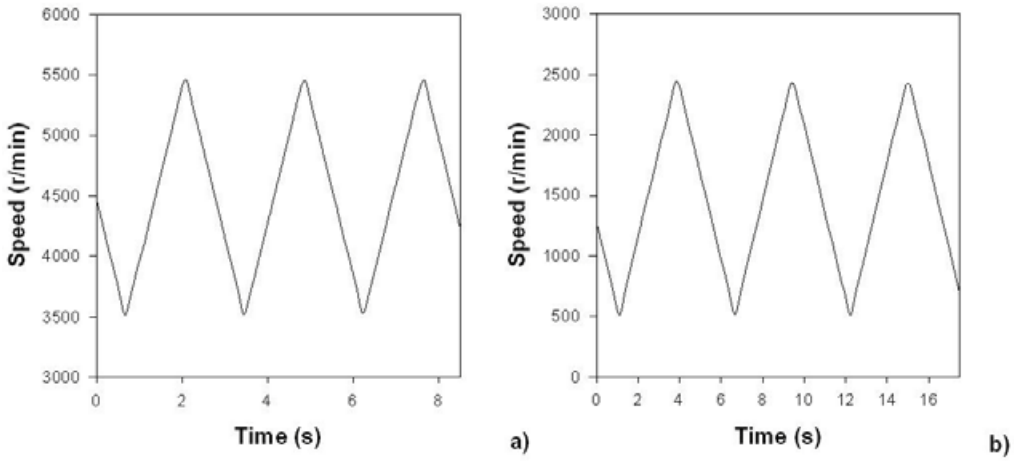

Fig. 6.5. Triangular speed profile a) 3500-5500 r/min, f=0.36 Hz. b)500-2500 r/min, f=0.18 Hz

As done in the case of the healthy machine, when dealing with the demagnetized motor, the fifth current harmonic and the third ZSVC harmonic are tracked by means of the VKF-OT algorithm when applying the above-explained speed changes. This procedure was applied under different load conditions. Fig. 6.6 presents experimental results for healthy and demagnetized SPMSMs running with a 3500-5500 r/min speed triangular profile with 30% and 100% load conditions.

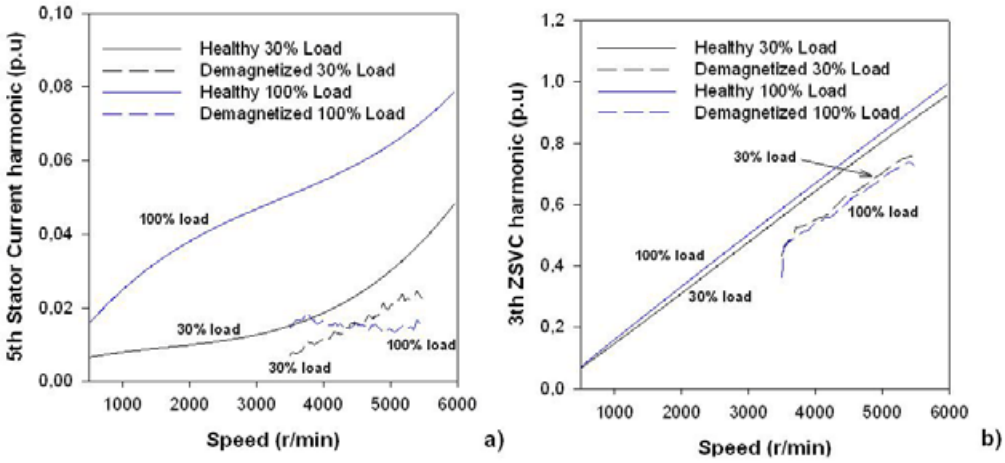

Fig. 6.6. Healthy and demagnetized harmonics amplitudes (3500-500 r/min, f=0.36 Hz). a) 5th Current harmonic amplitude b) 3th ZSVC harmonic amplitude

Results from Fig. 6.6 show that experimental values obtained from the partially demagnetized machine are below the reference polynomial fits obtained for the healthy machine. This is true for both the currents-based and the ZSVC-based methods. However, the ZSVC curves of the partially demagnetized SPMSMs are closer to the reference ones than in the case of the stator currents curves.

Fig. 6.7 shows experimental results obtained when a triangular speed change between 500 and 2500 r/min is applied.

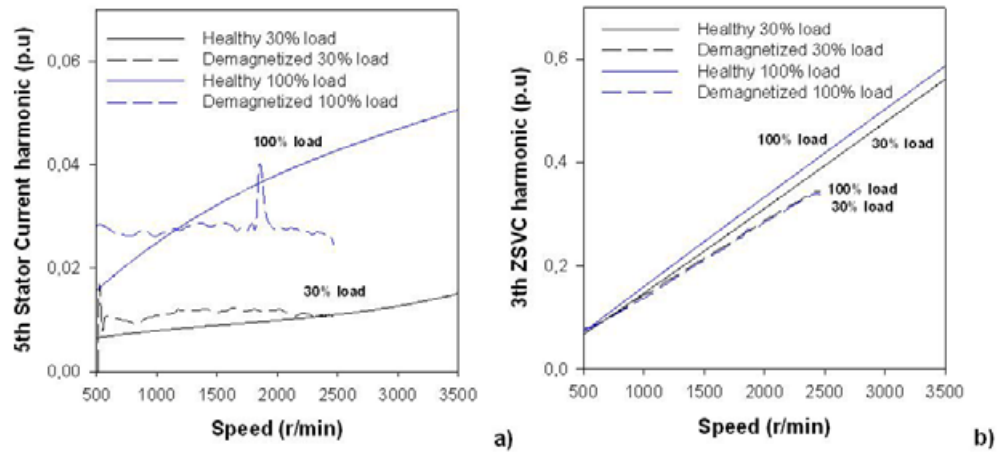

Fig. 6.7. Healthy and demagnetized harmonics amplitudes (500-2500 r/min, f=0.36 Hz). a) 5th Current harmonic amplitude b) 3th ZSVC harmonic amplitude

As shown in Fig. 6.7, it is difficult to diagnose demagnetization faults by the analysis of stator currents fifth harmonic at low speed, since some of the experimental points are above the reference curve obtained from the healthy motor conditions. Contrarily, the third ZSVC harmonic has a similar behavior than that obtained at high speed operation.

Fig. 6.8 details experimental values of the demagnetization index $1 - K_{dem}$ obtained from tests carried out under varying speed conditions.

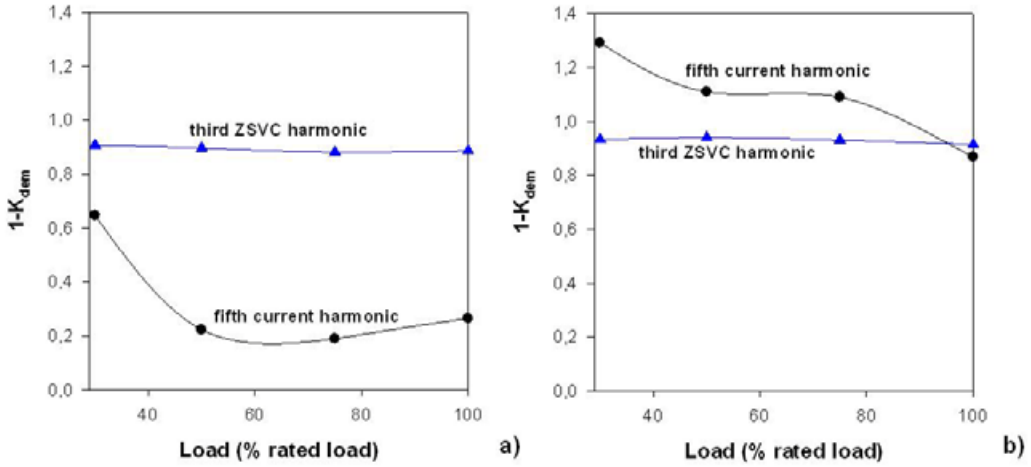

Fig. 6.8. Demagnetization index $1\text{-}K_{dem}$ obtained from experimental tests with healthy and partially demagnetized SPMSM by applying a triangular speed profile and different load conditions. a) 3500-5500 r/min. b) 500-2500 r/min.

Each data point shown in Fig. 6.8 was calculated by averaging the factors $1 - K_{dem}$ resulting from 30%, 50%, 75% and 100% load tests.

When analyzing the speed change from 3500 to 5500 r/min by means of both the stator currents and the ZSVC based methods, the demagnetization index $1 - K_{dem}$ is less than unity, thus making the diagnosis feasible. Although it is possible to quantify the fault severity by analyzing the third ZSVC harmonic, it is not possible from the analysis of the third harmonic of the stator currents.

In regard the data obtained from the 500-2500 r/min triangular speed change, it is possible to perform a quantitative fault diagnosis from the analysis of the third ZSVC harmonic. However, the fifth harmonic of the stator currents is greater than unity, thus it does not allow identifying such a fault. TABLE 6.1 presents the average values of demagnetization index $1\text{-}K_{dem}$ presented in Fig. 6.8.

TABLE 6.1. Experimental average values of the demagnetization factor $1 - K_{dem}$ obtained from the analysis of the fifth current harmonic and the third ZSVC harmonic.

Speed change	5th Current harmonic	3th ZSVC harmonic	Theoretical value
3500-5500 r/min	0.331	0.893	0.917
500-2500 r/min	1.090	0.928	0.917

6.3 Inter-turns short-circuit harmonics tracking

As done with demagnetization faults, detection of inter-turn short-circuits needs the actual motor speed. The VKF-OT algorithm is applied to track the ZSVC first harmonic component and the third one of stator currents. Fig. 6.9 shows a flow chart of the applied process in this section.

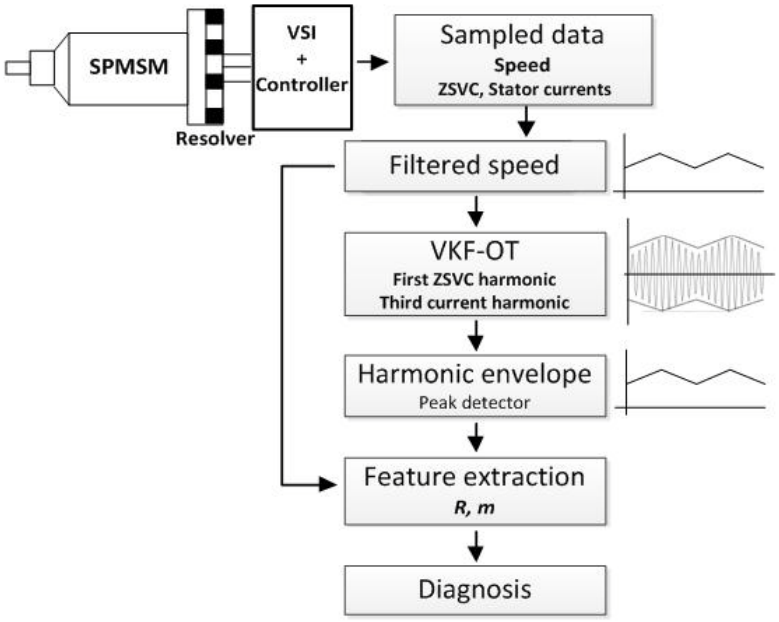

Fig. 6.9. Flow chart of the inter-turns short-circuits diagnosis process

According to section 5.1 the voltage drop in the shorted turns results in:

$$V_f = i_f R_f = \upsilon R_s (i_b - i_f) + \upsilon [L_s]^t \frac{d[i_{s,abc}]}{dt} - \upsilon^2 L \frac{di_f}{dt} + \upsilon \frac{d\lambda_{PM,b}}{dt} \tag{6.1}$$

The last term in equation above is the most significant one because of the important permanent magnets induction effect. Hence, the fundamental harmonic of the fault current i_f may be approximated as:

$$i_f \approx K \frac{d\lambda_{PM,b}}{dt} = k \frac{d\theta}{dt} sin\left(\theta - \frac{2\pi}{3}\right) = k\omega sin\left(\theta - \frac{2\pi}{3}\right) \tag{6.2}$$

Where θ is the rotor angular position and its time derivative is the angular speed ω. Hence, (6.2) predicts that for a given number of short-circuited turns, the fault current i_f is proportional to the motor speed. This result is corroborated experimentally, as shown in Fig. 6.10, being an experimental validation of the usefulness of equation (6.2).

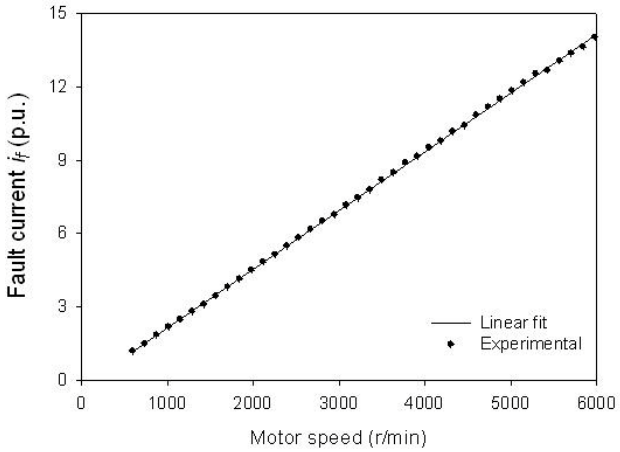

Fig. 6.10. Measured fault current i_f of a faulty SPMSM with 4 short-circuited turns. The results have been obtained under constant speed operation.

Next, the fault current i_f is measured in the case of 4 short-circuited turns when the SPMSM runs under non-stationary speed conditions. For this purpose a triangular speed profile with frequency 0.36 Hz is imposed within a speed interval range from 3500 to 5500 r/min. Fig. 6.11 shows the normalized speed profile and the normalized envelope of the fault current i_f. The envelope has been calculated by tracking the first harmonic component of the current i_f by means of the VKF-OT algorithm followed by the peak detector algorithm. Normalizations have been done by dividing the current value of the variable by its average value calculated over the analyzed time interval.

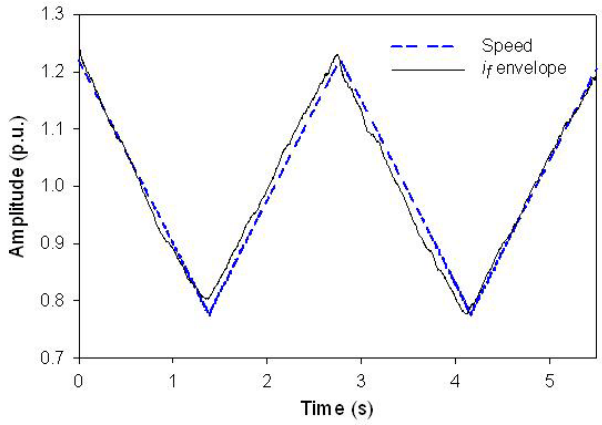

Fig. 6.11. SPMSM with 4 short-circuited turns running under a triangular speed profile from 3500 to 5550 r/min. Normalized triangular speed profile and normalized envelope of the first harmonic of the fault current i_f

Experimental results presented in Fig. 6.11 corroborate the assumption made in (6.2) which states that the fault current i_f is proportional to the current motor speed. However, under practical operating conditions the current i_f may not be measured. Hence, another fault indicator must be evaluated.

6.3.1 Behavior of stator currents third harmonic and the first one of ZSVC

Including (6.2) in (5.5), the first ZSVC harmonic component ($V_{0,1}$) may be approximated as (without unbalance):

$$V_{0,1} \approx k_1 \omega \sin\left(\theta - 2\frac{\pi}{3}\right) + k_2 \omega^2 \cos\left(\theta - 2\frac{\pi}{3}\right) + k_3 \frac{d\omega}{dt} \sin\left(\theta - 2\frac{\pi}{3}\right) \quad (6.3)$$

According to (6.3), the ZSVC first harmonic component has three terms. The first one is proportional to the speed, the second one is quadratic with the speed and the third one depends on speed time derivative. Depending on the imposed profile speed, each term in (6.3) has its own shape and its own central frequency. As the first term is proportional to the speed, it is the easier to track. This term is the one analyzed in this work.

In Fig. 6.12 the first term in (6.3) is tracked by means of VKF-OT algorithm when imposing a triangular speed profile. Next, a peak detector and an envelope extractor algorithm are applied. Afterwards, the tracked harmonic is normalized with respect to the third ZSVC harmonic amplitude (fundamental component) of a healthy SPMSM operating at 6000 r/min.

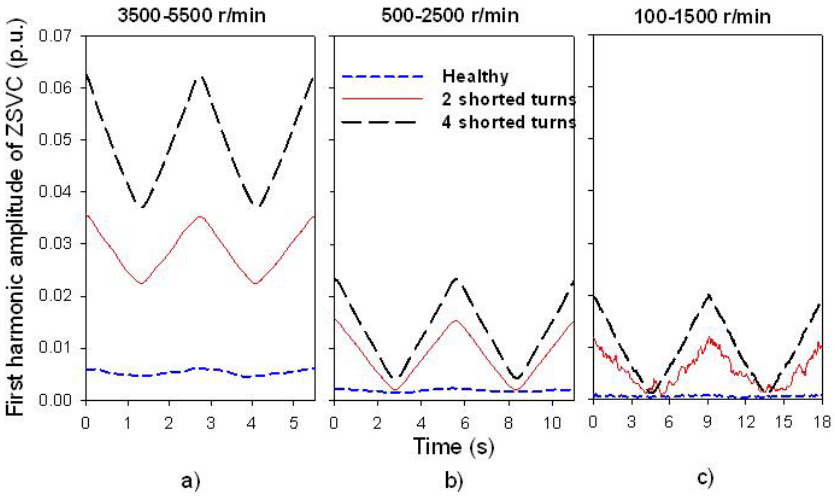

Fig. 6.12. Experimental envelope of the first ZSVC harmonic when the healthy and the faulty SPMSMs run under a triangular speed profile. The reference ZSVC value is 46 V. a) Speed change (f = 0.36 Hz) from 3500 to 5500 r/min. b) Speed change (f = 0.18 Hz) from 500 to 2500 r/min. c) Speed change (f = 0.108 Hz) from 100 to 1500 r/min.

Fig. 6.12 shows that the normalized value of the first ZSVC harmonic has the same shape than the imposed speed profile. It also proves that its amplitude increases with the number of turns in short-circuit. Similarly as done with the ZSVC, Fig. 6.13 tracks the normalized value of the third harmonic of the stator current in phase B by means of VKF-OT algorithm when the same triangular speed profile is applied. Next, the peak detector and the envelope generator algorithm are applied.

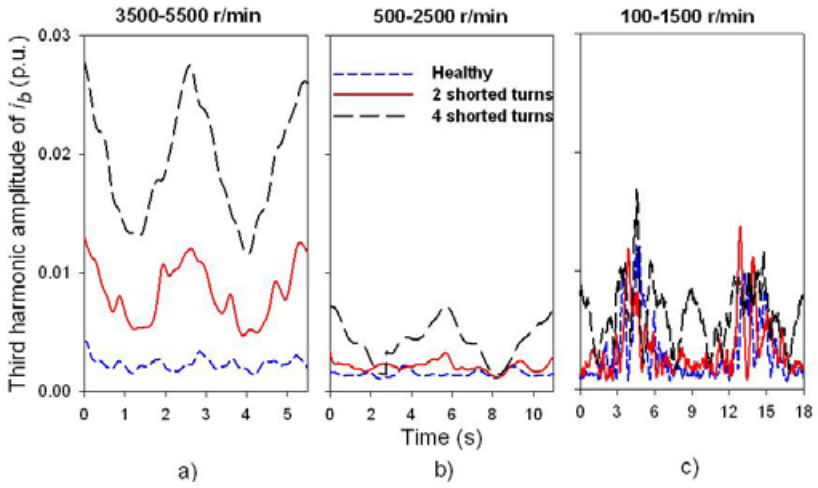

Fig. 6.13. Experimental envelope of the third current harmonic when the healthy and the faulty SPMSMs run under a triangular speed profile. a) Speed change (f = 0.36 Hz) from 3500 to 5500 r/min. b) Speed change (f = 0.18 Hz) from 500 to 2500 r/min. c) Speed change (f = 0.108 Hz) from 100 to 1500 r/min.

Experimental results from Fig. 6.12 and Fig. 6.13 show a similar behavior of the first term of the first ZSVC harmonic and the third harmonic of the stator currents. However, the method based on the ZSVC is more sensitive and accurate than the stator currents-based method, especially at low speed with few shorted turns. Fig. 6.13.c shows that at very low speed operation, the method based on the analysis of the third harmonic of the stator currents has no accuracy enough to track the fault harmonic. It is so because the ratio between the amplitude of the third harmonic and the amplitude of the fundamental one is very low (0.001 at 100 r/min and full load conditions for the SPMSM with four shorted turns). Conversely, the ratio between the first harmonic amplitude of the ZSVC and its fundamental harmonic is much higher (0.064). Hence, the ZSVC provides better sensitivity and accuracy, especially at low and very low speed operation since changes in the ZSVC-based results are magnified when compared to the ones based on the analysis of the stator currents.

It is worth noticing that the first ZSVC harmonic is mainly due to the short-circuit fault whereas the third one (the fundamental harmonic) is originated by the permanent magnets geometry ($d\lambda_{PM,0}/dt$). Additionally, both harmonics amplitudes are proportional to the machine speed. Hence the ratio between the first ZSVC harmonic and the third harmonic amplitude is nearly independent of the motor speed. Consequently, the ZSVC-based method presents improved sensitivity even under very low speed operation, as shown in Fig. 6.12.c.

The analyzed harmonics of the stator currents have a different behavior. The third stator currents harmonic amplitude (fault harmonic) depends on machine speed because of the permanent magnets induction effect. Consequently, the ratio between the stator current fault harmonic amplitude and the fundamental one diminishes with the speed, for a given load level. This fact lowers the sensitivity of such

a method, especially at low speed operation as detailed in Fig. 6.13.b. Consequently, to achieve accurate enough results, this method requires high resolution current sensors.

6.3.2 The m and R fault indicators

To develop fault indicators, first it is required to plot the values presented in Fig. 6.12 and Fig. 6.13 against the motor speed as shown in Fig. 6.14 and Fig. 6.15.

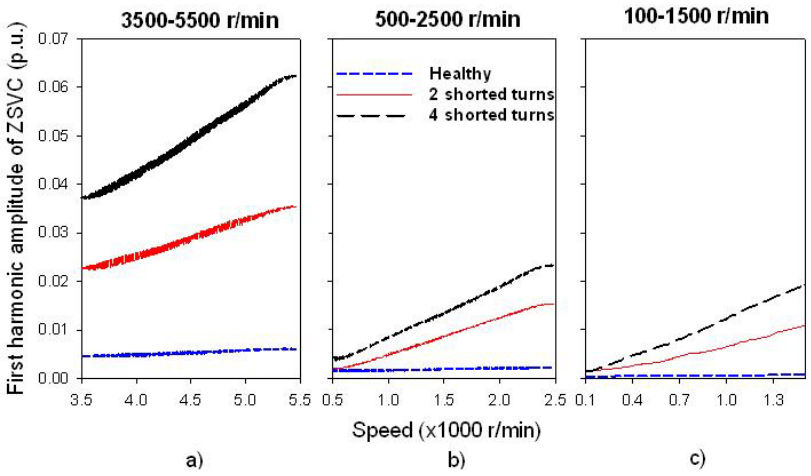

Fig. 6.14. Experimental envelope of the first ZSVC harmonic as a function of the motor speed when the healthy and the faulty SPMSMs operate under a triangular speed profile. The reference ZSVC value is 46 V. a) Speed change (f = 0.36 Hz) from 3500 to 5500 r/min. b) Speed change (f = 0.18 Hz) from 500 to 2500 r/min. c) Speed change (f = 0.108 Hz) from 100 to 1500 r/min.

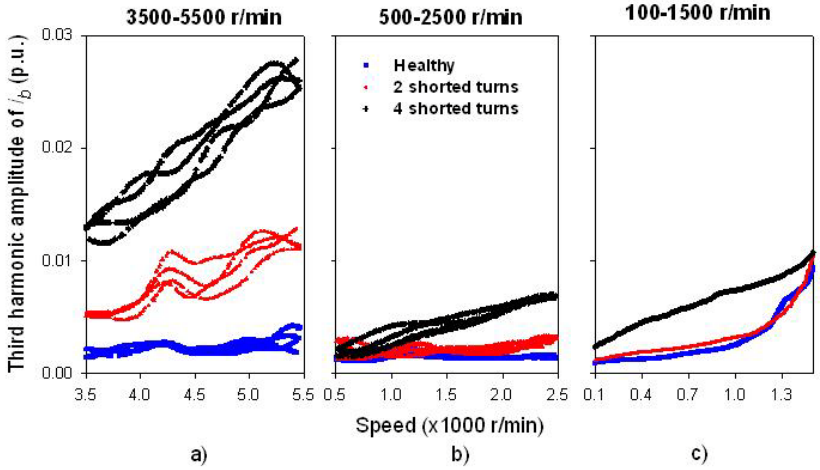

Fig. 6.15. Experimental envelope of the third current i_b harmonic as a function of the motor speed when the healthy and the faulty SPMSMs operate under a triangular speed profile. a) Speed change (f = 0.36 Hz) from 3500 to 5500 r/min. b) Speed change (f = 0.18 Hz) from 500 to 2500 r/min. c) Speed change (f = 0.108 Hz) from 100 to 1500 r/min.

Results shown in Fig. 6.14 clearly indicate that the amplitude of the first term of the first ZSVC harmonic increases proportionally with the motor speed. Consequently, this result is independent of the shape of the applied speed change profile. Similarly, results from Fig. 6.15 show that the amplitude of the third harmonic of the stator currents tends to increase proportionally with the motor speed. However, in this case the result is more disperse because of the abovementioned sensitivity problems, especially at lower speed operation.

As shown in Fig. 6.14 and Fig. 6.15, there is a clear link between the speed variation and the change in the magnitudes of the ZSVC first harmonic amplitude and the third one of the stator currents. Hence, two fault indicators are defined, the slope m of the curves in Fig. 6.14 and Fig. 6.15 and the correlation coefficient R.

Fig. 6.16 and Fig. 6.17 show the evolution of the two fault indicators R and m when analyzing the first harmonic component of the ZSVC and the third one of the stator currents against the motor speed. Both parameters have been calculated under different load conditions of the analyzed SPMSM when a triangular speed reference is applied.

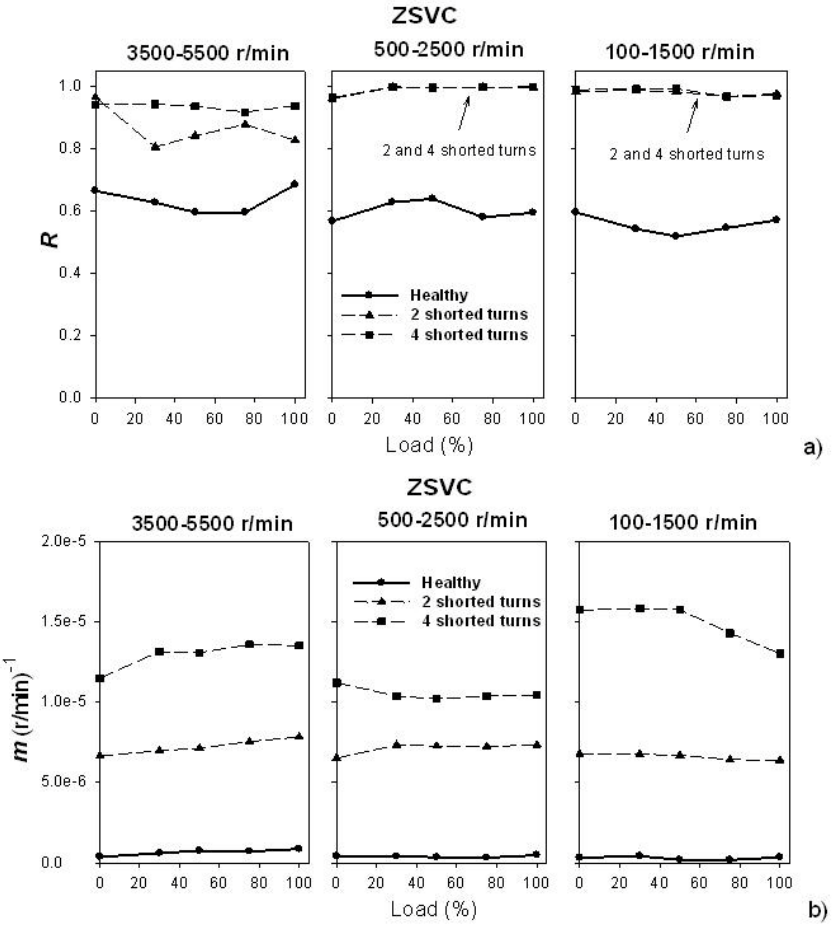

Fig. 6.16. Fault indicators *m* and *R* are calculated over the normalized envelope of the first ZSVC harmonic. a) Fault indicator *R*. b) Fault indicator *m*.

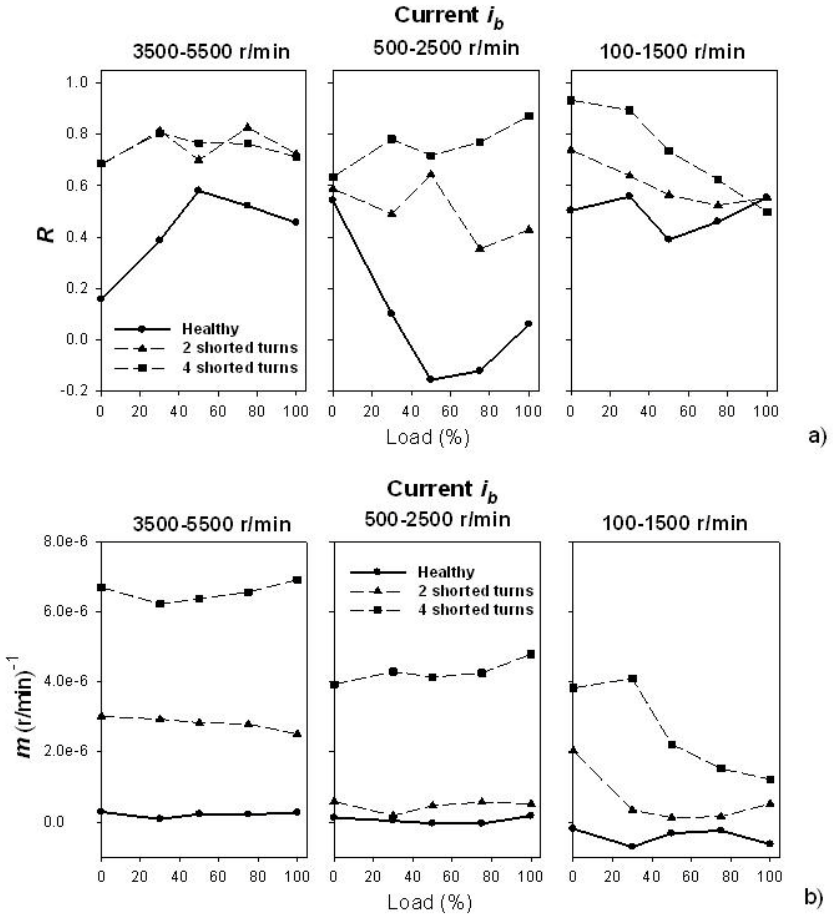

Fig. 6.17. Fault indicators *m* and *R* are calculated over the normalized envelope of the third stator current harmonic. a) Fault indicator *R*. b) Fault indicator *m*.

Although results presented in Fig. 6.16 and Fig. 6.17 are referred to the line current in phase B, similar experimental results were obtained for phases A and C.

The occurrence of an inter-turn fault is directly related to the correlation coefficient R. High values of the coefficient R indicate a high probability of fault occurrence, independently of the speed change applied. However, low values of R may indicate both, a healthy condition or that the sensor is not sensitive enough to detect the occurrence of a given fault level.

Experimental results presented in Fig. 6.16 and Fig. 6.17 show that the steeper the slope m, the more severe the fault. Hence, the severity of the analyzed fault may be quantified by means of the slope m since it increases with the number of short-circuited turns. Results from Fig. 6.16 and Fig. 6.17 show that the slope m is almost constant in front of load changes in all the speed range. Furthermore, the slope is nearly independent of both the profile of the speed change and its range of variation.

It is worth noticing that owing to their nature, both fault indicators m and R are designed to work under non-stationary speed conditions. The proposed system may be particularly useful during the start-up, since it allows dealing with any kind of speed change profile.

In the SPMSM analyzed, the most sensitive harmonic of the stator currents for detecting inter-turn faults is the third one, while the other harmonics are affected in a lesser extent [39] due to its particular stator windings configuration. However, depending on the stator windings configuration, other stator currents harmonics may be analyzed [82] by applying the methodology developed in this work. Contrarily, the ZSVC has the same behavior, independently of the configuration of the stator windings.

6.4 Conclusion

Nowadays, there are many applications in which motors operate under variable speed conditions. For this purpose, this chapter has dealt with demagnetization and inter-turns short-circuit fault detection in SPMSMs from the analysis of stator currents and ZSVC non-stationary signals.

The VKF-OT algorithm has been introduced successfully for tracking fault related harmonics under a wide speed range and different load levels. It has been shown the suitability of this algorithm to deal with the analyzed problems.

In the case of demagnetization faults, the tracked harmonics are the fifth when analyzing the stator currents and the third one when studying the ZSVC. Additionally, the demagnetization index presented in section 4.3 is applied.

In the case of inter-turns short-circuit faults, this chapter presents two reliable faults indicators especially focused to detect such faults under non-stationary speed conditions.

Experimental results have validated the methodology suitability for carrying out demagnetization and inter-turn faults diagnosis in SPMSMs operating under variable speed.

7. CONCLUSIONS AND FUTURE WORK

7.1 Conclusions

PMSMs have appealing features comprising compactness because of their high power and high torque density, high efficiency and reliability, simple construction, and precise torque control. Therefore, they are a highly suitable alternative for high performance systems such as traction drives, particularly for hybrid and electric vehicle power train with compact structure. On-line condition monitoring and diagnosis is an attractive tool that allows reducing unexpected failures occurrence. Consequently this thesis is dedicated to the magnetic and electrical faults diagnosis in PMSMs running under stable and non-stationary conditions.

This work has exhaustively analyzed demagnetization and electrical faults in PMSMs from a theoretical point of view. Next, the most suitable methods to detect such faults are identified. Subsequently the sensitivity and performance of these methods are evaluated by means of experimental measurements under steady-state conditions. Once the most suitable methods have been identified, their scope is extended to non-stationary conditions by using appropriate tracking algorithms

It is important to highlight that there is not a general approach for PMSM fault diagnosis, and in each case the diagnosis method depends on motor configuration, fault type and operational conditions.

For demagnetization faults, the main finding of this thesis is as follows:

- Due to geometric effects, the magnetic flux spectrum in a real PMSM has a high third harmonic amplitude besides others odd harmonics. Consequently, the back-emf has an important third harmonic component. However, if the PMSM is wye connected, no triplen harmonics will exist in the stator current, but they will exist in the ZSVC spectrum, and their amplitudes will decrease with the severity of the demagnetization fault. Therefore, third ZSVC harmonic monitoring is proposed as an alternative for demagnetization detection in PMSMs with integral windings and the third ZSVC harmonic amplitudes ratio between a faulty and a healthy PMSM can be used as a fault severity index.

In the case of electrical faults, the main conclusion of this work is as follows:

- Combined effects of resistive unbalance and stator windings inter-turn faults have been very little studied in general, and not studied in PMSMs in particular. In this work it is demonstrated that both types of faults greatly influence the third harmonic amplitude of the stator currents and the first harmonic of the ZSVC. Hence, by monitoring the stator currents and/or the ZSVC under different operating conditions of the PMSM, it is possible to establish a fault diagnosis scheme which allows discriminating both types of faults. In the case of a resistive unbalance, analyzed harmonics amplitudes remain nearly constant under motor speed changes, but increase linearly with the load level. Contrarily, in the case of short-circuit faults, studied harmonics amplitudes increase linearly with the motor speed but remain nearly constant under load changes

In the case of non-stationary analysis, the main finding of this work is as follows:

- The VKF-OT algorithm is introduced to track selected harmonics for detecting demagnetization and inter-turns short-circuit faults by analyzing non-stationary stator currents and ZSVC signals. The VKF-OT has the advantage that only extracts desired harmonics at each time by applying an adaptive band pass filter, which are the cases of demagnetization and electrical faults, where just certain frequencies are analyzed. Therefore VKF-OT is a compact solution since it includes both the harmonic extraction and tracking steps. From the VKF-OT output data it is possible to calculate fault indicators for both magnetic and electrical failures.

7.2 Future work

Some research topics that can be studied in the future are discussed as follows:

- Mechanical faults are among the most frequent faults related to electric motors. Bearing faults often might manifest themselves as rotor asymmetry faults, which are usually covered under the category of eccentricity-related faults. Consequently all these mechanical defects create distortions in the air gap flux distribution and may affect the ZSVC spectrum. As a consequence mechanical faults diagnosis by means of ZSVC should be studied.

- In this work it is demonstrated that the ZSVC is decoupled from the motor supply. However, its main disadvantage is the necessity of an accessible neutral point of the ststor windings. On the other hand in the case of stator current spectra analysis, this extra connection is not required, but their spectra may be distorted by the power supply. Therefore in order to improve the stator

currents method, the influence of motor controller and its associated power electronics should be investigated.

- In this thesis it is discussed the motor configuration influence on the fault diagnosis. Therefore for a full CBM structure it is interesting to design an expert system which can be able to combine and decide the most reliable method from those discussed in this work.

REFERENCES

[1] C. Ortega, A. Arias, C. Caruana, J. Balcells, and G. M. Asher, "Improved Waveform Quality in the Direct Torque Control of Matrix-Converter-Fed PMSM Drives," *Industrial Electronics, IEEE Transactions on,* vol. 57, pp. 2101-2110, 2010.

[2] J. Beerten, J. Verveckken, and J. Driesen, "Predictive Direct Torque Control for Flux and Torque Ripple Reduction," *Industrial Electronics, IEEE Transactions on,* vol. 57, pp. 404-412, 2010.

[3] R. Errouissi, M. Ouhrouche, C. Wen-Hua, and A. M. Trzynadlowski, "Robust Cascaded Nonlinear Predictive Control of a Permanent Magnet Synchronous Motor With Antiwindup Compensator," *Industrial Electronics, IEEE Transactions on,* vol. 59, pp. 3078-3088, 2012.

[4] K. Raggl, B. Warberger, T. Nussbaumer, S. Burger, and J. W. Kolar, "Robust Angle-Sensorless Control of a PMSM Bearingless Pump," *Industrial Electronics, IEEE Transactions on,* vol. 56, pp. 2076-2085, 2009.

[5] J. R. R. Ruiz, J. A. Rosero, A. G. Espinosa, and L. Romeral, "Detection of Demagnetization Faults in Permanent-Magnet Synchronous Motors Under Nonstationary Conditions," *Magnetics, IEEE Transactions on,* vol. 45, pp. 2961-2969, 2009.

[6] S. Rajagopalan, W. Roux, T. G. Habetler, and R. G. Harley, "Dynamic Eccentricity and Demagnetized Rotor Magnet Detection in Trapezoidal Flux (Brushless DC) Motors Operating Under Different Load Conditions," *Power Electronics, IEEE Transactions on,* vol. 22, pp. 2061-2069, 2007.

[7] Y. Zhang and J. Jiang, "Bibliographical review on reconfigurable fault-tolerant control systems," *Annual Reviews in Control,* vol. 32, pp. 229-252, 2008.

[8] P. Poure, P. Weber, D. Theilliol, and S. Saadate, "Fault tolerant control of a three-phase three-wire shunt active filter system based on reliability analysis," *Electric Power Systems Research,* vol. 79, pp. 325-334, 2009.

[9] W. T. Thomson and M. Fenger, "Current signature analysis to detect induction motor faults," *Industry Applications Magazine, IEEE,* vol. 7, pp. 26-34, 2001.

[10] L. Frosini and E. Bassi, "Stator Current and Motor Efficiency as Indicators for Different Types of Bearing Faults in Induction Motors," *Industrial Electronics, IEEE Transactions on,* vol. 57, pp. 244-251, 2010.

[11] R. N. Andriamalala, H. Razik, L. Baghli, and F. M. Sargos, "Eccentricity Fault Diagnosis of a Dual-Stator Winding Induction Machine Drive Considering the Slotting Effects," *Industrial Electronics, IEEE Transactions on,* vol. 55, pp. 4238-4251, 2008.

[12] B. M. Ebrahimi, J. Faiz, and M. J. Roshtkhari, "Static-, Dynamic-, and Mixed-Eccentricity Fault Diagnoses in Permanent-Magnet Synchronous Motors," *IEEE Transactions on Industrial Electronics, ,* vol. 56, pp. 4727-4739, 2009.

[13] Y. Shenbo and T. Renyuan, "Electromagnetic and mechanical characterizations of noise and vibration in permanent magnet synchronous machines," *Magnetics, IEEE Transactions on,* vol. 42, pp. 1335-1338, 2006.

[14] K. C. Kim, S. B. Lim, D. H. Koo, and J. Lee, "The Shape Design of Permanent Magnet for Permanent Magnet Synchronous Motor Considering Partial Demagnetization," *Magnetics, IEEE Transactions on,* vol. 42, pp. 3485-3487, 2006.

[15] S. Ruoho, J. Kolehmainen, J. Ikaheimo, and A. Arkkio, "Interdependence of Demagnetization, Loading, and Temperature Rise in a Permanent-Magnet Synchronous Motor," *Magnetics, IEEE Transactions on,* vol. 46, pp. 949-953, 2010.

[16] Z. Ping, Z. Jing, L. Ranran, T. Chengde, and W. Qian, "Magnetic Characteristics Investigation of an Axial-Axial Flux Compound-Structure PMSM Used for HEVs," *Magnetics, IEEE Transactions on,* vol. 46, pp. 2191-2194, 2010.
[17] J. Urresty, J. R. Riba, M. Delgado, and L. Romeral, "Detection of Demagnetization Faults in Surface-Mounted Permanent Magnet Synchronous Motors by Means of the Zero-Sequence Voltage Component," *Energy Conversion, IEEE Transactions on,* vol. 27, pp. 42-51, 2012.
[18] S. Grubic, J. M. Aller, L. Bin, and T. G. Habetler, "A Survey on Testing and Monitoring Methods for Stator Insulation Systems of Low-Voltage Induction Machines Focusing on Turn Insulation Problems," *IEEE Transactions on Industrial Electronics,,* vol. 55, pp. 4127-4136, 2008.
[19] R. M. Tallam, T. G. Habetler, and R. G. Harley, "Transient model for induction machines with stator winding turn faults," *Industry Applications, IEEE Transactions on,* vol. 38, pp. 632-637, 2002.
[20] J. Bockstette, E. Stolz, and E. Wiedenbrug, "Upstream Impedance Diagnostic for Three-Phase Induction Motors," in *Diagnostics for Electric Machines, Power Electronics and Drives, 2007. SDEMPED 2007. IEEE International Symposium on*, 2007, pp. 411-414.
[21] Y. Jangho, C. Jintae, L. Sang Bin, and Y. Ji-Yoon, "Online Detection of High-Resistance Connections in the Incoming Electrical Circuit for Induction Motors," *Industry Applications, IEEE Transactions on,* vol. 45, pp. 694-702, 2009.
[22] A. von Jouanne and B. Banerjee, "Assessment of voltage unbalance," *Power Delivery, IEEE Transactions on,* vol. 16, pp. 782-790, 2001.
[23] J.-C. Urresty, J.-R. Riba, and L. Romeral, "Application of the zero-sequence voltage component to detect stator winding inter-turn faults in PMSMs," *Electric Power Systems Research,* vol. 89, pp. 38-44, 2012.
[24] M. Chris, "Machine Condition Monitoring and Fault Diagnostics," in *Vibration Monitoring, Testing, and Instrumentation*, ed: CRC Press, 2007, pp. 1-35.
[25] R. Ahmad and S. Kamaruddin, "An overview of time-based and condition-based maintenance in industrial application," *Computers & Industrial Engineering,* vol. 63, pp. 135-149, 2012.
[26] V. T. Tran and B.-S. Yang, "An intelligent condition-based maintenance platform for rotating machinery," *Expert Systems with Applications,* vol. 39, pp. 2977-2988, 2012.
[27] M. J. Carr and W. Wang, "An approximate algorithm for prognostic modelling using condition monitoring information," *European Journal of Operational Research,* vol. 211, pp. 90-96, 2011.
[28] S. Nandi, H. A. Toliyat, and L. Xiaodong, "Condition monitoring and fault diagnosis of electrical motors-a review," *Energy Conversion, IEEE Transactions on,* vol. 20, pp. 719-729, 2005.
[29] Y. Han and Y. H. Song, "Condition monitoring techniques for electrical equipment-a literature survey," *Power Delivery, IEEE Transactions on,* vol. 18, pp. 4-13, 2003.
[30] P. J. Tavner, "Review of condition monitoring of rotating electrical machines," *Electric Power Applications, IET,* vol. 2, pp. 215-247, 2008.
[31] L. Hui, Z. Haiqi, and T. Liwei, "Gear Fault Diagnosis Based on Order Tracking and Hilbert-Huang Transform," in *Fuzzy Systems and Knowledge Discovery, 2009. FSKD '09. Sixth International Conference on*, 2009, pp. 468-472.
[32] S. Hui, J. Wei, and Q. Shie, "Order tracking by discrete Gabor expansion," *Instrumentation and Measurement, IEEE Transactions on,* vol. 52, pp. 754-761, 2003.
[33] J. Pons-Llinares, J. A. Antonino-Daviu, M. Riera-Guasp, M. Pineda-Sanchez, and V. Climente-Alarcon, "Induction Motor Diagnosis Based on a Transient Current Analytic Wavelet Transform via Frequency B-Splines," *Industrial Electronics, IEEE Transactions on,* vol. 58, pp. 1530-1544, 2011.
[34] S. Rajagopalan, J. A. Restrepo, J. M. Aller, T. G. Habetler, and R. G. Harley, "Nonstationary Motor Fault Detection Using Recent Quadratic Time Frequency

Representations," *Industry Applications, IEEE Transactions on,* vol. 44, pp. 735-744, 2008.
[35] A. K. S. Jardine, D. Lin, and D. Banjevic, "A review on machinery diagnostics and prognostics implementing condition-based maintenance," *Mechanical Systems and Signal Processing,* vol. 20, pp. 1483-1510, 2006.
[36] K. H. Kim, B. G. Gu, and I. S. Jung, "Online fault-detecting scheme of an inverter-fed permanent magnet synchronous motor under stator winding shorted turn and inverter switch open," *Electric Power Applications, IET,* vol. 5, pp. 529-539, 2011.
[37] Z. Guoxin, T. Lijian, S. Qiping, and T. Renyuan, "Demagnetization Analysis of Permanent Magnet Synchronous Machines under Short Circuit Fault," in *Power and Energy Engineering Conference (APPEEC), 2010 Asia-Pacific*, 2010, pp. 1-4.
[38] K. Gyu-Hong, H. Jin, N. Hyuk, H. Jung-Pyo, and K. Gyu-Tak, "Analysis of irreversible magnet demagnetization in line-start motors based on the finite-element method," *Magnetics, IEEE Transactions on,* vol. 39, pp. 1488-1491, 2003.
[39] L. Romeral, J. C. Urresty, J. R. Riba Ruiz, and A. Garcia Espinosa, "Modeling of Surface-Mounted Permanent Magnet Synchronous Motors With Stator Winding Interturn Faults," *IEEE Transactions on Industrial Electronics,,* vol. 58, pp. 1576-1585, 2011.
[40] B. M. Ebrahimi and J. Faiz, "Diagnosis and performance analysis of threephase permanent magnet synchronous motors with static, dynamic and mixed eccentricity," *Electric Power Applications, IET,* vol. 4, pp. 53-66, 2010.
[41] H. Jongman, L. Sang Bin, C. Kral, and A. Haumer, "Detection of Airgap Eccentricity for Permanent Magnet Synchronous Motors Based on the d-Axis Inductance," *Power Electronics, IEEE Transactions on,* vol. 27, pp. 2605-2612, 2012.
[42] J. Rosero, L. Romeral, E. Rosero, and J. Urresty, "Fault Detection in dynamic conditions by means of Discrete Wavelet Decomposition for PMSM running under Bearing Damage," in *Twenty-Fourth Annual IEEE Applied Power Electronics Conference and Exposition, 2009. APEC 2009.* , 2009, pp. 951-956.
[43] J. R. Stack, T. G. Habetler, and R. G. Harley, "Fault classification and fault signature production for rolling element bearings in electric machines," *Industry Applications, IEEE Transactions on,* vol. 40, pp. 735-739, 2004.
[44] J. R. Stack, R. G. Harley, and T. G. Habetler, "An amplitude Modulation detector for fault diagnosis in rolling element bearings," *Industrial Electronics, IEEE Transactions on,* vol. 51, pp. 1097-1102, 2004.
[45] L. Parsa and H. Lei, "Interior Permanent Magnet Motors With Reduced Torque Pulsation," *IEEE Transactions on Industrial Electronics, ,* vol. 55, pp. 602-609, 2008.
[46] F. Magnussen and C. Sadarangani, "Winding factors and Joule losses of permanent magnet machines with concentrated windings," in *Electric Machines and Drives Conference, 2003. IEMDC'03. IEEE International*, 2003, pp. 333-339 vol.1.
[47] J. Pyrhönen, T. Jokinen, and V. Hrabovcová, *Design of Rotating Electrical Machines*: John Wiley & Sons, 2009.
[48] G. Dajaku and D. Gerling, "Skewing effect on the PM Flux-Linkage high harmonics of the PM machines with delta winding," in *Power Electronics and Applications, 2009. EPE '09. 13th European Conference on*, 2009, pp. 1-7.
[49] R. Islam, I. Husain, A. Fardoun, and K. McLaughlin, "Permanent-Magnet Synchronous Motor Magnet Designs With Skewing for Torque Ripple and Cogging Torque Reduction," *Industry Applications, IEEE Transactions on,* vol. 45, pp. 152-160, 2009.
[50] P. J. Holik, D. G. Dorrell, P. Lombard, H. J. Thougaard, and F. Jensen, "A Multi-Sliced Finite Element Model for Induction Machines Incorporating Inter-bar Current," in *Industry Applications Conference, 2006. 41st IAS Annual Meeting. Conference Record of the 2006 IEEE*, 2006, pp. 819-826.
[51] R. Carlson, C. A. da Silva, N. Sadowski, Y. Lefevre, and M. Lajoie-Mazenc, "The effect of the stator-slot opening on the interbar currents of skewed cage induction motor," *Magnetics, IEEE Transactions on,* vol. 38, pp. 1285-1288, 2002.

[52] G. D. Kalokiris, T. D. Kefalas, A. G. Kladas, and J. A. Tegopoulos, "Special air-gap element for 2-D FEM analysis of electrical Machines accounting for rotor skew," *Magnetics, IEEE Transactions on,* vol. 41, pp. 2020-2023, 2005.

[53] D. G. Dorrell, P. J. Holik, and C. B. Rasmussen, "Analysis and Effects of Inter-Bar Current and Skew on a Long Skewed-Rotor Induction Motor for Pump Applications," *Magnetics, IEEE Transactions on,* vol. 43, pp. 2534-2536, 2007.

[54] J. In-Soung, H. Jin, and H. Dong-Seok, "3-D analysis of permanent magnet linear synchronous motor with magnet arrangement using equivalent magnetic circuit network method," *Magnetics, IEEE Transactions on,* vol. 35, pp. 3736-3738, 1999.

[55] B. M. Ebrahimi, J. Faiz, M. Javan-Roshtkhari, and A. Zargham Nejhad, "Static Eccentricity Fault Diagnosis in Permanent Magnet Synchronous Motor Using Time Stepping Finite Element Method," *Magnetics, IEEE Transactions on,* vol. 44, pp. 4297-4300, 2008.

[56] J. C. Urresty, J. R. Riba, L. Romeral, and A. Garcia, "A Simple 2-D Finite-Element Geometry for Analyzing Surface-Mounted Synchronous Machines With Skewed Rotor Magnets," *Magnetics, IEEE Transactions on,* vol. 46, pp. 3948-3954, 2010.

[57] A. G. Espinosa, J. A. Rosero, J. Cusido, L. Romeral, and J. A. Ortega, "Fault Detection by Means of Hilbert–Huang Transform of the Stator Current in a PMSM With Demagnetization," *Energy Conversion, IEEE Transactions on,* vol. 25, pp. 312-318, 2010.

[58] T. R. Jawad Ahmed Farooq, Abdesslem Djerdir, Abdellatif Miraoui, " Modelling and simulation of stator winding inter-turn faults in permanent magnet synchronous motors," *COMPEL: The International Journal for Computation and Mathematics in Electrical and Electronic Engineering,* vol. 27, p. 9, 2008.

[59] W. le Roux, R. G. Harley, and T. G. Habetler, "Detecting Rotor Faults in Low Power Permanent Magnet Synchronous Machines," *Power Electronics, IEEE Transactions on,* vol. 22, pp. 322-328, 2007.

[60] D. Casadei, F. Filippetti, C. Rossi, and A. Stefani, "Magnets faults characterization for Permanent Magnet Synchronous Motors," in *Diagnostics for Electric Machines, Power Electronics and Drives, 2009. SDEMPED 2009. IEEE International Symposium on*, 2009, pp. 1-6.

[61] O. Wallmark, L. Harnefors, and O. Carlson, "Control Algorithms for a Fault-Tolerant PMSM Drive," *Industrial Electronics, IEEE Transactions on,* vol. 54, pp. 1973-1980, 2007.

[62] J. Urresty, J. Riba, H. Saavedra, and J. Romeral, "Analysis of demagnetization faults in surface-mounted permanent magnet synchronous motors with symmetric windings," in *Diagnostics for Electric Machines, Power Electronics & Drives (SDEMPED), 2011 IEEE International Symposium on*, 2011, pp. 240-245.

[63] M. Stulrajter, J. Vittek, C. Caruana, and G. Scelba, "Signal processing of zero sequence voltage technique," in *Power Electronics and Applications, 2007 European Conference on*, 2007, pp. 1-8.

[64] A. Consoli, G. Scarcella, G. Scelba, S. Royak, and M. M. Harbaugh, "Implementation Issues in Voltage Zero Sequence-Based Encoderless Techniques," *Industry Applications, IEEE Transactions on,* vol. 44, pp. 144-152, 2008.

[65] P. Garcia, F. Briz, M. W. Degner, and A. B. Diez, "Diagnostics of induction machines using the zero sequence voltage," in *Industry Applications Conference, 2004. 39th IAS Annual Meeting. Conference Record of the 2004 IEEE*, 2004, pp. 735-742 vol.2.

[66] F. Briz, M. W. Degner, J. M. Guerrero, and P. Garcia, "Stator Windings Fault Diagnostics of Induction Machines Operated From Inverters and Soft-Starters Using High-Frequency Negative-Sequence Currents," *Industry Applications, IEEE Transactions on,* vol. 45, pp. 1637-1646, 2009.

[67] S. Ottonelli, M. Dabbicco, F. De Lucia, M. Di Vietro, and G. Scamarcio, "Laser-Self-Mixing Interferometry for Mechatronics Applications," *Sensors,* vol. 9, pp. 3527-3548, 2009.

[68] G. Giuliani, M. Norgia, S. Donati, and T. Bosch, "Laser diode self-mixing technique for sensing applications," *Journal of Optics A: Pure and Applied Optics,* vol. 4, p. S283, 2002.
[69] U. Zabit, R. Atashkhooei, T. Bosch, S. Royo, F. Bony, and A. D. Rakic, "Adaptive self-mixing vibrometer based on a liquid lens," *Opt. Lett.,* vol. 35, pp. 1278-1280, 2010.
[70] C. Bes, G. Plantier, and T. Bosch, "Displacement measurements using a self-mixing laser diode under moderate feedback," *Instrumentation and Measurement, IEEE Transactions on,* vol. 55, pp. 1101-1105, 2006.
[71] S. Nandi, "Detection of Stator Faults in Induction Machines Using Residual Saturation Harmonics," *Industry Applications, IEEE Transactions on,* vol. 42, pp. 1201-1208, 2006.
[72] P. Neti and S. Nandi, "Stator Interturn Fault Detection of Synchronous Machines Using Field Current and Rotor Search-Coil Voltage Signature Analysis," *Industry Applications, IEEE Transactions on,* vol. 45, pp. 911-920, 2009.
[73] S. M. A. Cruz and A. J. M. Cardoso, "Diagnosis of stator inter-turn short circuits in DTC induction motor drives," *Industry Applications, IEEE Transactions on,* vol. 40, pp. 1349-1360, 2004.
[74] A. Gandhi, T. Corrigan, and L. Parsa, "Recent Advances in Modeling and Online Detection of Stator Interturn Faults in Electrical Motors," *Industrial Electronics, IEEE Transactions on,* vol. 58, pp. 1564-1575, 2011.
[75] A. Bellini, F. Filippetti, C. Tassoni, and G. A. Capolino, "Advances in Diagnostic Techniques for Induction Machines," *Industrial Electronics, IEEE Transactions on,* vol. 55, pp. 4109-4126, 2008.
[76] M. Riera-Guasp, M. F. Cabanas, J. A. Antonino-Daviu, M. Pineda-Sanchez, and C. H. R. Garcia, "Influence of Nonconsecutive Bar Breakages in Motor Current Signature Analysis for the Diagnosis of Rotor Faults in Induction Motors," *Energy Conversion, IEEE Transactions on,* vol. 25, pp. 80-89, 2010.
[77] K. Sangshin, "Four-Leg-Based Fault-Tolerant Matrix Converter Schemes Based on Switching Function and Space Vector Methods," *Industrial Electronics, IEEE Transactions on,* vol. 59, pp. 235-243, 2012.
[78] W. Kesheng and P. S. Heyns, "A comparison between two conventional order tracking techniques in rotating machine diagnostics," in *Quality, Reliability, Risk, Maintenance, and Safety Engineering (ICQR2MSE), 2011 International Conference on*, 2011, pp. 478-481.
[79] VOLD, #160, H., SCHWARZ, B., RICHARDSON, and M., *Display operating deflection shapes from nonstationary data* vol. 34. Bay Village, OH, ETATS-UNIS: Acoustical Publications, 2000.
[80] B. Xu, H. Zhou, L. Sun, and J. Sun, "Weak-signal detection and the application in detection of electric motor faults," in *Electrical Machines and Systems, 2007. ICEMS. International Conference on*, 2007, pp. 1103-1106.
[81] K. S. Wang and P. S. Heyns, "Vold-Kalman Filter Order Tracking in Vibration Monitoring of Electrical Machines," *Journal of Vibration and Control,* vol. 15, pp. 1325-1347, September 1, 2009 2009.
[82] B. Mahdi Ebrahimi and J. Faiz, "Feature Extraction for Short-Circuit Fault Detection in Permanent-Magnet Synchronous Motors Using Stator-Current Monitoring," *Power Electronics, IEEE Transactions on,* vol. 25, pp. 2673-2682, 2010.